Master thesis

Design analysis for a small scale hydrogen peroxide powered engine for a Flapping Wing Mechanism Micro Air Vehicle

Delft University of Technology
Faculty of Mechanical, Maritime and Materials Engineering
Precision and Microsystems Engineering
Mechatronic System Design specialization

January 22, 2012

Supervisors:
Prof.dr.ir. A. van Keulen
Dr.ir. J.F.L. Goosen
Dr.ir. R.A.J. van Ostayen

Title:	Design analysis for a small scale hydrogen peroxide powered engine for a Flapping Wing Mechanism Micro Air Vehicle
Type of report:	Master Thesis
Author:	Tim van Wageningen
Email adress:	t.vanwageningen@student.tudelft.nl tim@riwik.nl
Student #:	WB1264990
Examination date:	24-01-2012
Examination #:	ME 12.003
Specialization:	Mechatronic System Design
Department:	Precision and Microsystems Engineering
Faculty:	Mechanical, Maritime and Materials Engineering
University:	Delft University of Technology

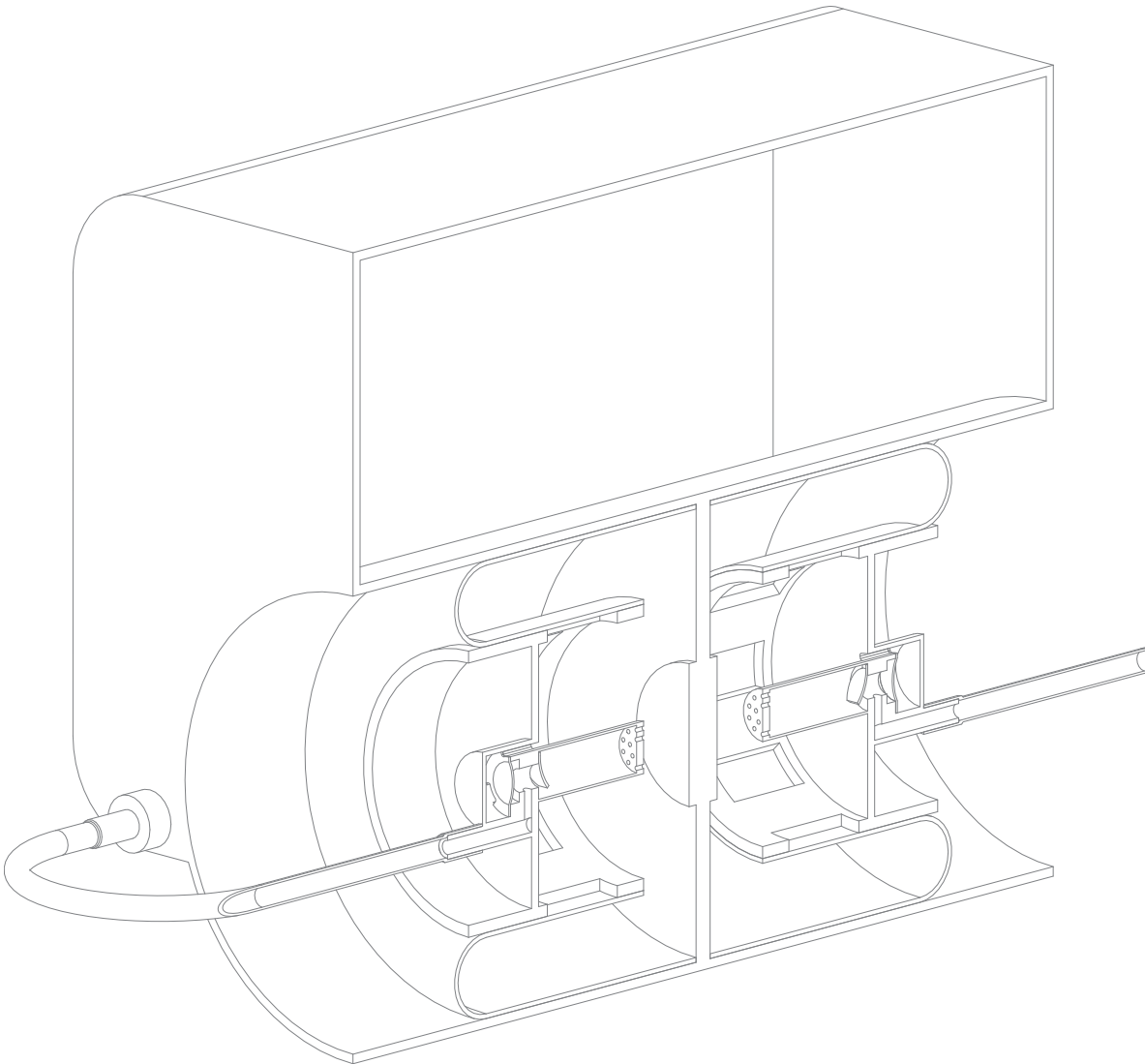

Contents

Summary

The main purpose of this thesis is to find a future direction for the engine project for the FWM of the Atalanta project. Based on previous work done by Arjan Meskers [60], it was indicated that hydrogen peroxide is a good candidate as energy source for small scale engines because of its ease of implementation and relatively high energy content. Using hydrogen peroxide as a starting point, further research has to be done to explore different possibilities for the FWM engine.

The first step is done in Chapter 1: an exploration of other projects on a similar scale. By learning from these projects that are described in literature, it is observed that certain directions are certainly not suitable for the FWM engine. For example, the bladed turbine has not the potential to become the FWM engine since the performance is too low and the requirements to make the system work are too substantial. Also, there is a clear indication that engines with a traditional cylinder piston assembly are dominated by leakage effects and therefore are also not successful on small scale. With this information a subset of the possibilities for the FWM engine is assembled in the form of concepts. These concepts are selected on their potential on small scale, their potential to be realized in a relatively short time span and their diversity.

A candidate that does have potential is the small scale heat engine, represented by Concept 3. The performance is too low of similar projects found in literature, but they are not optimized for the FWM situation. Also, an indication in literature is found that the power density of these types of engines has good scaling behavior. Another potential candidate for the FWM is formed by applying a solution for the leakage problems of the small scale piston cylinder assembly. In Concept 1 flexible material is used between a piston and cylinder such that no fluid can leak through the gap. The blade-less turbine, also called a Tesla turbine, is used in Concept 2. It is described in literature to have a good theoretical potential on small scale, although not much experimental projects are found.

The next step is to indicate what determines the performance characteristics for these small scale engines and how it relates to the requirements for the FWM engine. This is done in Chapter 2. The very basics for the thermodynamic cycle

theory is the Carnot cycle, which closely resembles the operation principle of Concept 3. This is used as a starting point for approximating the performance of the concepts.

The extension of the Carnot cycle is the Curzon Ahlborn model, which shows that the performance is completely determined by a certain potential and the utilization of that potential. The potential determines the magnitude of the incoming energy flow. The utilization determines how much of that incoming energy is converted into useful mechanical work. The nondimensionalization of the Curzon Ahlborn model shows that the utilization of the engine does not depend on any absolute scale, but merely on the ratio's between certain engine parameters. These findings are tested on a more complicated model of the same system. By introducing the energy balance of the working fluid into the model, a time response of its temperature is obtained. This model shows that similar characteristics can be expected regarding the potential and utilization. This information is used to formulate a search method for finding the optimal configuration of the engine model to ensure maximum utilization for a given potential. By making an estimate of the engine potential based on measurements found in literature, this search method is used to give an indication of the performance characteristics as function of the scale of the engine.

The study of Curzon Ahlborn type models is mainly focused on engines that have a compression and expansion step in the cycle and engines that use heat conduction as main energy transfer mode. Also all the models in the beginning of Chapter 2 are based on the assumption that work is extracted by a pressure force. Concept 2, the Tesla turbine, uses a different method of work extraction and has no compression step. Therefore, a separate model is presented at the end of Chapter 2 to characterize this concept. It is observed how the power output can be improved and how the efficiency is influenced accordantly. Measurements are found in literature from Tesla turbines at the exact scale that is opted for the FWM engine. These measurements are done with very small pressure differences, because the tests are done with a different application in mind. By combining the measurement results and the information from the simple model it is concluded that Concept 2 has no potential as FWM engine.

One of the selection criteria for the engine concepts was that they all have different operating principles. Consequently, they all have different types of energy inflows. The energy flows of the remaining two concepts are explored more thoroughly in Chapter 3. Heat flow is studied first, since it is indicated by literature as the most significant loss mechanism for small scale engines. The characteristics of the complex real life situation are modeled in a multi physics simulation and linearized around the scale of interest for the FWM.

The catalytic reaction is the primary energy inflow for all concepts, but based on measurements done by A.J.H. Meskers [60] it was observed that for Concept 1 the catalytic reaction characteristics might be critical. This is because the reaction time of small drops was found to be in the same order as the opted

cycle time for the FWM in its current size. To study the characteristics of the catalytic reaction in more detail, a model is constructed based on the energy balance and fitted to the experimental data.

The last energy flow identified is the exhaust fluid flow in concept 1. Due to time restrictions a full detailed analysis of this subject needs to be done in future work, but a basic analysis using the theory of gas dynamics is given. By approximating the shape of the exhaust as a round nozzle and assuming that friction has not much influence, the mass flow is given as function of a pressure difference.

The findings of Chapter 3 are used in Chapter 4 to construct two models for the two remaining concepts. A numerical method for finding the steady state of these models is discussed and tested by comparison with analytical results. The performance of the models is obtained using these steady states. For Concept 3 it is observed that the performance is too low for the FWM in its current size, but has potential if the geometric scale of the system is reduced. This is due to favorable power density scaling of Concept 3. Of course this is only true if the operation principle of the real engine closely resembles the model. In the model a fixed temperature difference between the two heat sinks is assumed. This might be problematic in a real situation because it will be more difficult to accomplish a temperature difference when the geometric scale is reduced.

For Concept 1, the engine model is a combination of the energy balance of the species inside the cylinder and the exhaust flow model described in Chapter 3. To reduce the sensitivity of the conclusions to the uncertainties of these models, two sets of parameters are used. One is considered optimistic and the other pessimistic. It was found that the performance for both sets is in the right region for the FWM engine requirements. This suggests that among the considered concepts, Concept 1 is the best way forward for the engine project of the FWM.

Nomenclature

α, Π	Non dimensional engine parameter
α_w	Fitted constant characterizing wing performance
$\bar{E}_{react}$	Molar energy release during decomposition
β	Volumetric expansion coefficient gas
ΔH_{evap}	Evaporation enthalpy water
$\Delta M_{uf,n}$	Mass of used fuel during cycle n
ϵ	Surface emittance
η	Efficiency
ν	Viscosity
ϕ	Angle of wing
ρ	Density
σ	Stefan-Boltzmann constant
τ	Shear stress
θ	Compression ratio working fluid
φ	Rotation
a	Speed of sound

c_v	Volumetric heat capacity working fluid
c_p	Isobaric heat capacity working fluid
C	Heat conductance constant
C_x	Damping constant vertical movement FWM
C_d	Damping constant wing movement FWM
C_l	Lift constant wing movement FWM
C_b	Concentration H_2O_2 in bulk
C_i	Heat capacity of species i
C_s	Concentration H_2O_2 at surface catalyst
Da	Diffusive based Damköhler number
E	Energy
E_{hover}	Energy used for hovering FWM during cycle n
f_{cycle}	Cycle frequency
$f_{r,w}$	Weight per weight ratio fuel
f	Ratio parameter of engine model
F_{wd}	Total drag force of wings
F_{xd}	Drag force of FWM in vertical direction
F_{lift}	Lift force of wings
g	Gravitational acceleration
Gr	Grashof number
h_{cyl}	Height cylinder FEM model
h_{conv}	Convective heat transfer constant

I_{tot}	Total inertia wings FWM
k	Stiffness wing angular movement
k	Adiabatic index
k_t	Transportation rate constant
k_{react}	Reaction rate constant
L	Length of wing
M_{act}	Moment that engine FWM needs to supply
M_{avg}	Average molar mass of fluid
m_{tot}	Total mass FWM system, including fuel
m_{device}	Total mass FWM system, excluding fuel
Ma	Mach number
n	Molar quantity of substance
p	Pressure
P	Produced power
Q	Displaced heat
r	Radius
R_{gas}	Universal gas constant
S_g	Geometric scaling factor
t	Time
t_{end}	Maximum flight time
T	Temperature
T_{sat}	Saturation temperature

u	Velocity fluid relative to belt
U	Linearized heat transfer constant
v_{air}	Volume of air in compressed air tank
v_{fuel}	Volume of fuel in compressed air tank
V	Volume
W	Mechanical work
W_{adi}	Work extracted from fluid due to adiabatic expansion

Chapter 1

Design Study: Small Engines

1.1 Introduction

The context of this master thesis is the Atalanta project, which aims to design a small insect inspired device that uses flapping wings to fly. In Figure 1.1 an example is shown, which is a design done by Casper Bolsman [2]. The flexible rings are exited by an actuator with the resonance frequency of the device, such that the wings go through a flapping motion. The actuation currently used is based on electromagnetic forces, but the power density of such systems is too low. In order for the FWM (Flapping Wing Mechanism) to fly, another actuation principle is needed.

This subject was studied by Arjan Meskers [60], who indicated that chemical energy based systems have the most potential to provide a system with high power density at small scales. Especially the chemical decomposition of hydrogen peroxide (H_2O_2) shows good potential at small scale, since it is a mono propellant and has a relatively high energy density. Because it is a mono propellant, the process of decomposition is relatively easy to implement. As the name suggests, there are no other species needed for the chemical reaction, other than the catalyst. This differs from more conventional fuels since they normally need to be mixed with another species in order for the reaction to take place. The mixing of different reactants at small scale is complicated [66], since flow characteristics are usually laminar at small scale. Another reason for choosing H_2O_2 is the fact that it does not emit toxic products.

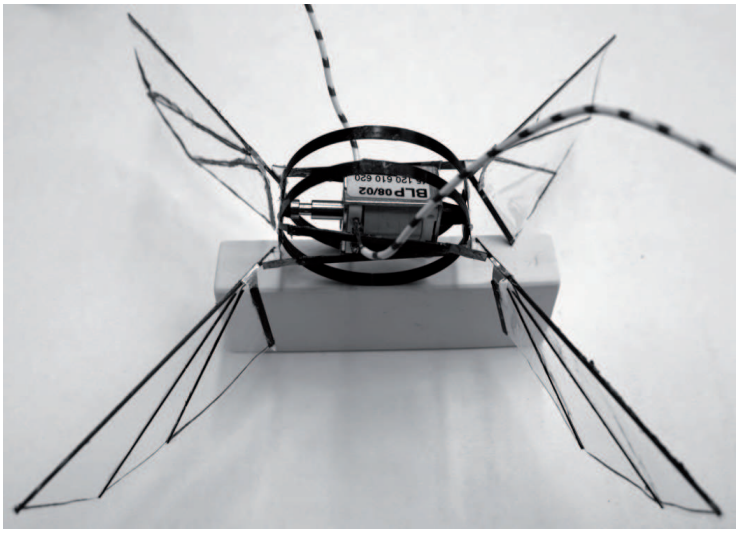

Figure 1.1: Picture of one of the concepts for the FWM designed by Casper Bolsman. (Source:[2])

The product of the decomposition of H_2O_2 is a hot gas, containing water vapor and oxygen gas. The reaction stoichiometry is given by:

$$H_2O_2\,(aq) \rightarrow H_2O\,(l) + \frac{1}{2}O_2\,(g)\,, \tag{1.1}$$

which also releases 98 kJ of energy for every mole of fuel. This energy is used to heat up the liquid water and the oxygen. At some point the water is evaporated such that the only product of the decomposition is a hot gas mixture. The energy that is contained within the gas needs to be converted to mechanical power. For normal scale engines this is typically done by either a piston cylinder assembly or a turbine stage. A third option is to use the energy from the hot gas as a external energy source for the engine, which would make it a external decomposition engine. All three options have been implemented at small scale to some degree, as is discussed in Section 1.3.

The ideal outcome of the Atalanta project is a system that can fly for a long period of time while having enough capacity to carry additional equipment on board, like cameras or other types of sensors. The ideal geometric scale of such a system depends on many factors, for instance the scaling behavior of the wings and the resonance structure shown in Figure 1.1. To choose the right engine concept for the FWM, the scaling behavior of the engine also needs to be put into perspective. This will be the aim of this master thesis:

> *Find an engine design that uses H_2O_2 to supply power to the FWM and indicate what scaling characteristics are involved.*

Material	Specific Volume [cm^3/gram]
Aluminum	0.37
Steel	0.13
Titanium	0.22
Silicon	0.43
Magnesium	0.58
Nylon	0.87
Copper	0.11

Table 1.1: Overview of different materials with their specific volume. (Source:[1])

To do this, first an estimate of the performance requirements for the engine concept are given in Section 1.2. To get a sense of the implications and limitations of engine design at small scale the scaling characteristics of some fundamental engineering elements are discussed in Section 1.3. In Section 1.4 and 1.5, an inventory is given of which subsystems are needed to form a complete engine system, which are combined into concepts in Section 1.6. In Chapter 2, the thermodynamic properties that influence the performance of a small scale engine are described. In Chapter 3, an overview is given of the physical processes that can be found in an engine that uses H_2O_2 decomposition as a power source. In Chapter 4 two models are presented that are used to make an estimate for the performance of two of the concepts.

1.2 Estimating Specifications

1.2.1 Dimension Requirements

The H_2O_2 engine will be designed specifically for the flapping wing mechanism (from here on FWM) as it is described by C. T. Bolsman [2], while keeping in mind that the system needs to have favorable scaling properties. In Figure 1.1, one of the concept versions of the FWM is shown. The engine is fitted inside the rings, which limits the maximum dimensions of the engine. The ring has a diameter of 28 mm and width of 25 mm [2]. The maximum volume the engine can attain if the design shown in Figure 1.1 is used, is in that case $1.5{\cdot}10^{-5}m^3$ or 15 cc. The main focus of this design report will not be on the size constrained, since modifications to the FWM design might provide more space for the engine.

C. T. Bolsman [2] indicated that for the FWM design at the current scale, an engine mass of approximately 1 gram is allowed. To get a sense of how much material 1 gram is, in Table 1.1 a list of different materials is given with their volumes for 1 gram material. In order to stay under the weight limit of the FWM, only a small portion of the available volume can be used by material.

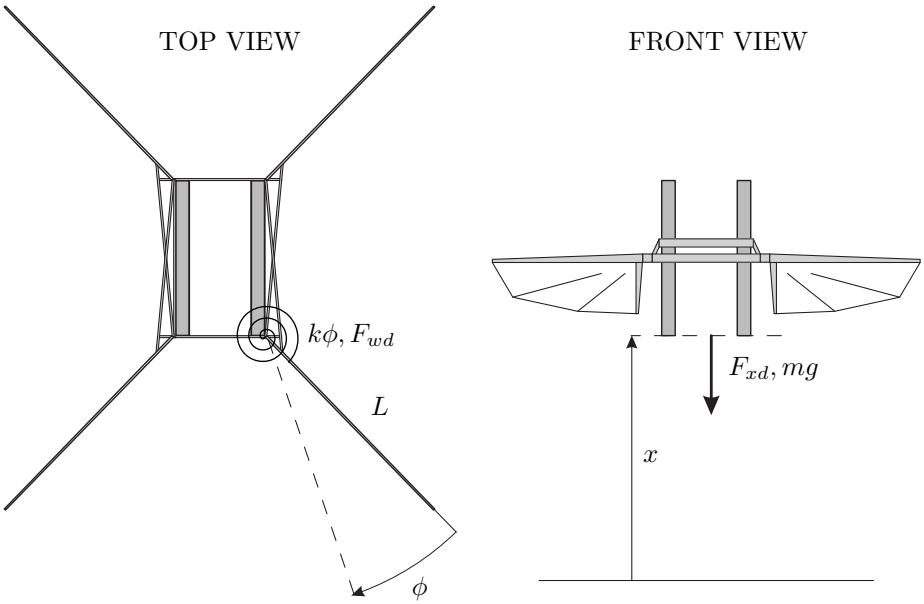

Figure 1.2: diagram of the flapping wing mechanism for which the engine will be designed, defining the two degrees of freedom used in the analysis, wing angle ϕ and height x.

1.2.2 Power Requirements

One of the benefits of using flapping wings is that is easy to stay at one place, making position control of the device easy. This flight mode is called hovering. In this section, the power needed for hovering will be used for finding the relation between weight and maximum flight time.

To analyze the dynamics of the FWM, the wings are approximated as 4 pendulums with one degree of freedom, rotation ϕ. The rotation is counteracted by a linear spring and a damping force F_{wd} caused by the air resistance, as is described by Reference [2]. For simplicity, the force required to actuate this system is replaced by the torque required to move the wings with the needed amplitude. By doing this, the mechanism that converts the force delivered by the engine to a torque on the wings is neglected. The complete system hovers a distance x above the ground and is subjected to the gravity field g. In the x direction the device experiences a drag force F_{xd} due to air resistance, which is assumed to be linear with $\dot{x}$, see Figure 1.2. The equations of motion of this system become:

$$
\begin{aligned}
I_{tot}\frac{d^2\phi}{dt^2} + F_{wd}L + k\phi &= M_{act}, \\
m_{tot}\frac{d^2x}{dt^2} + F_{xd} + m_{tot}\left(t\right)g &= F_{lift}.
\end{aligned}
\tag{1.2}
$$

Here I_{tot} is the rotation inertia of all four wings and m_{tot} is the mass of the complete system. L is the length indicating the point on the wing where the forces are acting. The damping force F_{xd} accompanying movement x, the damping force of the wing F_{wd} and the generated lift can be approximated by [2]:

$$
\begin{aligned}
F_{xd} &= C_x\dot{x}, \\
F_{wd} &= C_dL^2\dot{\phi}^2 sgn\left(\dot{\phi}\right), \\
F_{lift} &= C_lL^2\dot{\phi}^2.
\end{aligned}
\tag{1.3}
$$

Here C_d and C_l are the drag and lift coefficients of the wing. Since the mechanism is designed to operated in a resonating state, it is likely that the rotation of the wings can be approximated with a sinus of a certain amplitude. Using this assumption, the required torque on the wings can be calculated:

$$
\begin{aligned}
\phi &= A_n cos\left(\omega t\right), \\
M_{act} &= C_dL^3A_n^2\omega^2\left(cos\omega t\right)^2 sgn\left(cos\omega t\right),
\end{aligned}
\tag{1.4}
$$

with wing rotation amplitude A_n and angular frequency ω. Here it is assumed that the engine is operating with a frequency equal to the eigenfrequency of the device. With this frequency, the least amount of energy needs to be put into the system in order to move the wings [2]. This is because all momentum forces of the device are counteracted by elastic forces (ideally) and the engine only needs to supply the energy dissipated by the drag forces.

The power needed to hover will decrease as the total mass of the system decreases, which happens because of the fuel consumption by the engine. In order to keep the analysis simple, the mass variation due to fuel consumption over one cycle of the wing movement is neglected from here on. This means that m_{tot} can be assumed constant in Equation 1.2. The resulting function for the mass becomes:

$$
m_{tot,n} = m_{ini} - \sum_{n=1}^{n}\Delta m_{uf,n},
\tag{1.5}
$$

with mass of the system $m_{tot,n}$, the initial mass m_{ini} and used amount of fuel $m_{uf,n}$ in cycle n. For cyclic engine types like piston engines, this approximation is not unrealistic because these types of engines discard the used fuel in short periods. For engines that have a continuous mass flow it might be less accurate. But since the total flight time will be much longer than the cycle time of the FWM, the influence of this assumption will be small. By combining Equation 1.5 and (1.2), the motion in the x direction during one wing period can be calculated:

$$\begin{aligned} x_n &= B_1 cos\,(2\omega t) + B_2 sin\,(2\omega t) + B_3 t + B_4, \\ B_3 &= -\frac{2m_{tot,n}g - A_n^2 C_l L^2 \omega^2}{2C_x}. \end{aligned} \tag{1.6}$$

To keep hovering, the device needs to be at the same height at the end of the wing period as it was at the beginning. That means that constant B_3 should be zero. The resulting wing amplitude A_n in cycle n is given by:

$$A_n = \sqrt{\frac{2m_{tot,n}g}{C_l L^2 \omega^2}}. \tag{1.7}$$

Here it is seen that the damping in the x direction has no influence on the needed power from the engine during hovering. As the device moves up and down, just as much work by the friction force is done downwards as during the upwards movement. With a known wing amplitude, the power needed from the engine can be calculated. To do this, the relation between the fuel consumption and the generated power needs to be determined, which is done in Chapter 2. For now it is assumed that the fuel consumption rate $\dot{m}_{fuel}$ depends linearly on the generated power. This results in the following function for the used amount of fuel during one wing period:

$$\begin{aligned} P_{hover,n} &= M_{act,n}\dot{\phi}_n, \\ E_{hover,n} &= \int_{t1}^{t1+\frac{2\pi}{\omega}} M_{act}\dot{\phi} dt = \alpha_w m_{tot,n}^{3/2} \\ \alpha_w &= \frac{8C_d}{3\omega}\left(\frac{2g}{C_l}\right)^{3/2} \\ \Delta m_{uf,n} &= \frac{E_{hover,n}}{\eta\Phi}. \end{aligned} \tag{1.8}$$

The constant η is the efficiency of the engine and Φ the energy density of the fuel. The energy that is needed for one complete cycle of the FWM is given by E_{hover}. The average power $\bar{P}_{hover}$ over one cycle that the engine needs to

deliver will be useful during the design of the H_2O_2 engine. From this, also the needed power density P_{dens} of the complete system can be calculated:

$$\begin{aligned} \bar{P}_{hover} &= \frac{E_{hover}}{t_p} = \frac{\alpha_w}{t_p} m_{tot}^{3/2}, \\ P_{dens} &= \frac{\bar{P}_{hover}}{m_{tot}} = \frac{\alpha_w}{t_p} \sqrt{m_{tot}}. \end{aligned} \tag{1.9}$$

From measurements done by Reference [2], it was observed the FWM at its current stage needs approximately 0.5 W for lifting 4 gram, which results in a P_{dens} of 125 W/kg. This value can be used to determine if the concepts analyzed in this report are suitable for the FWM in its current size. By combining Equation 1.5 and (1.8), the resulting relation for the mass of the device becomes:

$$m_{tot,n} = m_{ini} - \sum_{m=1}^{n-1} \frac{\alpha_w}{\eta \Phi} m_{tot,m}^{3/2}. \tag{1.10}$$

The engine design has influence on the parameters η and m_{tot}. Note that the term within the summation gives the fuel consumption [kg] for every cycle n. The total mass of the device is the sum of the flapping wing mechanism, fuel tank, control systems and engine. The qualification for the best engine in terms of flight duration can be extracted from Equation 1.10. To optimize the flight time, the fuel consumption during every cycle needs to be minimal. This means that the engine needs to have a large efficiency and a low mass according to:

Design objective for the engine:

Minimize: $\frac{m_{device}^{3/2}}{\eta}$

Constraint: $P_{out} = \gamma \bar{P}_{hover}$

The constraint comes from the needed power while the device is hovering. The device also needs to climb and accelerate which probably demands more power than just for hovering, which is why the constant γ is added.

In nature, flying insects like flies and beetles use a similar mechanism to generate lift. The power needed to hover for different insects has been studied numerically by S. Mao et al. [45], who report specific power requirements of approximately 30 W/kg for a hawkmoth. The hawkmoth has approximately the same wing span and stroke frequency as the FWM designed by Reference [2].

Using the given performance requirements in combination with Equation 1.8, a value for α_w can be calculated:

$$\alpha_w = \frac{\bar{P}_{hover} t_p}{m_{tot}^{3/2}} = \frac{0.5 \cdot 1/30}{0.004^{3/2}} = 66.9. \tag{1.11}$$

To calculated the maximum flight time of the device for a given fuel mass, Equation (1.10) can be used. To solve Equation (1.10), it is assumed that the used fuel per one wing period is small compared to the total device mass, such that Equation (1.10) can approximated with:

$$\begin{aligned} \dot{m} &= \frac{E_{hover}}{\eta \Phi t_p}, \\ m_{tot,t} &= m_{ini} - \int_{t=0}^{t} \dot{m} dt, \\ &= \frac{4}{\left(\frac{\alpha_w}{\eta \Phi t_p} t + \frac{2}{\sqrt{m_{ini}}}\right)^2}. \end{aligned} \tag{1.12}$$

The resulting maximum flight time will be longer using this approximation, since the average mass over one period will be smaller. But for small changes in mass the difference will be small. The maximum flight time t_{end} is defined by the time at which all the fuel is consumed.

$$\begin{aligned} m_{tot,t=t_{end}} &= m_{device}, \\ t_{end} &= \frac{2\eta \Phi t_p}{\alpha_w} \left(\frac{1}{\sqrt{m_{device}}} - \frac{1}{\sqrt{m_{device} + m_{fuel}}} \right). \end{aligned} \tag{1.13}$$

Using Equation 1.13 an estimate of the maximum flight time for the FWM in its current size can be given. With an engine efficiency η of 5%, an energy density of the fuel Φ of $2.9{\cdot}10^6$J/kg, a wing cycle period t_p of 1/30, 1 gram of fuel and 3 gram device weight, the estimated flight time t_{end} in hovering mode is 6 minutes. Reducing the total mass of the device to 2 grams (1 gram for FWM and 1 for the engine) and the total fuel weight to 2 grams results in a estimated flight time is 16 minutes. Note that the used α_w is an estimate that comes from Equation 1.11, where the required power and mass are used based on measurements done by Reference [2]. Looking at the definition of α_w in Equation 1.8 it is assumed that it is contant over the whole flight time. The energy density is based on the decomposition enthalpy of hydrogen peroxide. As will be shown in Section 3.3, not all of this energy will be available to generate power since a lot of it is needed to evaporate the water and heat the reaction products. Also, the efficiency is assumed to be constant over the whole power range of the engine, which is also not the case (Section 2.3).

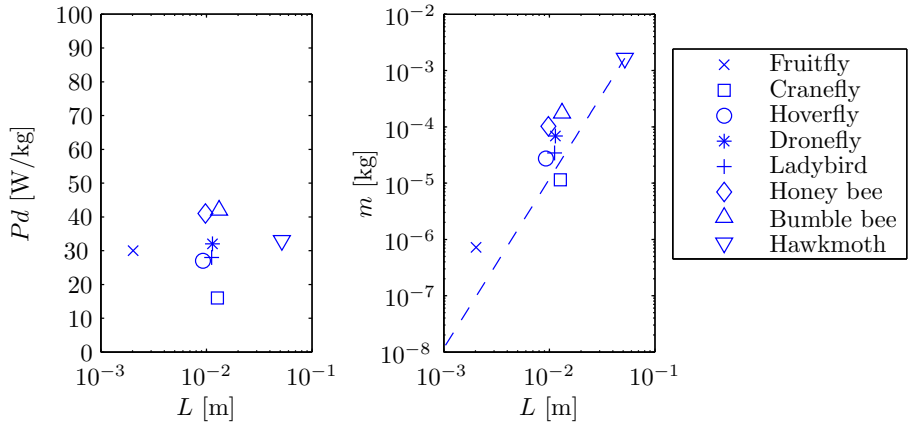

Figure 1.3: Left: the needed power density for hovering for different insects, plotted against their respective wing length L. Right: bodymass of the insects, plotted agains their wing lenght L. The dotted line shows mass of a hawkmoth assuming that its bodymass is proportional to L^3. (Source:[45])

Scaling

The previous calculation shows how the engine mass influences the needed power density to hover a FWM, while assuming that the scale of the FWM remains the same. As stated before, in the future it is desired to further reduce the size of the FWM. To select a appropriate engine design for the H_2O_2 engine, we need to know how the required power density depends on the scale of the FWM.

As the FWM is scaled down, the operating frequency will go up and the wing span will go down. This means that the characteristic parameters of the wing, C_l and C_d, will also change. If the wing length L is taken as reference for the scale of the FWM, the mass of the FWM is proportional to L^3 as a result of geometric scaling (Section 1.3). The influence of scaling on the wing performance parameters C_l and C_d is described by S. Mao et al. [45], who calculated these parameters for different insects wings. In Figure 1.3, the resulting power density P_d that is needed to hover is given for different insects. In the left figure, the body mass of these insects is plotted against the wing length L, which shows that is scales approximately according to L^3.

As can be seen from Figure 1.3, the required power density remains approximately the same for insects of very different sizes and is approximately 30 W/kg. Assuming that nature knows best, the required power density for the FWM is considered to be independent of scale. The 125 W/kg requirement of the current FWM combined with the 30 W/kg found in nature can be used to make a judgment of the suitability of the different concepts described in Section 1.6.

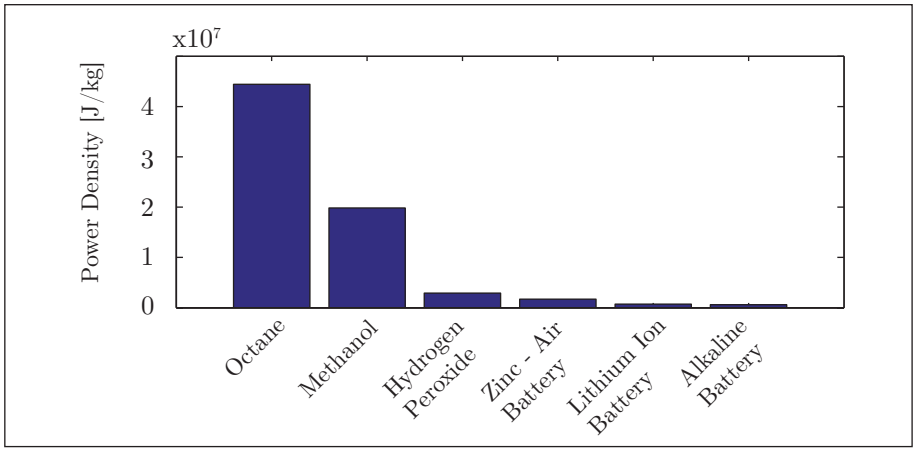

Figure 1.4: Comparison of the energy density for different chemical energy sources and different battery technologies.(Source:[63])

1.3 Small Engine Complications

A lot of research is done on miniaturization of engines, see for example References [10, 11, 47, 46]. The main interest is to provide an alternative for battery systems or to find a solution that powers small unmanned vehicles. Hydrocarbon fuels have a high energy density compared to conventional battery technologies, as is shown in Figure 1.4. High test peroxide (HTP), which is a concentrated hydrogen peroxide water solution, also has a considerable larger energy density then the battery technologies, but not as much as the hydrocarbon fuels. The reason for choosing HTP as energy source has to do with complexities resulting from scaling effects. There are some complications with using combustion technologies at small scale.

These problems are mainly caused by the increased of ratio between surface area over volume [46, 15]. Because of this increase, surface area phenomena like friction and heat flow become more dominant, while volume phenomena like mass and internal energy become less effective. One of the major difficulties of using hydrocarbon fuels at small scale arises from this: sustaining the flame front during the combustion. The quenching distance of the flame becomes small, such that its hard to achieve complete combustion [20].

Another problem arises with the mixing of the fuels. At small scales, the viscosity effects are more dominant than inertia effects, which means that most flows will be laminar. In laminar flows mixing occurs only via diffusion, which results in slow mixing rates [63]. This requires long residence times of the reactants inside the combustion chamber compared to normal sized systems. Longer residence times means that the flow rate need to be smaller, which in most cases means that the power output is smaller.

Effect	Scaling factor exponent x
Mass	3
Surface	2
Material stress from gravity	1
Material stress from fluid pressure	0
Material stress from inertia	2
Material stress from thermal expansion	0
Maximum load limited by buckling	2
Structure stiffness	1
Natural frequency	-1
Moment of inertia	5
Heat flow by conduction	1
Heat flow via radiation	2
Gas flow (laminar flow)	3
Pressure loss (laminar flow)	0

Table 1.2: Overview of different scaling effects with their appropriate scaling exponent. Source:[6, 39]

To illustrate the scaling phenomena a little better, it is useful to introduce the geometric scaling factor S_g. It is defined as the ratio between the characteristic dimensions of two engine of the same shape but different size, for example the stroke of a cylinder based engine. To study the effect of scaling, it is assumed the shape of the engine remains the same but all dimensions are multiplied by the same factor S_g. For example, consider the mass of a engine. If S_g of 0.5 is applied, the total volume of the material that makes up the smaller engine will be a factor 0.125 (0.5^3) smaller than the volume of the original sized engine. This is because volume is a function of three dimensions, which are all reduced by a factor 0.5. Since the mass is proportional to the volume, it is also a factor 0.125 smaller:

$$Mass \propto (S_g)^x \, , x = 3. \tag{1.14}$$

Following the analysis given by J.C. Cool [6], some of the effects caused by geometric scaling have been summed in Table 1.2 with the appropriate scaling factor exponent x from Equation (1.14). By applying these scaling effects to a normal piston engine, it can be shown that the produced power is proportional to the geometric scaling factor with $x = 2$ [6]. This relation applies only when it is assumed that the engines of different dimensions have the same combustion pressure and the same operating speed. Also loss influences like heat leakage are neglected. Performance measurements of small combustion engines (in the order of 100 gram weight) show that the exponent is closer to 4 for real engines [4]. This would mean that the power density is proportional to the geometric scaling factor. The difference is caused by the loss effects.

Because the ratio between the produced power and the power lost reduces for smaller engines [46], there is a certain geometric scale at which these two quantities are equal and the engine produces no power at all. Based on a model of an engine using the Stirling cycle, it has been stated that the minimum engine size is in the order of 1 mm [64]. Below this value the thermodynamic efficiency of the engine is close to zero. This value depends on the chosen materials for the construction of the engine, as well as operating frequencies and temperatures. For normal combustion engines the minimum engine size was predicted to be around 3 mm, based on measurements of small scale engines [46]. Similar data for engines based on decomposition of hydrogen peroxide have not been found.

1.4 Other projects in the same field

Next a overview is given of some projects that are relevant for the H_2O_2 engine design. The list is probably incomplete, but the most successful projects are described with their performance characteristics and problems that were encountered during the testing. Also

1.4.1 Small Turbine Engines

Small or micro turbine engines are used increasingly for distributed power generation. Power output can range between several Watts [10] to several kilowatts [65]. The advantages of small turbine engines compared to typical piston engines include higher power density and a more simplistic design [65].

MIT Micro Turbine

A millimeter scale turbine fueled by hydrogen is designed at the gas turbine laboratory at the Massachusetts Institute of Technology [10]. With use of MEMS production technologies the engine is build out of 6 layers of silicon wafers. The target weight of the system is around one gram, which includes a electric generator and some other devices to run the turbine. With an airflow in the order of grams/sec and a rotational speed above 10^6 rpm the output power should be in the order of 20 Watt. The high rotational speeds are achieved with air bearings. Expected operating temperatures are around 1700 K and is limited by creep of the material at high temperatures [65].

Various aspects of the micro turbine have been investigated and tested, but a standalone system has not been realized yet. One of the issues with a turbine of this small scale that is identified by the research team is the reaction time of the fuel [15]. As the engine scales down, the residence time of the fuel in the combustor scales down with it. The reaction time on the other hand does not, which means that in comparison a much larger combustor is needed for the

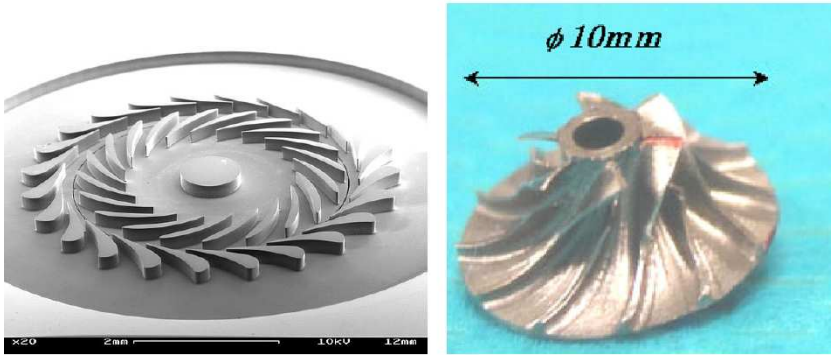

Figure 1.5: Left: Image of the compressor and turbine of the MIT turbine.(Source:[10]) Right: turbine of the Toyko university project. (Source:[32])

same fuel combustion rate. Heat leakage is another problem that becomes more significant when the scale of the engine is lowered, influencing the efficiency of the engine and the maximum power that can be produced. It is estimated that the ratio between the heat energy that is lost and heat energy that is generated is two orders larger than with normal sized turbines [15]. Similar negative effects of scaling are found because of viscous friction forces in the flow of the gas.

The project shows the capabilities of combustion of fuel and the conversion of gas pressure to mechanical motion on a micro scale. The requirements for controlling the turbine include a sensor for the airflow measurement and a digital controller for the fuel control valves. The valves are also a topic of research at MIT and have been successfully realized. Especially the sensors integrated with MEMS technology are indicated as problematic, since high temperatures are required for production of the turbine. Another challenge for a complete standalone system is the starting procedure. It is suggested that it can be done with a integrated micro electric motor, but the requirements for the power density of such a design lay two orders from what is currently accomplished.

Tokyo University Micro Turbine

Another project at the university of Tokyo in corporation with IH Heavy Industries has focused on a 100 Watt micro turbine [32]. In Figure 1.5, a picture of the 10 mm turbine is shown. The intended application of the engine is to supply power for mobile robots. Design specifications include a compression ratio of 3, a rotational speed of the turbine of 870 000 rpm and a flow rate of 2 gram per second. The intended overall efficiency is 5%. Both hydrogen and methane fuels have been tested. The combustion efficiency was around 99.9%. Encounterd problems include heat insulation and bearing design. Since the thermal efficiency of the engine drops significantly if the wall temperature increases, it is

important to provide good insulation [32]. Instabilities were found when using hydrostatic bearings for the turbine shaft.

Leuven University Micro Turbine

The university of Leuven developed a small turbine system that has a tested power output of 28 Watt [28]. The system does not include the combustor and compressor needed for a stand alone system. The weight of the turbine, including housing, is 36 gram. The rotational speed of the blades is around 160 krpm. The overall efficiency is 18%, with the bigest losses from the blade profile (32%) and the exit losses (34%). With Reynolds numbers between 1 and 43, all flows were considered laminar.

University of Berkeley Micro Tesla Turbine

V.G. Krishnan et al. from the Berkeley university report the results of experiments with small scale Tesla turbines [56]. 1 cm disks where used to expand a flow with a rate between 1 and 15 cc/s to generate a power output between 10 and 45 mW. Only small pressure differences were used, between 0.1 and 0.3 bar. The efficiency of the turbine improved for a decreasing pressure difference, with a maximum of 36.6 %. Two models were tested, one with 20 disks and one with 13 disks. The mass of the device was not reported, although the mass of the disks can be calculated from the given dimensions. With a disk mass 0.08 gram, the total disk weight varies between 1 and 1.5 grams. One of the main efficiency losses is caused by the entrance and exit disturabances of the flow. This makes the design of the entrance nozzle an important factor for the overall perforance. In this design nozzle losses are coped with by keeping the flow rate low which limits the power output of the device.

For the H_2O_2 engine, a small bladed turbine is one of the options, although the high operating temperatures and exceptional high rotating speeds that are needed to make the engine operate seem not that desirable for the FWM vehicle. Some kind of transmission should be constructed that converts the fast rotational motion into a 30 Hz translational motion. The Tesla turbine shows better efficiencies at low power outputs and has much lower rotational speeds, but the power density needs to be at least one order higher to be suitable for the H_2O_2 engine.

1.4.2 Small Wankel Engines

Berkeley University Wankel Engine

At the university of Berkeley a micrometer scale Wankel engine is designed and constructed that operates on a hydrogen fuel, see Figure 1.7. At a rotational

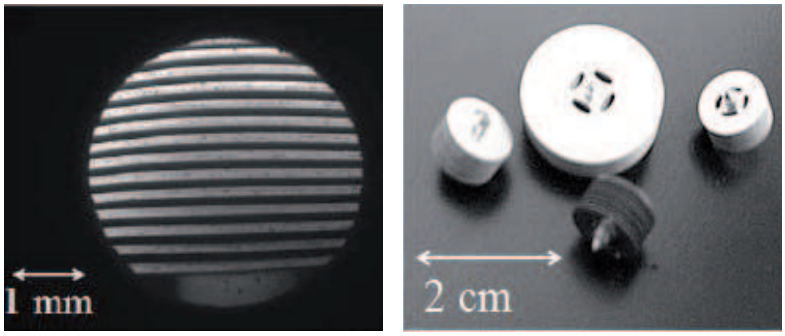

Figure 1.6: Example illustrations of the Tesla turbine systems tested by the Berkeley university. Left: close up of the gaps between the disks. Right: different rotors tested. (Source: [56])

speed of 9300 rpm a power output of 4 Watt was measured for an engine with a displacement of about 350 mm^3 [11]. Another version produced 1 Watt at 5000 rpm. Ignition of the fuel is done via self ignition assisted by a heat source. The goal of the project is to design an engine with 2.4 mm diameter and a power output of 0.1 Watt.

Birmingham University Wankel Engine

Simultaneously another small Wankel engine is developed at the university of Birmingham [16]. The project focuses both on liquid CO_2 and normal combustion fuels. The combustion version has a operating speed between 2500 and 18000 rpm, with an output power of 12 Watt at 17000 rpm.

Both projects use MEMS fabrication techniques to produced the rotor and combustion chamber, which is particularly suitable for a Wankel engine because of its 2D shape. Since the rotational speed and produced power are in the same order of what is desired for the H_2O_2 engine, the small Wankel engine is an interesting option. A big benefit over a normal piston engine is that the timing of the inlet and outlet is automatically controlled by the rotor of the engine, which simplifies the design.

1.4.3 Micro Heat Engines

Washington State University Micro Heat Engine

Washington State university is developing a micro heat engine called the P^3 [47]. It operates with an external heat source, which could be provided by combustion or solar energy for example. It uses two thin membranes with a cavity between them which is filled with a working fluid. By deflecting the

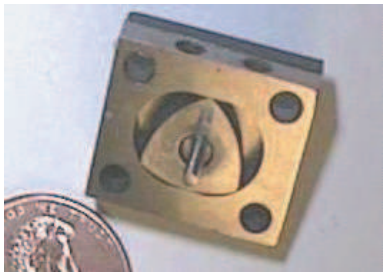

Figure 1.7: Wankel engine with 13 mm diamater combustion chamber (Source:[11])

membranes, the working fluid comes into contact with either the hot side of the engine or the cold site, see Figure 1.8. For this deflection active control is needed. On one of the membranes a layer of piezoelectric material is placed such that the deformation of the membranes is converted to electrical energy. With a deflection of the membranes of approximately 60 μm and a cycle frequency of 370 Hz an electrical power output of 56 μWatt was measured [47].

University of Freiburg Micro Heat Engine

A similar device is designed at the university of Freiburg, which uses bistable membranes such that the thermal switching of the membranes is automatic [49]. Just like with the P^3 engine, there is an external heat source and a cold heat sink to provide the energy flow, see Figure 1.8. With a temperature difference of 37 K, a 80 μm stroke and a operating frequency of 0.7 Hz, a power output of 1.3 μWatt was measured. Higher operating frequencies can be obtained by increasing the temperature difference.

The operating frequency and stroke of these devices is far from what is needed for H_2O_2 engine. But the idea of using only heat energy to drive the engine reduces the requirements on the decomposition process. With automatic thermal switching as it is used by T. Huesgen et al. [49] the hydrogen peroxide decomposition process can be done at a steady rate, such that there is no need for valves or nozzles to regulate the control of this process.

1.4.4 Micro Stirling Engines

A Stirling engine uses an external heat source as energy supplier, just like the micro heat engines of the previous sections. It generates power by alternatively heating and cooling a working fluid. This is accomplished by moving the working fluid between a hot and a cold side of the engine with a displacer, see Figure 1.9. What separates a Stirling engine from a normal hot air engine is that some part of the engine functions as a regenarator [40], which improves the efficiency significantly. In order to drive the pistons, usually a fly wheel mechanism is used

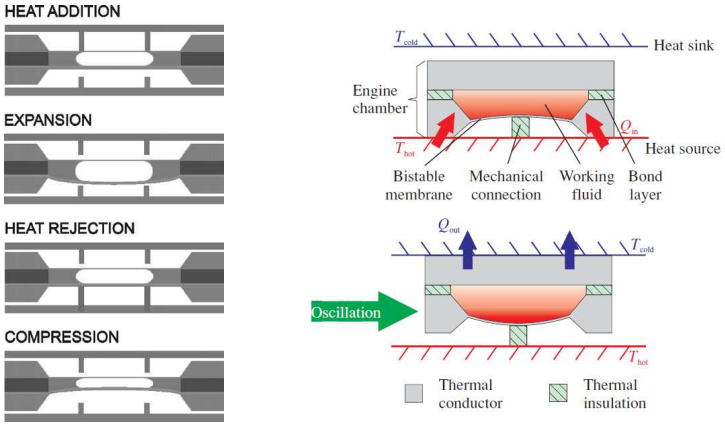

Figure 1.8: Left: schematic representation of the micro heat engine called P^3 developed at the Washington State university.(Source:[47]).Right: schematic representation of the Freiburg university micro heat engine.(Source:[49]

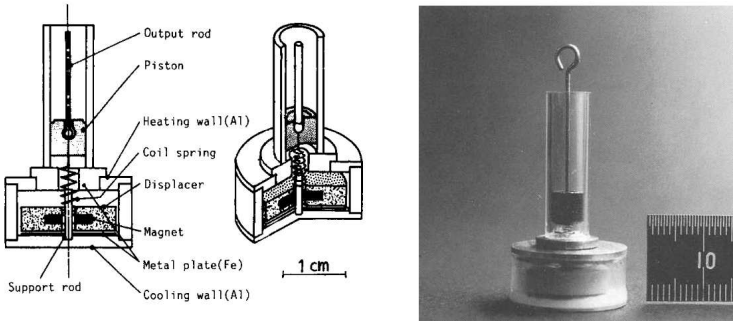

Figure 1.9: Left: schematic overview of the miniature Stirling engine from the Tokyo university, designed in 1989. Right: picture of the test engine. (Source:[39])

for conventional scale engines. Because of scaling effects, the storage capacity is not high enough for small scale systems. Other designs use the resonance cause by the gas pressure stiffness, but this is also not applicable because the frequency becomes to high for small scale engines [39].

A small version of the Stirling engine is designed and build at the university of Tokyo [39]. Various designs for the movement of the pistons are considered, including a 'snap-action' spring and a magnet. With a engine mass of 10 gram, a swept volume of 0.05 cc, an operating frequency of 10 Hz, and a temperature difference of 100 K, a power output of 10 mW was realized.

There are other examples of small scale Stirling engines, but these are not well documented. The example from the Tokyo university has not enough power and is to heavy for the H_2O_2 engine. Perhaps with updated materials and

modern production technologies a better design can be constructed. Similar to the micro heat engines, a benefit of this design is the low requirement on the decomposition process.

1.4.5 Micro Otto Engines

KAIST Internal Combustion Engine

At the Korea Advanced Institute of Technology a small Otto cycle based engine is designed and tested [20]. The design, see Figure 1.10, uses a piston with two combustion chambers on each side. By the movement of the piston an exhaust gate is automatically opened, much like a normal 2 stroke petrol engine. For the testing of the engine, a mix of hydrogen and air was used. A high voltage potential needs to be supplied to an electrode in order to ignite the fuel. For the production, multiple layers of photosensitive glass are used on which the engine design is patterned with UV light. During the test it was observed that leakage effects dominated the engine performance. At 1.8 bar, not only leakage between the wall and the piston was observed, but also between the different glass layers. Heat loss was also a problem. The research team suggests that a better production method and better insulation should help prevent the problems.

Ritsumeikan University Internal Combustion Engine

At the Ritsumeikan University a similar device is designed, only here the piston is connected to a spring such that a reciprocating motion is obtained [51]. As can be seen in Figure 1.10, the device also includes a electric generator. Combustion is obtained by a spark plug. At a compression ratio of 5, a operating frequency of 610 Hz and a combustion temperature of 850 K, the theoretical design predicts a electric power output of 40mW, but no test results are found.

1.4.6 Decomposition Units

Micro H_2O_2 Decomposition Unit Uppsala University

A small H_2O_2 decomposition unit for a micro rocket is developed at the Uppsala university in Sweden [27]. A honeycomb structure is fabricated out of silicon using typical MEMS fabrication techniques, see Figure 1.11. Over the honeycomb structure a layer of catalyst is depositioned, either silver of manganese oxide. The catalyst bed is suspended by very thin arms in order to minimize the conductive heat losses. The size of the holes is a trade off between flow resistance and providing a large contact area. With a supply pressure of 4 bars, a mass flow of 2.5 gram/sec was measured.

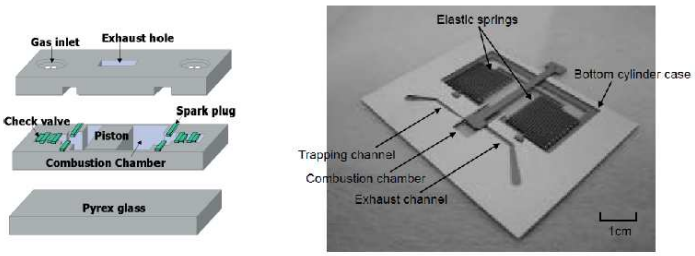

Figure 1.10: Left: schematic overview of the KAIST internal combustion engine.(Source:[20]) Right: picture of realized Ritsumeikan University engine. (Source:[51])

Micro H_2O_2 Decomposition Unit MIT

A small steam generator developed by MIT [22] is shown in the middle of Figure 1.11. The device is designed for homogeneous decomposition of H_2O_2. The fuel and liquid catalyst are pumped into a mixer, after which they enter a reaction room. In the first stage of the reaction room the liquid H_2O_2 decomposes and the released products are heated and evaporated. At some point, the evaporation point of H_2O_2 is reached and it starts to evaporated as well. The length of the reaction chamber is designed such that all the H_2O_2 is decomposed. Measured temperatures reach between 360 and 623 K. Experiments with different weight percentages of the fuel (amount of H_2O_2 in the fuel) have shown that fuel with 74% weight percentage is needed to fully decompose all reactants. The device is designed for a fuel volume flow of about 7 mL per minute.

Micro H_2O_2 Decomposition Unit Vermont University

A small decomposition unit is designed at the university of Vermont [21]. Its suggested application is the propulsion of very small space vehicles. The target specifications for the complete system include a total volume of 1 cm^3, mass of 100 gram and a power consumption of 1 Watt. High concentration H_2O_2 (90%) is pumped through the reaction chamber. The silver catalyst is deposited on small pillars, as seen in Figure 1.11 on the left. To prevent the fuel from the reaction chamber to flow back into the supply channel, a injector was added to the design. The target mass flow of the fuel was around 390 μg/sec. Different reaction chamber lengths were tested, between 1 and 2.5 mm, but no full decompositoin of the fuel was achieved. One of the suggested reasons was the observed bubble formation between the pillars, formed by the released gas. This reduced the effective area of the reaction chamber. Another encountered problem was

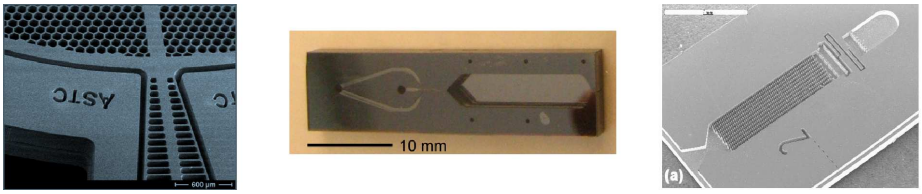

Figure 1.11: Left: design of Uppsala University.(Source:[27]) Middle: MIT ejector pump.(Source:[22]) Right: Vermont University decomposition unit.(Source:[21])

that epoxy was used during the fabrication, which acts as weak catalyst on its own.

1.5 System Functions

In this section the engine design will be split up in smaller pieces, which will be useful for constructing concept designs. The engine as a complete system is subdivided based on some general functions that most version of the engine should have. After the subdivision, a list of implementations of those function is given.

1.5.1 Identifying System Functions

In order to decompose H_2O_2 it first needs to be stored in some sort of container. From there the fuel will require some kind of delivery system to arrive at the catalyst site. Then the decomposition can take place in the decomposition unit. When the hot gas is generated, its energy needs to be extracted in the form of mechanical work. This is the function of the expansion unit. The mechanical work needs to be converted into the right form by a conversion unit in order to drive the flapping wing mechanism. This results in 5 different system functions:

1. Fuel storage
2. Fuel delivery
3. Decomposition
4. Expansion
5. Conversion

In some cases these functions can be integrated or are not needed. For instance, if it turns out that the catalyst can be placed directly into the container, there is no need for a fuel delivery system. Also the conversion unit might not be necessary if the expansion unit is in the form of a cylinder, since it already produces the right translational motion needed for the FWM. Since the engine

system needs to be as light and simple as possible, the design that has the most integration of these functions is likely to be the best for this particular situation. Below some notes on the different functions are given:

Storage

The fuel will be a large part of the total system weight. As for all areal vehicle's, the weight distribution is important for FWM. The center of gravity must be kept in the middle of the device. The tank design needs to be such that if the fuel volume is reduced, the center of gravity does not shifts too much. As indicated by A.V. Jensen [59], H_2O_2 has a small self decomposition rate, which means that for long storage periods, some kind of venting system must be used.

Delivery System

In Section 1.3 it was stated that small scale systems have large area over volume ratio's. For fluid flow, this means that viscous forces will be large and will dissipate more power than in conventional scale systems. Also, as shown by the projects described in Section 1.4, systems to control fuel flow, like conventional pumps and electronic control systems, are large and heavy. Some sort of smart integration of the fuel delivery to the catalyst is desirable in the H_2O_2 engine.

Expansion Unit

There are multiple ways to extract mechanical energy from the reaction products. The most obvious one is by directly expanding the generated hot gas such that pressure does mechanical work. This is the chosen and proven method of almost all engines used in daily life, from aircraft turbines to car engines. The other way is by conducting the heat energy from the hot gas to another working fluid, which expands and compresses it in a closed cycle. This can be found in all external combustion engines like a Stirling engine. Although it might appear as a detour to first conduct the energy by heat transfer before mechanical work can be generated, scaling shows that for small systems heat transfer rates are fast. A big benefit is that the decomposition process and the expansion process are decoupled, which means that no complicated fuel delivery systems like pumps and control systems are needed.

The expansion process itself can also be done in two ways: in a steady state manner as is found in turbines or in a cyclic manner used by piston engines. With a steady state process, first the energy is converted into kinetic energy, after which the mechanical work is delivered by aerodynamic forces. In cyclic expansion process, the mechanical work is mostly delivered by pressure difference. The difference between them is that with a steady state process there is a spatial temperature difference inside the working fluid, which causes internal

losses. Also, because the working fluid must be moving in order to generate the aerodynamic forces, the viscous friction losses of steady state processes are larger. On the other hand, cyclic expansion processes usually suffer from leakage and friction of the sealing used in most cylinder type engines, which also reduces engine efficiency.

Other projects described in Section 1.4.1 that use a turbine, report exhaust temperatures around 1500 K. This indicates that the efficiency of bladed turbine engines at these scales is very poor. Also the rotational speeds above $1{\cdot}10^6$ rpm are problematic for a FWM, since this rotational motion needs to be converted to a translational motion of 30 Hz. A final complication is the needed axillary equipment to operate the turbine, which are large and heavy.

1.5.2 Implementations

For each of the identified functions a couple of solutions are shown in Figure 1.12. The ideas are inspired by other projects on a similar scale and by the input of the PME (Precision and Microsystems Engineering) department at the Technical University Delft. Note that some of these 'subsolutions' might not be the best in their own category, but by combining them with other subsolutions a good overall engine design might emerge. A short description of each subsystem will be given below. As can be seen in Figure 1.12, the subsystems are placed in a grid with each its own location code, for instance A1 is the basic tank.

A1: Basic Tank

For storing the fuel, the most simple solution is a hollow container, much like a regular car fuel tank.

A2: Balloon Tank

Storing the fuel in a balloon might be an attractive option for the engine design. Since the balloon is deformable, it has a particular pressure vs inflation characteristic, as is described at B2.

B1: Gravity Force

Using the gravity of the earth as driving force to transport the fuel to the reaction chamber is a very simple solution. The mayor benefit is that there are no moving parts or delicate conditions needed for the system to work. A downside is that when the tank becomes almost empty due to fuel consumption,

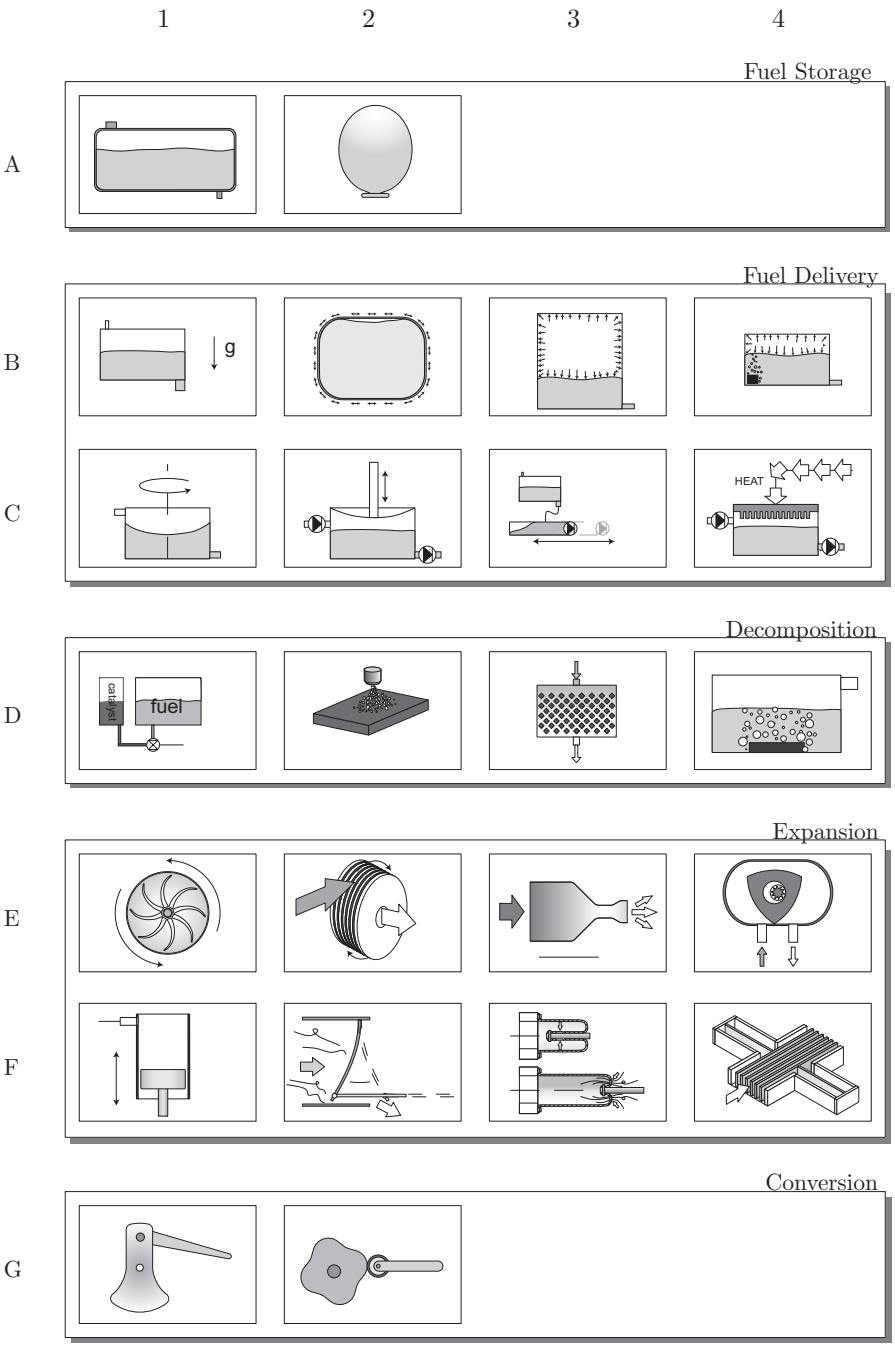

Figure 1.12: Schematic representations of subsystems as they are described in Section 1.5.2. They are placed in a grid with a vertically assigned letter and horizontal assigned number.

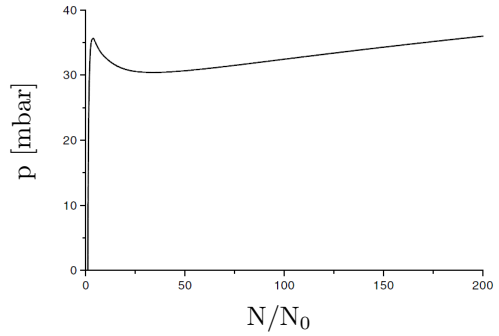

Figure 1.13: Balloon filling characteristics, with pressure in millibars and amount of substance N normalized by the initial amount of substance in the balloon. (Source:[26])

the available pressure is gone. The pressure p at the bottom of the tank is proportional to the height h of the fuel in tank according to:

$$p = \rho g h, \tag{1.15}$$

Assuming that initially there is 5ml fuel on board and the tank dimension are such that the initial fuel height is 1 cm, the supply pressure varies from 140 Pa to zero.

B2: Elastic Energy

By placing the fuel in a balloon, the elastic energy stored in the balloon can be used as motive force for the fuel. The energy is added to the system when refueling, as the elastic material of the balloon expands. Balloons are usually made from polymers, where long chains give the high elongation capabilities. In Figure 1.13 a typical inflation curve of a rubber balloon is shown [26]. The behavior is the result of the balloon shape and the chosen material. After the balloon reaches a certain peak pressure, the pressure drops to a lower level after which the pressure increases approximately linear again. As can be seen in Figure 1.13, if the balloon is almost empty there is still a considerable amount of pressure inside the balloon. This is a benefit for the H_2O_2 engine, since it makes it easy to use the last bit of fuel. The obtainable pressure depends on the design and material of the balloon [26], which would require some testing.

B3: Compressed Air

Using compressed air inside the tank as driving force is a simple and easy solution. When assuming that the temperature is constant and the air behaves as a ideal gas, the ideal gas law can be used to calculate the pressure inside the tank:

$$\begin{aligned} pv_{air} &= nR_{gas}T, \\ \Delta p &= p_{ini}\frac{\Delta v_{fuel}}{v_{air,ini} + \Delta v_{fuel}}. \end{aligned} \tag{1.16}$$

Here Δp is the difference between the initial pressure inside the tank and the pressure after Δv_{fuel} fuel has be used. To keep the influence of fuel consumption on the supply pressure inside the tank as small as possible, the initial volume of compressed air should be many times the volume of the fuel. A larger tank would also mean that it is heavier, so a trade off should be made.

B4: Catalyst Inside Tank

By putting a small element of catalytic material inside the tank, the oxygen gas that is released by the reaction can be used to supply some pressure to the fuel. The needed rate of gas formation in order to keep the pressure inside the tank constant can be calculated by assuming that the ideal gas law applies:

$$\begin{aligned} p &= \frac{nR_{gas}T}{v_{gas}} = constant, \\ \frac{dn_{O_2}}{dt} &= \frac{1}{R_{gas}T}\frac{dv_{fuel}}{dt}. \end{aligned} \tag{1.17}$$

Here it is assumed that the rate of the reaction is small such that the temperature is approximately constant. The catalytic reaction of H_2O_2 is described in detail in Section 3.3, but for now it is assumed that the rate k $[mole/s/kg]$ is proportional to the mass of the catalyst. The amount of mole H_2O_2 $n_{H_2O_2}$ in the tank changes due to the reaction and due to fuel consumption. The amount of mole O_2 n_{O_2} in the gas above the fuel only changes due to the reaction:

$$\begin{aligned} \frac{dn_{H_2O_2}}{dt} &= \left(-m_{cata}k + \frac{dv_{fuel}}{dt}\right)\frac{n_{H_2O_2}}{v_{fuel}}, \\ \frac{dn_{O_2}}{dt} &= -0.5m_{cata}k\frac{n_{H_2O_2}}{v_{fuel}}. \end{aligned} \tag{1.18}$$

Note that $n_{H_2O_2}/v_{fuel}$ is the molar concentration c of hydrogen peroxide in the fuel. The factor 0.5 comes from the reaction stoichiometry of H_2O_2 decomposition into water and oxygen: for every mole of H_2O_2, half a mole of oxygen is released. To get an approximation of how much catalyst is needed inside the

tank, assume that the fuel flow is 0.1 μL/sec and the temperature is 20°C. For a weight ratio of the fuel of 80% $c \approx 3.15 \cdot 10^3$ [mole/m^3]. The reaction constant is in the order of $2 \cdot 10^2$ mole/s/kg, depending on the type of catalyst (Section 3.3). The amount of catalyst needed intitially becomes:

$$\begin{aligned} m_{cata,ini} = \frac{-2}{R_{gas} T k c} \frac{dv_{fuel}}{dt} &= \frac{2 \cdot 0.1 \cdot 10^{-9}}{8.314 \cdot 293.15 \cdot 2 \cdot 10^2 \cdot 3.15 \cdot 10^3}, \\ &\approx 1 \cdot 10^{-13}\ [kg]. \end{aligned} \tag{1.19}$$

This rough approximation of the needed catalyst mass shows that it will be difficult to achieve constant pressure inside the tank because the needed mass is very small. Also, concentration and temperature changes will have influence on the needed catalyst mass. Some kind of flow control is needed to control the rate at which fuel is decomposed in the tank.

C1: Rotating Tank

By rotating the tank an additional acceleration field is created which can be used to drive the fuel out of the tank. This subsystem might be a good combination with a continuous expansion unit like a turbine or Wankel engine if the rotational speeds are not too high. The pressure at the bottom of the tank is a combination of gravity forces (in the y direction) and centrifugal forces (in the x direction):

$$\begin{aligned} \frac{dp_y}{dy} &= \rho g, \\ \frac{dp_x}{dx} &= \rho \omega^2 x, \\ p_{bottom} &= \rho \left(hg + 0.5 \omega^2 r^2 \right), \end{aligned} \tag{1.20}$$

where r is the distance from the rotational center, ρ is the fuel density and ω is the rotational speed. Assume a cylindrical tank with a volume of 4 mL and a radius of 1 cm. With a rotational speed of 30 Hz, the pressure at the bottom of the tank becomes

$$\begin{aligned} p_{bottom} &= 1250 \left(\frac{4 \cdot 10^{-6} \cdot 9.81}{\pi 0.01^2} + 0.5 \left(30 \cdot 2\pi \right)^2 0.01^2 \right), \\ &\approx 27\ [mbar]. \end{aligned} \tag{1.21}$$

A benefit from this subsystem is that the fuel pressure is still considerable compared to the initial pressure when the fuel tank becomes more empty, which is important for making full use of the onboard fuel of the FWM.

C2: Pumping

By using 2 unidirectional valves, a simple pump mechanism can be realized. These valves are usually constructed using MEMS fabrication techniques. The driving force could be supplied by the expansion process itself in the case cyclic expansion is used. Other possibilities include electrostatic or piezoelectric actuation. N.T. Nguyen [62] reports on various pump designs with a volume flow in the order of μL/sec, using different actuating techniques.

C3: Acceleration

This is similar to the rotating tank idea (C1), but in this case for a reciprocating motion instead of rotation. The FWM designed by C.T. Bolsman [2] has a operating frequency of 30 Hz and approximate stroke of 6 mm. The maximum acceleration that is achieved by such a motion is $0.5 \cdot 6 \cdot 10^{-3} \left(2\pi \cdot 30\right)^2 \approx 10g$. A benefit besides the large acceleration is that there is a link between how much energy is needed (stroke and frequency of the motion) and the fuel pressure.

C4: Heat

Another variation of a pump, but with heat energy as the actuating mechanism. By periodically heating the gas inside the air it is expanded and contracted, which pressurizes the fuel.

D1: Homogeneous Decomposition

By mixing a liquid catalyst with the fuel, decomposition can be achieved. This way gas formation has less effect on the decomposition process compared with heterogeneous decomposition. One of the problems with small scale systems is that mixing occurs primarily via diffusion, which is a slow process. Also the refilling of large quantities of catalyst for every fuel tank is undesirable.

D2: Droplet Decomposition

Droplet decomposition has benefits when using a cyclic expansion process, because it can be done directly inside the expansion chamber. This form of integration is desirable for the H_2O_2 engine, as described earlier. One condition is that the reaction needs to be fast enough in order to generate enough power.

This is studied by Meskers [60] and explained in Section 3.3. The generation of small droplets is not uncommon on MEMS scale, with the largest application found in inkjet printers and fuel injectors [9].

Many forms of actuating principles can be used for generating microdroplets, including: pneumatic, piezoelectric, electrostatic and inertial actuation [9]. For the H_2O_2 engine, pneumatic and inertial actuation appear to be the logical choice since they are easily integrable with the other subsolutions. With pneumatic actuation, a pressure difference is used to generate an airflow through a nozzle. This airflow pulls out the fluid from a separate channel and creates the droplets [9]. Also a flexible diaphragm can be used. The pressure difference deflects the diaphragm and pushes the fluid through a small nozzle such that droplets are created [19]. Inertial actuation uses a fast moving fluid reservoir with a small opening through which the fluid can escape. J. Duncre [8] reports on a design with an opted droplet size of 60 μm.

D3: Separate Catalyst Chamber

Inspired by the Vermont University example shown in Section 1.4. The fuel needs to supplied at high pressure at the entrance of the decomposition unit, which means that the requirements on the fuel delivery system are large. Problems with bubbles have to be overcome.

D4: Bulk Decomposition

Placing the catalyst material directly into the main reservoir of the fuel is probably the simplest decomposition subsolution. This mode of decomposition has been thoroughly studied in literature and is described in Section 3.3. A continuous supply of hot gas is generated, with a rate that depends on the concentration of the fuel and catalyst mass. This subsolution is suitable for continuous expansion units and by using some sort of valve it could also be used for cyclic expansion.

E1:Bladed Micro Turbine

The idea to use a bladed MEMS scale turbine design is inspired by the projects of the MIT, Tokyo University and Leuven University. As described earlier, the high rotational speeds and poor efficiencies reported by A.H. Epstein [10] indicate that this subsolution is not suitable for the H_2O_2 design. It is only noted here to provide a complete overview of the possibilities.

E2: Micro Tesla Turbine

A Tesla turbine uses viscous forces that are created by fluid flow to generate power. Conventional bladed turbines have poor efficiencies when they are scaled down. Viscous turbines like the Tesla are expected to have a theoretical maximum efficiency of 38%, which is independent of scaling [43]. In Section 1.4 a project about a micro tesla turbine was desribed, with a power output in the order 45 mW with an efficiency of 17 % and a rotational speed of 7000 rpm. The power density of the demostrated design was not in the right order for the H_2O_2 engine, but might be increased by chosing other construction materials and increasing the pressure difference. For the engine design, a very simple overall system can be construced in combination with a bulk decomposition unit (D4). For the conversion to the right motion, the rotationals speeds are in the same order of the opted operating frequency for the FWM. This means that no complex transmision mechanims are needed, just the conversion of rotation to translation.

E3: Jet Propulsion

A small ejector pump can be used to propulse a moving part of the engine. The specific thrust increases linearly with a decreasing geometric factor, which is why small scale ejector pumps are attractive for space applications [21]. For power applications, low efficiencies can be expected because of high exhaust temperatures.

E4: Wankel Engine

Also inspired by other demonstration projects, the Wankel engine shows good performance on small scale. The rotational speeds used in these types of systems is in the same order as the opted operating frequency of the FWM, which makes the conversion of the rotational motion to translation easy. The timing of the inlet and outlet gates is automatically handled because the shape of the rotor so there is no need for valve systems. Leakage has a large influence on the performance, which is hard to overcome on small scale.

F1: Piston Engine

A piston cylinder assembly has the benefit of producing the right translational motion for the FWM. As shown by D.E. Park et al. [20], special measures have to be taken in order to prevent leakage from dominating engine performance. The university of Leuven worked on a special seal for cylinder-piston assemblies to prevent leakage [7]. Although the seal was designed for actuation purposes, a similar idea might also be applied for small scale piston engines.

F2: Deformable Plate

A thin flexible plate is attached to the top of a duct. By suppling a pressure difference, the gas will push the plate outward, such that the gas can escape and the pressure inside the duct drops. The plate deforms back such that the pressure can increase again. A benefit of this subsolution is that it is simple and provides the right translational motion for the FWM. The performance will be low because the achievable compression ratio will be low and leakage will be prominent.

F3: Flexible Cylinder

The flexible cylinder has the same benefits of F1, but without the leakage problem. There are also no problems with lubrication or with strict fabrication tolerances. Looking closely at the figure of F3 shows another benefit of using flexible material. By forming holes in the material at the right location, an automatic exhaust port can be constructed. A suitable material for a flexible cylinder would have a high temperature resistance, which is not common for flexible materials. One of the potential materials is nylon fabric, frequently used in balloons. It has melting point up to 300°C, depending on the composition. Friction in the material might reduce the engine performance.

F4: Tesla Piston

The Tesla piston uses a number of movable parallel plates to extract power from a moving fluid via viscous forces. The leakage problem from F1 is used here as a benefit, which will result in better performance for small scale systems.

1.6 Concepts

Now that the functions of the engine are identified, some functional concepts can be constructed. Note that these concepts only connect the subsolutions discussed in the previous section and probably will not work in the dimensions that are shown in the figures. These concepts are selected because they have the most potential as a working engine design, it is not guaranteed that all these concepts have the potential to meet the needed specifications of the H_2O_2 engine. In the next two chapters, it will be discussed what determines the engine performance, how it depends on scaling and based on that the concept with the most potential for meeting the specifications can be selected. Next a short description of each concept is given.

1.6.1 Concept 1, Two Stroke Engine

The first concept uses subsolutions A1, B1, C3, C4, D2 and F3 from the previous section. In Figure 1.14 an illustration is given of the cross section of the device. The engine operates by using the spring of the FWM to compress the gas inside the two cylinders. As can be seen in the two lowest images in Figure 1.14, there is a mass that is attached to a thin flexible membrane, which will go from left to right as because of the acceleration of the reciprocating motion. The motion of this mass pumps new fuel into the chamber. Because the pressure is the same on left of the fuel chamber as it is on right of the nozzle, the fuel will be pushed out because of its inertia and because the pump mass will push it out. The valves seen in the figure are operated automatically by the pressure differences and because of inertia. There is also a valve at the point where the fuel pipe enters the tank, but this is not shown in the figure. As the droplets are pushed out of the nozzle, the pressure will increase rapidly and the flexible material of the cylinder will be pushed outward. At some point the gaps in the cylinder will be exposed to the ambient pressure and the hot gas inside the cylinder can escape.

Since the pumping mechanism is based on the inertia of the pumping mass and of the fuel, it will work only if the geometric scale of the system is large enough. Inertia effects scale down faster than surface tension effects, as explained in Section 1.3. At some point, the inertia forces caused by the reciprocating motion will not be bigger than the surface tension of the fuel at the nozzle, such that the fuel will not move at all. Depending on what scale this will occur, another pumping mechanism needs to be used for the H_2O_2 engine. Apart from the pumping mechanism, the flexible cylinder will remain useful at small scales since stresses due to pressure will not increase when the engine is scaled down.

1.6.2 Concept 2, Tesla Engine

The second concept uses subsolutions A1, D4, E2 and G2. Figure 1.15 shows what the device could look like. There are three moving parts, the Tesla turbine and the two wheels attached to the crank. These wheels push the flexible ring of the FWM outward in a sinusoidal motion. The catalyst material is directly placed in the fuel tank. This can easily be extended to a system that regulates the fuel flow towards the catalyst material, such that the engine can be throttled. The hot gas released by the decomposition rises to the top of the engine and is expanded between the disks of the Tesla turbine. In the middle of the disks the gas can escape to the outside environment.

This concept is a little easier in terms of implementation compared to concept 1. The only requirement for this engine to work is that there is fuel inside the tank. As can be seen in Figure 1.15, there is no compression stage in this device, as might be expected in a normal turbine engine. One of the main reasons to add a compression stage to a turbine is to increase the maximum combustion

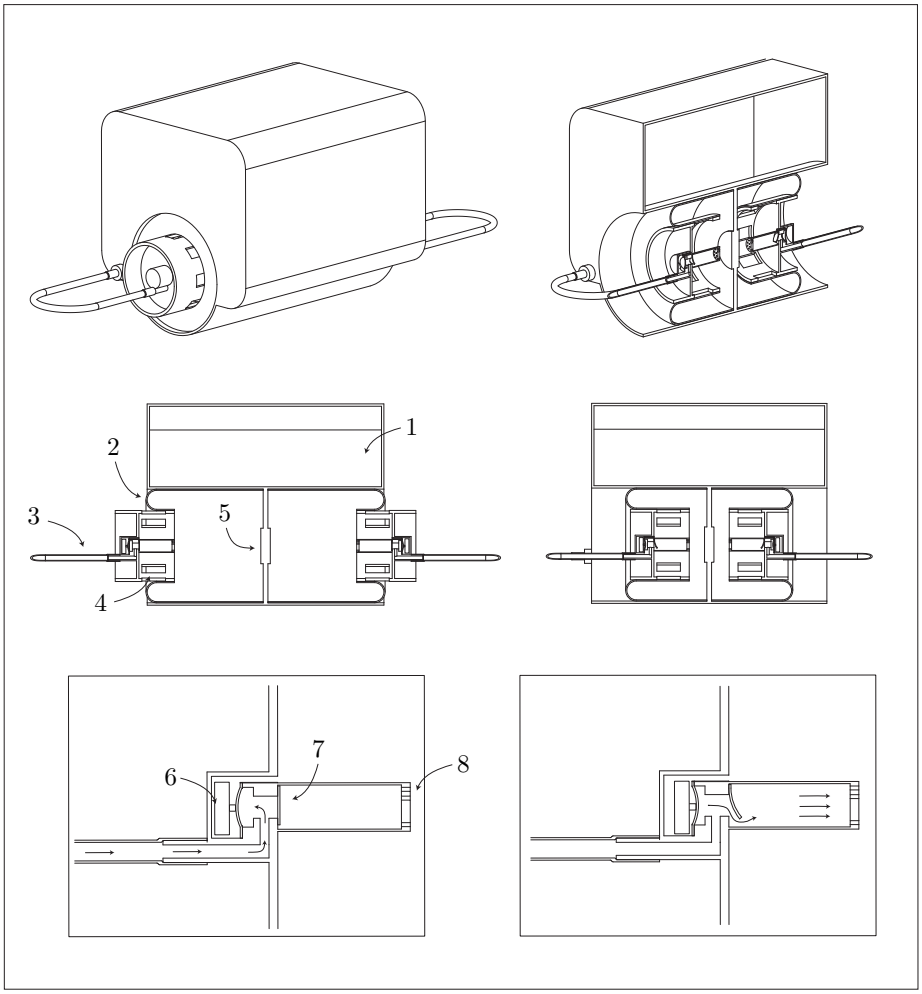

Figure 1.14: Concept 1. The three images on the left show the deformable cylinder in its extended position, on the right in the contracted position. The two closeups show the working of the fuel pump. 1: fuel tank 2: deformable material 3: fuel pipe 4: exhaust ports 5: catalyst material 6: pumping mass 7: flexible valve 8: nozzle.

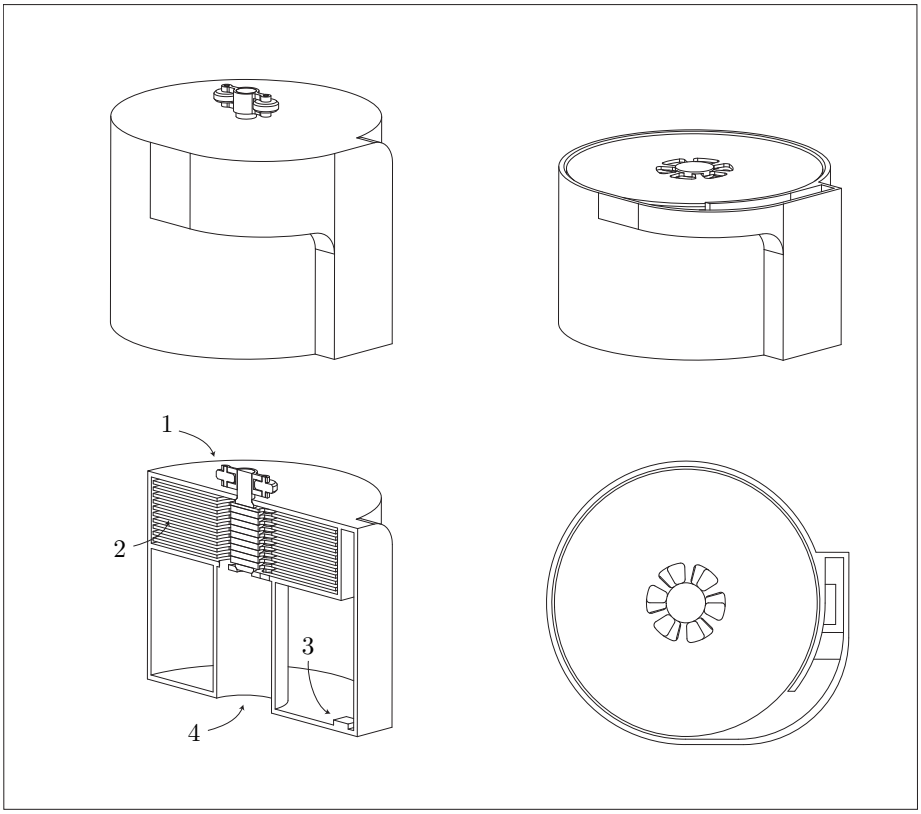

Figure 1.15: Concept A1B3D3E2G3. Top left: small Tesla turbine engine. Top left: housing cut open. Bottom right: cross section 4: Bottom left: top view of the top left image. 1: crank and wheels 2: disks 3: fuel inlet port 4: exhaust port 5: catalyst material.

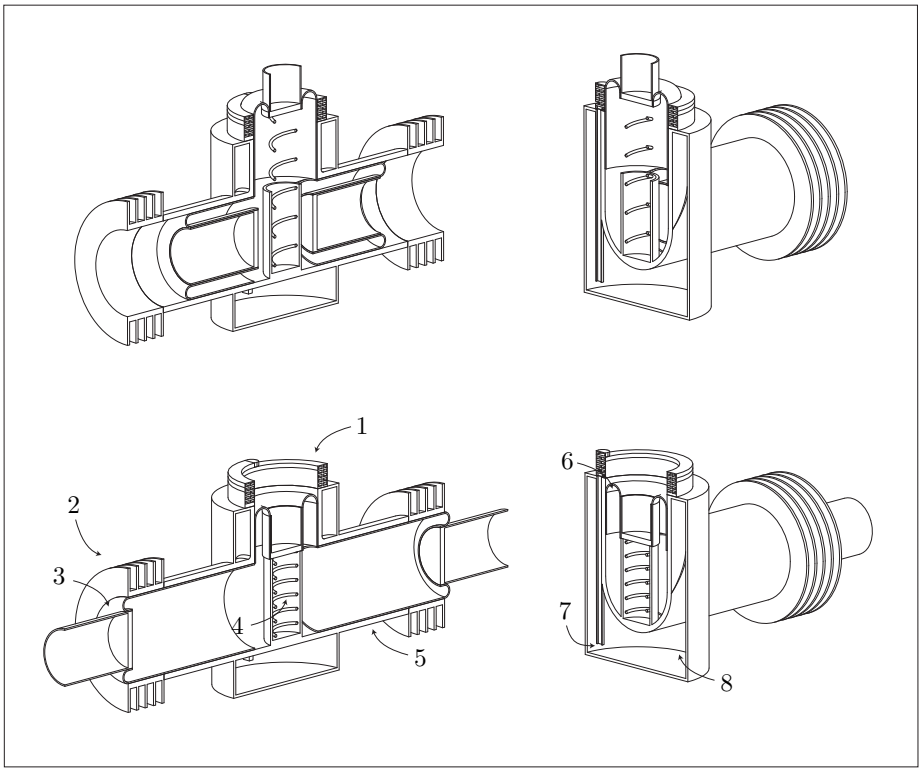

Figure 1.16: Cross sections of concept 3, the top 2 images show the engine in its contracted position, the bottom two in its extented position. 1: decomposition unit 2: cold sink 3: one of three flexible cylinders 4: prestressed spring 5: isolating material 6: flexible cylinder that comes into contact with decomposition unit in the contracted position 7:fuel entry point of decomposition unit 8: fuel tank with compressed air.

rate of hydrocarbon fuels [5]. The increased density of oxygen allows for more combustion, increasing the power density of the engine. For the monopropellant H_2O_2 the compressed air conditions will not increase the decomposition rate, so a compressor stage will not benefit the engine performance.

1.6.3 Concept 3, Heat Engine

Concept 3 uses subsolutions A1, B3, D3 and F3. The configuration represents what a heat engine might look like at small scale. Although the engine shown in Figure 1.16 looks bulky, remember that it has a stroke of only 6 mm. Fuel is stored in a pressurized tank, while it is pushed out trough the decomposition unit. Inside this unit catalyst material is applied to the side walls. The channels through which the fuel flows are configured in a helix shape.

As the two horizontal flexible cylinders are pushed inwards by the spring stiffness of the FWM, the pressure of the working fluid rises. At some point, the pressure pushes on the vertical flexible cylinder with such magnitude that it overcomes the prestress of the spring. At this point it extends towards the decomposition unit which has a hot inner surface. When they make contact, heat will conduct into the working fluid. The horizontal cylinders are pushed outwards again by the spring stiffness of the FWM and the added heat energy. The extension causes the pressure to drop and the vertical cylinder goes back to its original position. When the horizontal cylinders reach the most extended position, they come into contact with the cold heat sinks. Heat energy left in the working fluid is removed via the sinks into the ambient air.

For this specific layout of an heat engine, the radius of the vertical cylinder is a trade off between compression ratio and the rate at which energy is added to the working fluid. For a large radius, the contact area between the vertical cylinder and the decomposition unit is large, but the compression ratio is low. Also, the spring stiffness and prestress of the spring are critical parameters in this design, since they directly determine the timing of the contact between the decomposition unit and the vertical cylinder.

Now that 3 concepts are formed from the subsolutions of the previous section, it needs to be determined what performance can be expected from them. This will be done in the next chapters.

Chapter 2

Engine Performance

2.1 Introduction

Previous research has pointed out that hydrogen peroxide is a promising energy carrier for power systems of small scale [60]. Its energy density in terms of weight and volume is lower than that of other more traditional fuels like petrol, but since H_2O_2 is a mono propellant, the energy conversion process can be kept relatively simple. There is no need for a ignition mechanism or mixing of reactants like is needed with gasoline. The peroxide decomposes into water and oxygen as soon as it has come in contact with the catalyst. The decomposition is exothermic, such that the reaction products are vaporized. Assuming that our system is going to use the potential of hot gas to generate power, a further subdivision of possible system layouts can be made, as was done in Section 1.6.

What separates these concepts in terms of thermodynamics are the different energy flows that go through the engine. This is shown schematically in Figure 2.1. Recurring steps in every concept are the decomposition and work extraction steps. For Concept 1 and 3, the work is extracted by a piston for which the extracted work W is given by:

$$W = \int_{V_1}^{V_2} p dV, \tag{2.1}$$

where p is the pressure and V is the volume of the cylinder. For Concept 2, the work is extracted by viscous forces caused by the speed difference between the gas and the disks and is given by:

$$W = \varphi \int_{0}^{A_1} r\tau dA, \tag{2.2}$$

with disk rotation φ, wall stress τ, surface area A and disk radius r. This is fundamentally different from Concept 1 and 3, which will result in different scaling behavior of the performance characteristics. The same applies for the difference between Concept 1 and 3. With Concept 1, the energy is added to the expansion chamber via decomposition, for Concept 3 via heat conduction. These process have their own scaling behavior, resulting in a different engine performance.

In this chapter these differences are analyzed by starting with the most basic thermodynamic model. From this starting point, the complexity of the model is increased until the needed conclusions can be made. In thermodynamics the normal approach of analyzing the performance of an engine is by approximating its behavior with a model called a cycle. Since all the theory presented in this chapter is based on the Carnot cycle, a short introduction about this cycle is given in Section 2.2. It shows the fundamental relation between temperature and efficiency that will play an important role in the design of the H_2O_2 engine. Also, the relations that apply for the Carnot cycle can be used directly to analyze the performance of Concept 3, since it operates on the same physical principles. In Section 2.3, the extension from an ideal cycle to a more realistic situation is done by introducing the Curzon Ahlborn model. Here the fundamental relation between power output and energy efficiency is shown. In Section 2.4 the model is taken one step further, where the reversibility assumption used in Section 2.2 and 2.3 is replaced by the energy balance of the working fluid. This model can be used to make some approximations of the power output of Concept 3. In Section 2.5, the behavior of this power output as function of geometric scaling is discussed. The first 4 sections of this chapter are based on work extraction by pressure. In Section 2.6, the work extraction mode used by Concept 2 is analyzed. This subject is treated after the basic analysis of the Curzon Ahlborn model, since some of its elements come back in this section.

2.2 Work Generation by pressure

The foundation of the knowledge about thermodynamic processes dates back to the 18th century, in the time that James Watt studied and improved the operations of the steam engine. In the beginning of the 19th century Sadi Carnot started his studies on heat engines and observed that heat can be used as motive force [17]:

> 'Wherever there exists a difference of temperature, motive force can be produced' *Sadi Carnot*

This was illustrated with the concept of heat reservoirs, as seen in Figure 2.2. When the two reservoirs have different temperatures a heat flow will occur. This flow can be used to generate work. Carnot stated also that [17]:

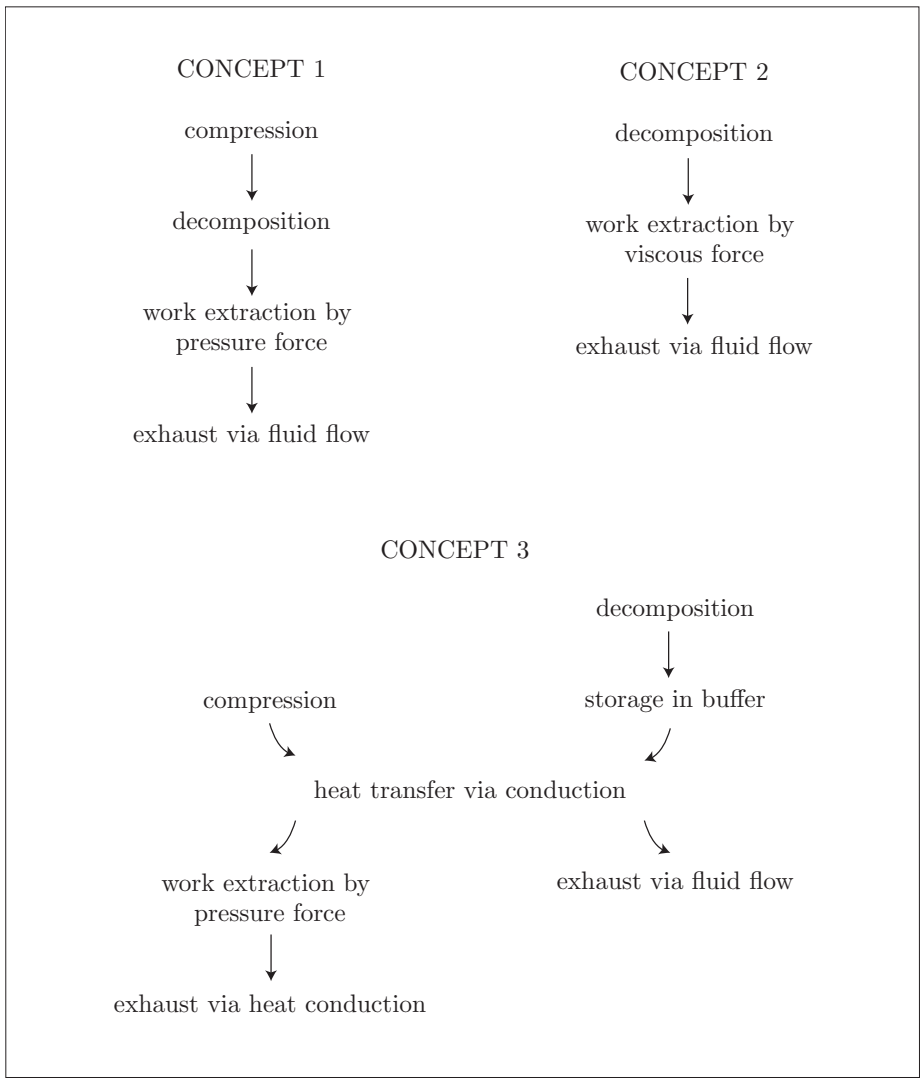

Figure 2.1: Diagram of the different energy flows in the concepts discussed in Section 1.6.

> 'The necessary condition for the maximum (work) is that in the bodies employed to realize the motive power of heat there should not occur any change of temperature which may not be due to a change of volume' *Sadi Carnot*

In a real system which utilizes heat to generate work, this means that there should be no temperature gradients since this would cause a heat flow that does not generate work. To keep the gradients at a minimum, all process which would cause a temperature difference, like expansion, should occur at an infinitely slow rate [17]. Carnot classified processes that fulfill this criterion as reversible. Reversible processes are only possible in theory, since they require infinite time and dimension scales if they are to be implemented in a real system. Since a reversible process produces the maximum amount of work, a real system that uses heat to generated work will never be more efficient than its reversible equivalent. It is useful to study reversible processes since they give the maximum performance limits of real processes.

To study the efficiency of reversible heat engines, Carnot introduced the Carnot cycle. He observed that if a thermodynamic process undergoes a cycle, which means that its end state is equal to the begin state, there is always some portion of the available heat flow needed to get back in the begin state. This means that the heat flowing out of a single heat reservoir can never be converted fully into work and that the efficiency can never reach 100 percent. This is illustrated by the 4 steps of the Carnot cycle, which describe the process of a working fluid in a piston assembly connected to two heat reservoirs:

1. Isothermal expansion while the working fluid absorbs heat from the hot reservoir.

2. Adiabatic expansion until the working fluid has reached the temperature of the cold reservoir.

3. Isothermal compression while the working fluid rejects heat to the cold reservoir, until the point is reached where the adiabatic compression step (4) can bring the working fluid back in the begin state.

4. Adiabatic compression which brings the working fluid back in its begin state.

A diagram of a possible physical implementation of the Carnot cycle is seen in Figure 2.3. By analyzing the different steps of this cycle the important relation between temperature and efficiency can be derived. The following is based on the steps taken in D. Kondepudi et al. [17], which gives a more detailed explanation.

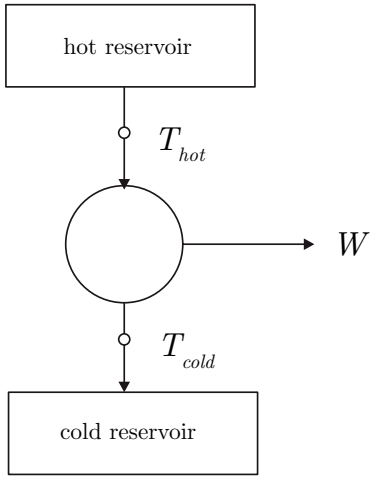

Figure 2.2: diagram of a heat engine with two heat resevoirs

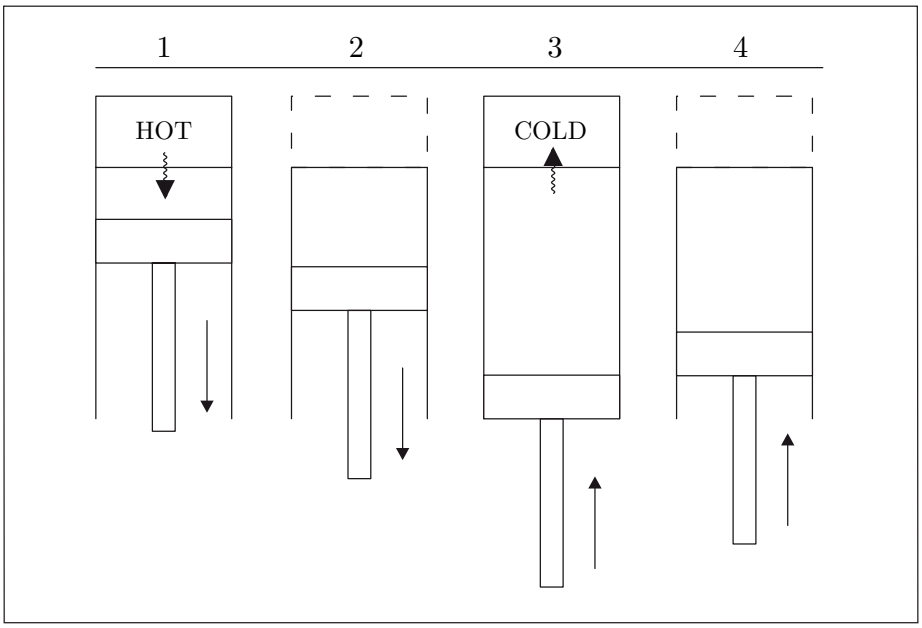

Figure 2.3: the steps that are taken during a Carnot cycle with the corresponding state numbers

The Carnot Efficiency

In Step 1 the heat Q_{in} is added to the process, which is equal to the work W generated during this step by the expansion if the process is reversible. The following sign convention is used: Q is positive if the flow is towards the system and W is positive if the work is done by the system. Assuming the ideal gas law applies:

$$pV = nR_{gas}T, \tag{2.3}$$

which gives a relation for the pressure p, volume V, amount of working fluid n, temperature T and universal gas constant R_{gas}. The work and heat flow during step 1 can be calculated with:

$$\begin{aligned} W_{1\to 2} &= \int_1^2 pdV = nR_{gas}T_{hot}ln\left(\frac{V_2}{V_1}\right), \\ Q_{1\to 2} &= W_{1\to 2}. \end{aligned} \tag{2.4}$$

Step 2 brings the working fluid in balance with the cold reservoir, which is needed to allow isotherm (reversible) compression during step 3. Since this process is adiabatic, the pressure and volume are governed by the polytropic relation:

$$\begin{aligned} &\left(pV^{\gamma}\right)_1 = \left(pV^{\gamma}\right)_2, \\ &W_{2\to 3} = \int_2^3 pdV = \frac{nR_{gas}\left(T_3 - T_2\right)}{\gamma - 1}, \\ &Q_{2\to 3} = 0. \end{aligned} \tag{2.5}$$

Step 3 is the same as step 1, but with compression instead of expansion. Step 4 is the compression step, which is like step 2 also adiabatic and polytropic. It can be shown that if the heat engine of Figure 2.3 is reversible, the relation between the volumes of the different steps is given by [17]:

$$\left(\frac{V_2}{V_1}\right) = \left(\frac{V_3}{V_4}\right) \tag{2.6}$$

With this condition, the first law of thermodynamics, and assuming that the system does not gain any internal energy during the cycle, the total work output during one cycle can be calculated:

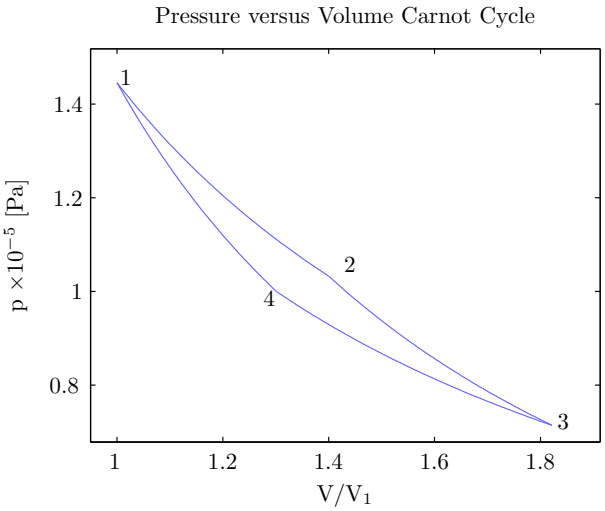

Figure 2.4: pressure versus volume characteristic for the Carnot cycle. The volume is normalized for the smallest volume that the working fluid has during the cycle.

$$\begin{aligned} W_{net} &= \sum W, \\ W_{2\to3} &= -W_{4\to1}, \\ W_{net} &= Q_{1\to2} + Q_{3\to4}. \end{aligned} \tag{2.7}$$

In Figure 2.4 the pressure and volume throughout the Carnot cycle are plotted. Note that the area within the blue line represents the generated work. By defining the efficiency of the cycle as the ratio between the generated work and the thermal energy that enters the system and using Equations (2.4) and (2.5), the efficiency is given by:

$$\begin{aligned} \eta_{rev} &= \frac{W_{net}}{Q_{1\to2}}, \\ \eta_{rev} &= 1 - \frac{T_3}{T_1} = 1 - \frac{T_{cold}}{T_{hot}}. \end{aligned} \tag{2.8}$$

This relation, called the Carnot theorem, shows that if the temperature difference between the hot and cold reservoir is higher, the efficiency of the reversible process will be higher. It will never reach unity, since the difference in temperature will always be less than infinite. The reversible cycle and its relations are useful for the analysis of thermodynamic processes. By assuming that a part of the engine operates reversible, the relation between the generated work and efficiency can be determined. This will be used in Section 2.3.

Up to this point it is assumed that the processes of the engine occur in a reversible manner. This means for example that there are no temperature or pressure gradients. For this to be true in a real process, it must be infinitely slow. That is why at the maximum efficiency of the Carnot cycle, the power output of the heat engine will actually be zero. To take in consideration that the process must occur in finite time to produce power the theory of endoreversible thermodynamics must be applied. It will indicate which effects reduce the power and efficiency of a thermodynamic cycle. Since these effects usually depend on geometric dimensions, a prediction can be given about how the system will behave when it is scaled down.

2.3 The Curzon Ahlborn model

2.3.1 The basic model

The first effect that is illustrative for real processes is the time needed to transfer the heat quantities into the system. In an internal decomposition system like Concept 1, the maximum rate at which heat can be added to the system is given by how much fuel can be decomposed per unit time. For a external decomposition engine like Concept 3, the generated heat must also be transferred via a heat exchanger. K. H. Hoffman et al. [31] modeled this effect as thermal resistances that are present between the heat reservoirs and the reversible part of the engine. This resistance limits the magnitude of the heat flow for a given time period. The model presented below and seen in Figure 2.5 is called the Curzon Ahlborn heat engine. A detailed explanation of the model can be found in Reference [31] and in Appendix A. The model is primarily based on external combustion engines because the assumption that energy enters an internal combustion through heat conduction has no real meaning [33]. The basic idea of the Curzon Ahlborn model is to show the effect of time on a reversible engine. Because only a certain amount of energy can be transferred to the engine for a given cycle time, the amount of work that can be generated is also limited. Following the analysis given in Reference [31] and only looking at the heat conduction for now, the following applies:

$$\begin{aligned} Q_{hot} &= t_h C_h \left(T_{hot} - T_{w,h}\right), \\ Q_{cold} &= t_c C_c \left(T_{cold} - T_{w,c}\right), \end{aligned} \tag{2.9}$$

where Q is the amount of energy that is transfered from or to the reservoirs. The time t_h is the duration of the heat addition step, C_h is the heat conduction constant, T_{hot} is the temperature of the hot reservoir and $T_{w,h}$ is the temperature of the working fluid during the heat addition step (for the cold side h=c). Curzon and Ahlborn indicated that if these relations are applied to the Carnot cycle, a different efficiency characteristic is obtained. Assuming that the internal part of

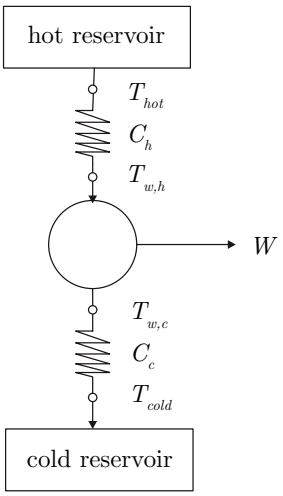

Figure 2.5: diagram of the Curzon Ahlborn heat engine, which is characteristic for external decomposition engines.

the heat engine still operates reversible, the relation between the heat streams is given by the entropy balance:

$$\frac{Q_{hot}}{T_{w,h}} - \frac{Q_{cold}}{T_{w,c}} = 0. \tag{2.10}$$

Since the difference between the working fluid temperatures is lower than the difference between the reservoir temperatures, the maximum efficiency of the conversion process will be lower. The first law of thermodynamics still applies and gives the relation between the work and the heat flows:

$$\begin{aligned} W_{irr} &= Q_{hot}\left(1 - \frac{T_{w,c}}{T_{w,h}}\right), \\ \eta_{irr} &= 1 - \frac{T_{w,c}}{T_{w,h}} < 1 - \frac{T_{cold}}{T_{hot}}. \end{aligned} \tag{2.11}$$

with the irreversible efficiency n_{irr}. The working fluid temperatures $T_{w,h}$ and $T_{w,c}$ will always be closer to each other than the reservoir temperatures, otherwise there will be no energy flowing at all. The usefulness of endoreversible thermodynamics for the study of the H_2O_2 engine comes from the relation between the power that is generated and efficiency of the cycle. Continuing the analysis given in Reference [31], the power P is given by:

$$P = \frac{W}{t_{cycle}}, \tag{2.12}$$

with the duration of the cycle t_{cycle}. A simplification is done here. The time for the expansion and compression steps are neglected such that the total cycle time becomes equal to the time needed for the adding and removing the heat [31]:

$$\begin{aligned} t_{cycle} &= t_h + t_c, \\ t_c &= t_h f_t. \end{aligned} \tag{2.13}$$

Here t_h stands for the time taken for the heat addition process and t_c for the heat removal process, f_t is the fraction that relates the two times together, which makes it easy to see the influence of different time ratios. The same is done for the heat transfer constants of Equation 2.9, using the fraction f_c:

$$C_c = C_h f_c. \tag{2.14}$$

The last relation that is needed relates the generated work to the internal temperature of the working fluid. Since it is assumed that the heat engine uses a reversible process to convert heat into work, one can look at the Carnot process presented earlier for this relation. As shown before, the work of the two adiabatic steps of the Carnot cycle are equal but opposite. The net work output is given by [17]:

$$W_{irr} = nR_{gas} ln\left(\frac{V_2}{V_1}\right)(T_{w,h} - T_{w,c})\,. \tag{2.15}$$

Here n is the amount of moles of working fluid that engine effectively uses, R_{gas} is the universal gas constant and V_2/V_1 is a ratio between two characteristic volumes of the engine (see Carnot cycle). This relation in combination with the relations for heat transfer, energy and entropy gives 5 formulas for 5 unknown variables: $T_{w,h}$, $T_{w,c}$, W, Q_{hot} and Q_{cold}. Solving this set of equations results in an equation for the produced work in terms of the control variables: T_{hot}, T_{cold}, C_{hot}, f_c, f_t and t_{cycle}. For details, see Appendix A.

In Figure 2.6 the main characteristics of the model are plotted. The time dependency of the efficiency is interesting to note. For very large cycle times, the efficiency converges to the Carnot efficiency and for small cycle times the efficiency becomes zero. The time at which the efficiency is zero can be calculated. At cycle times lower than this minimum, the model will become invalid because of the reversing of the heat outflow. The plot also shows a clear maximum of the produced power for a given set of engine parameters. This maximum can be obtained by searching for the condition:

$$\frac{\partial P}{\partial t_{cycle}} = 0. \tag{2.16}$$

With this condition the well known Curzon Ahlborn efficiency is obtained, Equation (2.17), which gives the efficiency at the maximum power point. Similar to the Carnot efficiency, it is only dependent on the temperatures of the reservoirs:

$$\eta_{CA} = 1 - \sqrt{\frac{T_{cold}}{T_{hot}}}. \tag{2.17}$$

The maximum power output P_{max} is found by solving Equation (2.16) for the cycle time and inserting this in the equation for the power output. This shows that the maximum power output for the Curzon Ahlborn model is given by a formula of the form:

$$P_{max} = C_h T_{hot} f\left(\eta_{rev}, f_t, f_c\right). \tag{2.18}$$

The details of the function f are given in Appendix A. Equation 2.18 shows that the maximum power output is proportional to the heat transfer constant C_h. It will be shown that this result also applies to more complicated models. With differentiation the optimal relation between the timing ratio f_t and the heat conductance ratio f_c can be found:

$$\begin{aligned} &\frac{\partial P}{\partial f_t} = 0, \\ &f_t = \frac{1}{\sqrt{f_c}}. \end{aligned} \tag{2.19}$$

which shows the importance of the timing variables of the engine. The Curzon Ahlborn model gives a good indication of how the cycle time influences the engine characteristics. By making the variables of the model non dimensional, the influence of the other parameters can also be observed.

2.3.2 The nondimensionalized model

By applying nondimensionalization more understanding can be obtained about the influence of the parameters other than the cycle time. By rewriting and combining terms found in the formulas for the efficiency and the produced power, it can be shown that the entire model depends on only two independent parameters. For this purpose, the suggested engine parameters are:

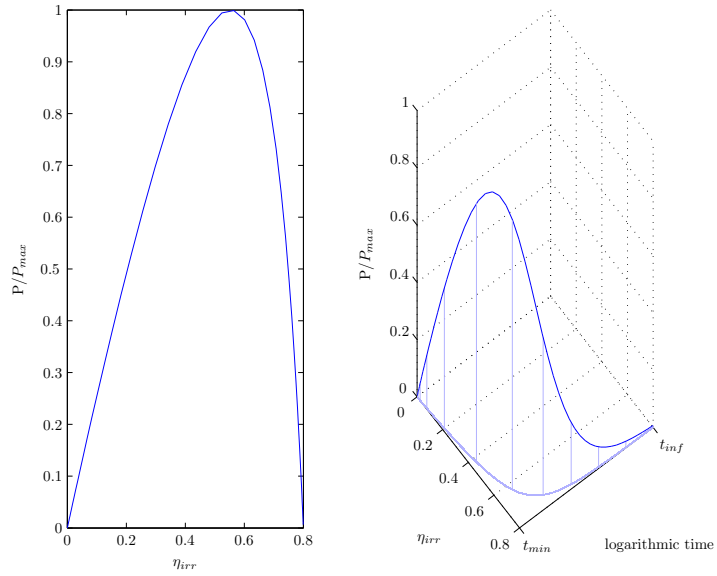

Figure 2.6: A: plot of the normalized power versus the efficiency of heat engine with irreversibility caused by heat resistance, also called the Curzon Ahlborn heat engine. The temperature ratio between the hot and cold reservoirs is taken as 0.8. B: same plot but the time dimension is added.

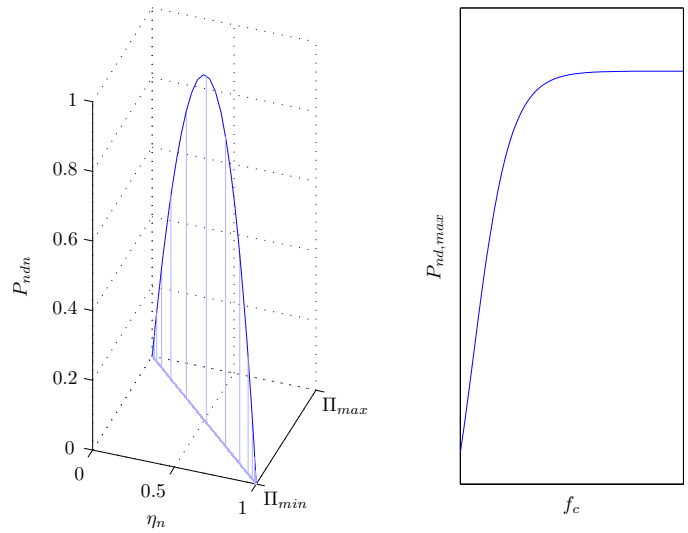

Figure 2.7: A: nondimensional version of the Curzon Ahlborn model, showing the influence of the parameter Π. B: maximum non dimensional power as function of the ratio between the two heat conduction constants, with the Condition (2.16) applied. Note that this quantity is used as normalization factor for the power in plot A.

$$\eta_{rev} = 1 - \frac{T_c}{T_h},$$
$$\alpha = \frac{C_h t_{cycle}}{n R_{gas} ln\left(\frac{V_2}{V_1}\right)}, \tag{2.20}$$
$$\Pi = \frac{\alpha + (f_t + 1)}{\alpha - \frac{f_t+1}{f_t f_c}}.$$

The parameter α includes all the physical quantities of the engine. The suggested non dimensional and normalized performance parameters are:

$$\eta_n = \frac{\eta_{irr}}{\eta_{rev}},$$
$$P_{nd} = \frac{P}{C_h T_h}, \tag{2.21}$$
$$P_{ndn} = \frac{P_{nd}}{P_{nd,max}}.$$

with normalized efficiency η_n and normalized and nondimensionalized power output P_{ndn}. Here the power is nondimensionalized by the inlet heat conductance C_h and the inlet temperature T_h. The reason for this choice became apparent while different performance parameters were tested. Using these new parameters and combining them with the results obtained for the normal Curzon Ahlborn model, results in:

$$\eta_n = \Pi - \frac{\Pi - 1}{\eta_{rev}},$$
$$P_{ndn} = \frac{(\Pi - 1)\left(\Pi\left(\eta_{rev} - 1\right) + 1\right)}{\Pi\left(1 - \sqrt{1 - \eta_{rev}}\right)^2}. \tag{2.22}$$

These two functions are plotted in Figure 2.7 for a Carnot efficiency n_{rev} of 80%. Note that there are no separate physical parameters of the engine in the performance parameters given in Equation (2.22). From the definition of the dimensionless parameter Π it can be seen that C_h has the same influence on the performance as the cycle time. The amount of working fluid n and the chosen volume ratio have an inverse effect. This suggests that if the power of the CA engine is nondimensionalized for the inlet conductance and the inlet temperature, the other engine parameters have no independent influence on the engine performance. Note also that both C_h and T_{hot} could be interpreted as the potential of the engine to generate power, especially if T_{cold} and f_c are

kept constant throughout the analysis as is done here. For the engine design of the FWM, this would mean that after these potentials are chosen, any amount working fluid or cycle time could be chosen. As long as the ratio's between these parameters is constant, the performance is not influenced. This seems a bit abstract, so this hypothesis will be tested with a more complicated engine model in the next section. For the efficiency, it is seen that α has a similar role as t_{cycle} had in the previous section. If α goes to infinity the efficiency of the engine converges to the Carnot efficiency.

If Condition (2.19) for f_t is applied, the maximum nondimensional power $P_{nd,max}$ is a function of η_{rev} and f_c only. The right plot of Figure 2.7 shows that the maximum generated power eventually converges to a limit for a given η_{rev}, showing that at some point the power of the engine does not increase for an increased ratio between the heat conductances.

For the H_2O_2 engine, it is know that there is a certain relation between produced power and efficiency that indicates that there is an optimal engine layout. Also this model shows that a certain α gives this optimal engine configuration. This means that the rate at which energy is added to the engine (here C_{hot}) needs to be in proportion with the amount of working fluid.

2.3.3 Adding a dissipative term

When an engine is scaled down, surface effects become more and more dominant over volume effects. Heat flow is one of these so called surface effects because it is proportional to the effective surface area over which heat transfer occurs. In real engines a large portion of the efficiency loss is due to heat flow to the environment. Heat loss can be modeled in several different ways, depending on the assumptions used for the heat transfer rate and the internal temperatures of the engine. The most common model for heat loss assumes that the working fluid temperature and the produced work are not affected by heat loss, but that it only affects the efficiency of the engine [31, 57, 33]. More detailed models use the energy balance of the working fluid as governing equation and use the working fluid temperature as a control, both with uniform temperature [55] and non uniform temperature of the gas [54]. The models have also been implemented for other thermodynamic cycles than the Carnot cycle [57] and for different heat transfer laws [35]. For the non uniform temperature models finite element methods are used. Other studies have looked at the effects of scaling on a micro heat engine which was already realized [33]. It was shown that the thermal efficiency of a heat engine reduces as the engine size is reduced, due to increasing heat leakage. Also a optimum of the power density can be found for a certain engine size. In the following, an overview of the theory that is given in different references is presented, to show what the consequences of heat leakage are on the H_2O_2 engine.

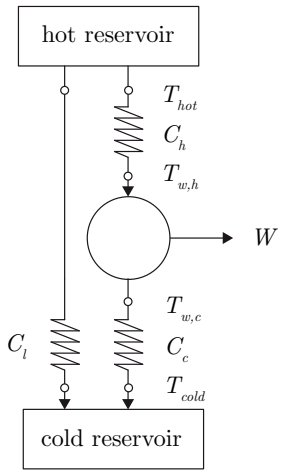

Figure 2.8: diagram of the model that can be used for identifying the heat loss effect on the ideal Carnot cycle.

To keep the model for heat leakage simple it is assumed that the temperature of the gas can be considered uniform. This will be valid if the thermal resistance of the gas and the cylinder wall will be small compared to the thermal resistance of the system to the environment, see Section 3.2. Further it is assumed that the heat transfer coefficient for the heat leakage can be approximated by its average value, where in reality it will vary as the volume of the gas. In Figure 2.8 a diagram is shown of the model that is used.

The diagram shows a direct bypass of energy from the hot to the cold reservoir, with a heat flow constant of C_l. The amount energy Q_{loss} that is lost through this resistance is [34]:

$$Q_{loss} = t_{cycle} C_l \left(T_{hot} - T_{cold}\right) \tag{2.23}$$

For convenience, the heat conductance constant of the loss term is expressed as a ratio of C_h:

$$C_l = C_h f_l \tag{2.24}$$

In this model the operation of the engine itself is not influenced. The same operating temperatures are reached and the same portion of energy that flows through C_h is converted into work. The dissipative term only influences the efficiency [31]:

$$\eta_{i+l} = \frac{Q_{hot} - Q_{cold}}{Q_{hot} + Q_{loss}} \tag{2.25}$$

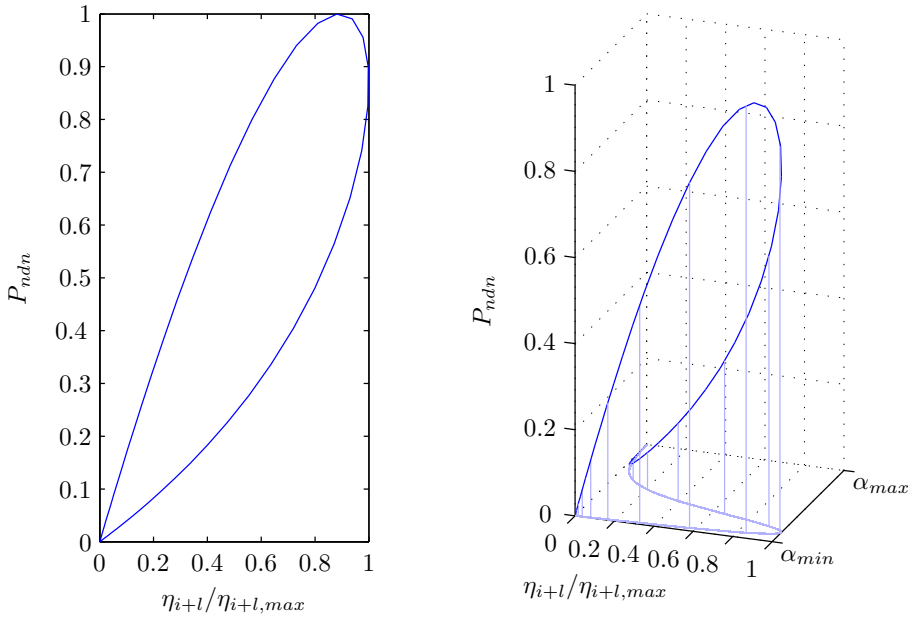

Figure 2.9: The Curzon Ahlborn model with a dissipative term. Left: the normalized and nondimensionalized power versus the normalized efficiency. Right: the third dimension added, of which the left plot is a projection.

Or with the nondimensional parameters used for the standard Curzon Ahlborn model:

$$\eta_{i+l} = \frac{\eta_{irr}}{1 + f_l\,(f_t + 1 + \alpha)\,\eta_{rev}} \tag{2.26}$$

As α goes to infinity, the efficiency will approach zero. Interesting to note is that even though n and the volume ratio do not appear directly in Equation (2.23), their influence on the efficiency is similar in relation with t_{cycle} as it was with standard Curzon Ahlborn model. Equation (2.26) also shows that, just like with the Carnot engine, a new maximum efficiency can be found, named from here on $\eta_{i+l,max}$. In this case it depends on the reservoir temperatures and the ratio's f_t, f_c and f_l and is not as elegant as the Carnot efficiency or the Curzon Ahlborn efficiency, see Appendix A. In Figure 2.9 the new characteristics are plotted for a specific η_{rev}, f_t and f_c. Because the efficiency converges to zero as α approaches infinity, a loop shape characteristic is obtained, which is representative for real engines of various types [58, 12]. Because of this loop shape the maximum power point and the maximum efficiency point are much closer together as they were with the Cuzon Ahlborn model, and come closer to each other when the dissipative term becomes bigger.

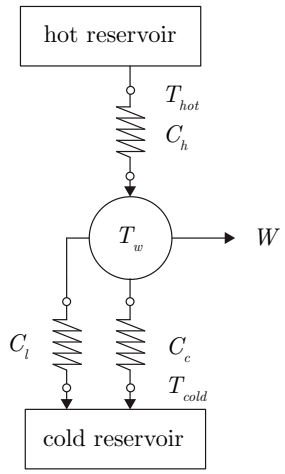

Figure 2.10: diagram of the model using the energy balance to model heat leak.

2.4 Engine model based on energy balance

The assumption that heat leakage does not influence the internal temperatures of the engine might have a big influence on the observations made above. As demonstrated in Section 3.2, the time that a fluid loses a certain amount of heat energy decreases rapidly when the volume decreases. This is because of the increased ratio between surface area and volume. When this time is a significant portion of the cycle time of the engine, there will not only be a large bypass heat flow as was modeled earlier, but also the working temperatures of the engine will be lower. This means that the Carnot efficiency will be lower, which adds up to the reduced efficiency of the bypass heat leak. Also, the internal workings of the engine are still assumed to be reversible. To check if the observations made in the previous section still apply when these assumptions are dropped, a new model will be introduced here. This model is based on the energy balance of the working fluid, and perhaps is a bit more closer to reality as the Curzon Ahlborn model was. This gives also the opportunity to test the statement made in the previous section: if the engine power is nondimensionalized for its potential to generate power, the physical engine parameters have no independent influence anymore on the generated power.

The model

By dropping the reversible and bypass heat leakage assumption, a set of new assumptions need to be formulated. Again, it is assumed that the working fluid inside the cylinder is uniform in temperature and pressure and the heat flow is governed by Fourier's heat conduction law. To determine what the influence is of heat leak on cycle temperatures of the engine, it is assumed that there

is a heat leak during every step of that cycle. This heat leak is also modeled according to Fourier's heat conduction law, the magnitude is determined by the working fluid temperature and the cold reservoir temperature. A diagram of the model is shown in Figure 2.10. By looking at the resulting energy balance of the working fluid, the following applies:

$$\begin{aligned} dU &= dQ - dW, \\ dW &= pdV, \\ dQ &= C_R \left(T_R - T\right) dt, \\ dU &= nc_v dT, \end{aligned} \tag{2.27}$$

where U is the internal energy of the working fluid, Q is the heat flow through the working fluid boundary and W is the pressure work done by the working fluid. C_r and T_r are the heat transfer rate constant and the reservoir temperature. These equations can be rewritten for the working fluid temperature, for which an analytical solution is found.

$$\begin{aligned} \frac{dT}{dt} &= A_3 - \left(A_4 + A_5 \frac{1}{V}\frac{dV}{dt}\right) T, \\ A_3 &= \frac{T_R C_R}{c_v n}, \\ A_4 &= \frac{C_R}{n c_v}, \\ A_5 &= \frac{R_{gas}}{c_v}. \end{aligned} \tag{2.28}$$

The constants T_R and C_R are different for each of the 4 steps of the engine cycle. This differential equation can be solved when a certain relation between time and the volume of the working fluid is assumed. The method of integration constants can be applied when:

$$\begin{aligned} V &= \left(A_1 sin\left(\omega t + \phi\right) + A_2\right)^x, \\ &= V_n^x. \end{aligned} \tag{2.29}$$

Notice the x constant in this function, which is needed for solving the resulting integral (see Appendix A). A more normal assumption for the volume function would be a normal sinus function, but by choosing the constant A_1 and A_2

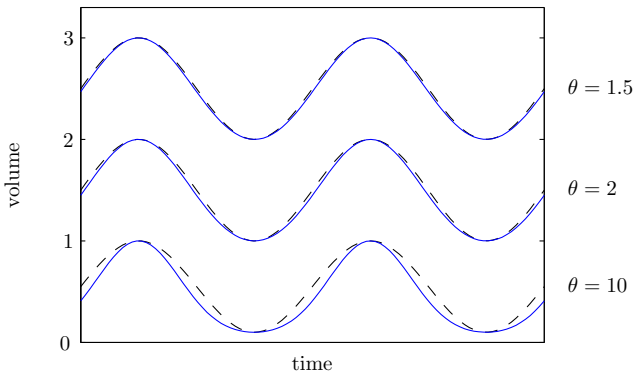

Figure 2.11: Comparison between the assumed function for the volume, Equation (2.29), and a normal sinus function, which is expectable for a normal cylinder based engine. The solid blue lines represent the assumed function for different compression ratios θ, the dotted lines are simple sinus functions fitted to those functions

appropriately V will have the same minimum and maximum as a normal sinus function. As can be seen in Figure 2.11 the maximum deviation from a normal sinus function is neglectable for small compression ratios θ. At the cost of making a little bit strange assumption for the volume function, an analytical solution can be found for the working fluid temperature. The resulting time function for the working fluid temperature has the form of:

$$T = \frac{1}{V_n}\left(A_2\omega^2 A_8 - A_4 A_8 \frac{dV_n}{dt} + \frac{A_7}{e^{A_4 t}}\right) + A_4^2 A_8, \tag{2.30}$$

where the A constants depend on the specific step of the engine. The four steps that can be identified for most engines are the same steps used in the Carnot cycle, see Section 2.2. In Figure 2.12 a timeline of these steps is shown. Just like with the Curzon Ahlborn model, a certain timing between these steps needs to be determined. In this model the time taken by the compression and expansion steps is not neglected, so the complete definition of the timing cannot be captured with one parameter (f_t in the previous section). Again, the start of the heat addition step (t_1) will be constrained to the time at which the volume of the working fluid is minimum. The start of the heat removal step (t_3) will be at maximum volume. To define the duration of each step, two new parameters are used: f_{t1} and f_{t2}. f_{t1} defines the ratio between the time of the heat addition and the expansion step, f_{t2} for the heat removal and compression step.

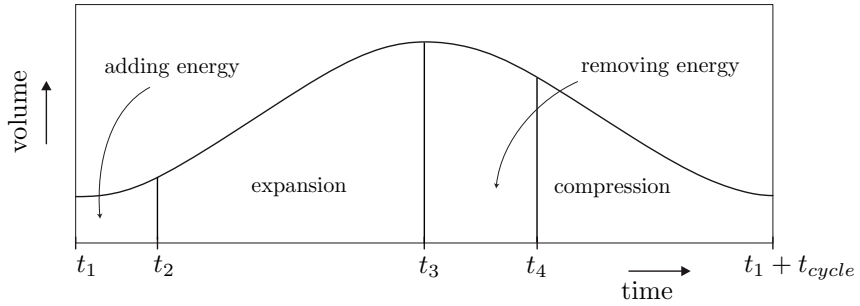

Figure 2.12: Timing of the energy balance based model, accompanied with a typical volume profile

$$f_{t1} = \frac{t_2 - t_1}{0.5 t_{cycle}},$$
$$f_{t2} = \frac{t_4 - t_3}{0.5 t_{cycle}}. \tag{2.31}$$

By using 4 sets of different A constants and the timing as it is defined by Equation (2.31), 4 equations are obtained which can be solved for the characteristic temperatures of the cycle that determine the engine operation at steady state. With this steady state operation the engine performance can be evaluated, for details see Appendix A.

Checking the reversible assumption

First the reversible assumption of Section 2.3 is checked, by chosen the A constants such that no heat leak is taken into account. Since a reversible engine has maximum efficiency it is expected that the modeled engine without the reversible assumption will have a lower maximum efficiency. Notice that in comparison with Curzon Ahlborn model, the only additional engine parameters are A_1, A_2, f_{t1}, f_{t2} and A_5. A_1 and A_2 determine the size and the compression ratio of the working fluid, f_{t1}, f_{t2} determine the timing of the different steps of the engine and A_5 is a fixed quantity determined by the choice of the working fluid type. For some choice of these parameters, the efficiency of this model should converge to the maximum achievable, the Carnot efficiency. By taking the limit values of the heat flows for infinite cycle time, the maximum work output can be determined for a certain set of engine parameters. The resulting maximum efficiency depends only on the chosen reservoir temperatures and the volume ratios that determine the timing of the 4 different steps of the engine cycle:

$$
\begin{aligned}
t_{cycle} &\to \infty, \\
\eta_{irr,max} &= 1 + \frac{Q_{out,lim}}{Q_{in,lim}}, \\
&= 1 - \frac{(1-\eta_{rev})\left(1 + ln\left(\frac{Vn4}{Vn3}\right)\right) - \frac{Vn2}{Vn3}}{(1-\eta_{rev})\frac{Vn4}{Vn1} - \left(1 + ln\left(\frac{Vn2}{Vn1}\right)\right)}.
\end{aligned}
\tag{2.32}
$$

The limiting case is found when the duration of the heat adding step and the duration of the heat removal step are chosen to be nearly zero. The efficiency then converges to:

$$
\begin{aligned}
f_{t1,t2} &\to 0, \\
\eta_{irr,max} &= \frac{2A_1}{A2 + A1}.
\end{aligned}
\tag{2.33}
$$

This will always be lower than one, since $A_1 < A_2$, but can be higher than the Carnot efficiency. This is because no constraints on the direction of the heat flows of the engine are incorporated into the model. Just like was seen with Curzon Ahlborn engine, the heat flow at the cold reservoir reverses from direction and Equation (2.32) will no longer be valid. With some further investigation perhaps one could extract the upper and lower limits on the timing parameters of the engine such that the engine will always produce work, but that is not done here. Note that the A_1 and A_2 constants directly determine the volume of the working fluid of the engine according to Equation (2.29) and thereby the compression ratio. The maximum efficiency $\eta_{irr,max}$ shows that the compression ratio directly determines the maximum obtainable efficiency of the engine. For low compression ratios, $\eta_{irr,max}$ will be lower than the Carnot efficiency and even for infinite cycle times the engine efficiency will not converges to the Carnot efficiency.

In Figure 2.13, a comparison is shown between the Curzon Ahlborn model and the energy balance model. Different timing schemes were used, but the compression ratio, heat conductances and volume of the engine were kept constant. As explained in the previous section, the efficiency using the CA model quickly approaches zero when the cycle time decreases. As seen in the right plot of Figure 2.13, this is not the case for the energy balance model. This is a direct consequence of dropping the reversible assumption. In the Curzon Ahlborn model, the temperatures of the working fluid converged to one single temperature for infinitely small cycle times, which results in zero work output and zero efficiency. Using the energy balance of the working fluid it is seen that for infinitely small cycle times a different behavior is obtained. The working

fluid temperatures of the EB model also converge to a steady value, but each to a different value depending on the physical parameters of the engine. In the CA model, the working fluid temperatures are only a function of how much energy flows into the working fluid. The cycle time decreases, which decreases the total amount of energy and thus the working fluid temperatures converge to one another. In the EB model the working fluid temperatures also depend on the actual compression and expansion. The total amount of energy flow also decreases for smaller cycle times, but still work is produced. Since the working fluid temperature is hardly influenced by the small energy inflow, it can be considered constant during the heat exchange steps. In that case, according to Fourier's law of heat conduction Equation (2.23), the heat flow and hence the produced amount of work is proportional to the cycle time.

So by dropping the reversible inner workings assumption, a new upper limit on the efficiency is obtained. Also a different temperature characteristic was found for small cycle times. But what about the produced power of the engine? First it must be said that no analytical expression for the produced power is found, because the heat flows in the engine can only be calculated when the cycle time is infinite, see Appendix A for details. This means that it is hard to obtain exact insight in what way the Curzon Ahlborn model differs from this model in terms of produced power. But by doing numerical simulations of the model, its characteristic can be compared with that of the Curzon Ahlborn model. In Figure 2.14 a plot is made of the power output characteristic as function of the cycle time for both the Curzon Ahlborn model and the energy balance model. Various configurations of the timing parameters are used and compared with the Curzon Ahlborn model, but the other parameters are kept constant just like in Figure 2.13. Again, the main difference between the CA en EB model is seen at small cycle times. Contrary to the CA model, there is still a power output for small cycles times with the EB model. As seen in Figure 2.14, the power output converges to a steady value, which can be understood from the fact that the work is proportional to the cycle time and the definition of power, Equation (2.12).

In general, it is seen that somewhat similar characteristics are found as were found with the Curzon Ahlborn model. For infinite cycle times the efficiency converges to its maximum and the maximum produced power is somewhere between minimum and maximum efficiency. The big difference is that the EB model does not have zero power output at infinity small cycle times. Also, the Curzon Ahlborn model always produces more power and has better maximum efficiency than the model of this section.

Checking the heat loss assumption

By changing the A constants of Equation (2.30), heat loss can be included in this model. As described earlier, heat loss directly lowers the efficiency because less of the available energy is converted into work, but also because it lowers

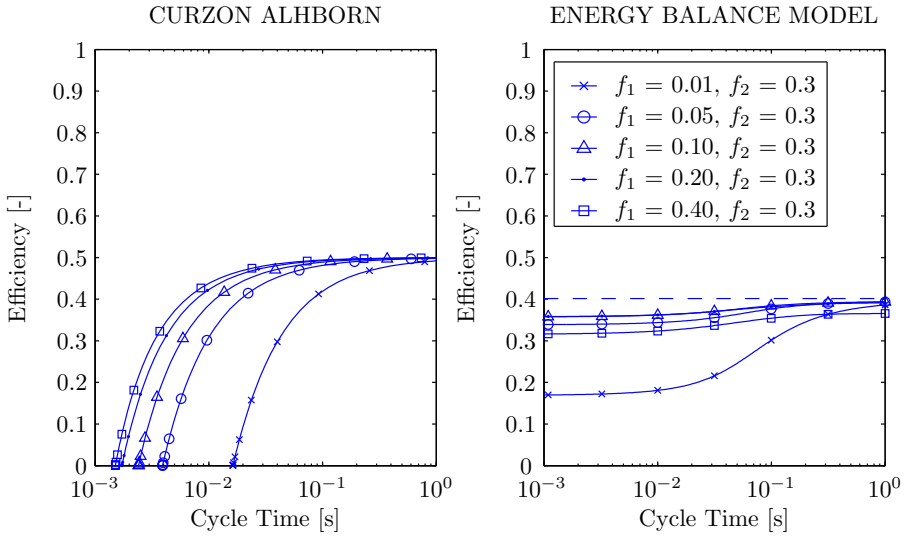

Figure 2.13: Comparison of the Curzon Ahlborn model (left) and energy balance model (right), showing the cycle efficiency versus cycle time. Different timing settings are used as shown in the legend. The maximum efficiency for the energy balance model according to Equation (2.33) is shown by the dashed line.

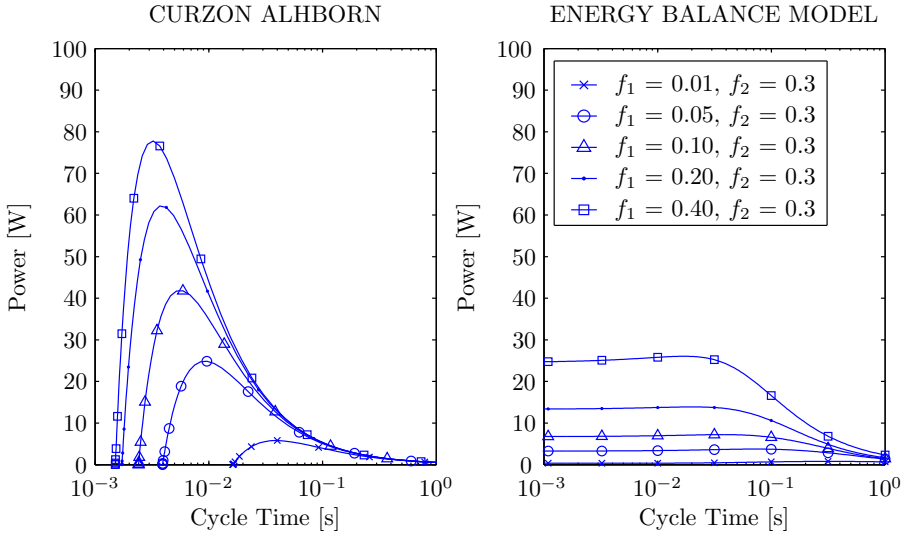

Figure 2.14: Comparison of the Curzon Ahlborn model (left) and energy balance model (right), showing the cycle power output versus cycle time. Different timing settings are used as shown in the legend.

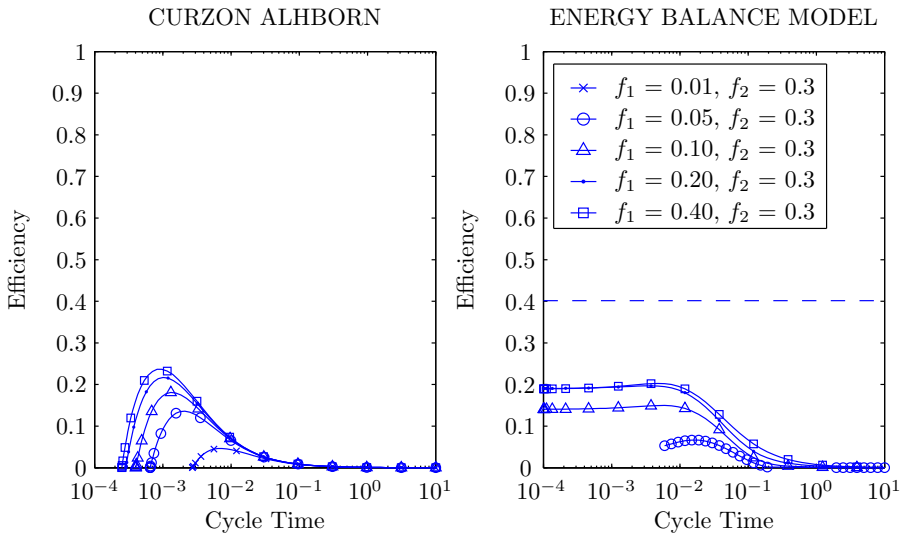

Figure 2.15: Left: Curzon Ahlborn model with shunt heat leak for various f_l values. Right: energy balance model with same engine parameters used for the Curzon Ahlborn model

the operation temperatures of the engine which lowers the Carnot efficiency. To see the influence of heat loss, the same engine parameters are used as was done before but now with a heat loss term added. Using the definition of the heat loss term in Equation (2.24), a f_l of 0.1 is used. In Figure 2.15 on the left the efficiency of the Curzon Ahlborn model is shown. On the right the energy balance model of this chapter is shown with the same axis span. For a f_l of 0.1 it is seen that for both the CA and the EB model, the efficiency approaches zero for large cycle times. As might be expected, the overall efficiency over the whole range is much lower in comparison with Figure 2.13. Another noteworthy observation from Figure 2.15 is the difference in cycle time when the heat loss term becomes dominant for the different models. The EB model is more efficient up to larger cycles times as the CA model.

Checking the hypothesis

In Section 2.3 the following statement was made:

> *If the engine power is nondimensionalized by its potential to generate power, the other dimensional engine parameters have no independent influence on it anymore.*

The term engine is defined here as a device that uses an external heat source, conduction and a cylinder to generate positive power. This is a tricky statement since the term 'potential to generate power' is not defined in a general way. But

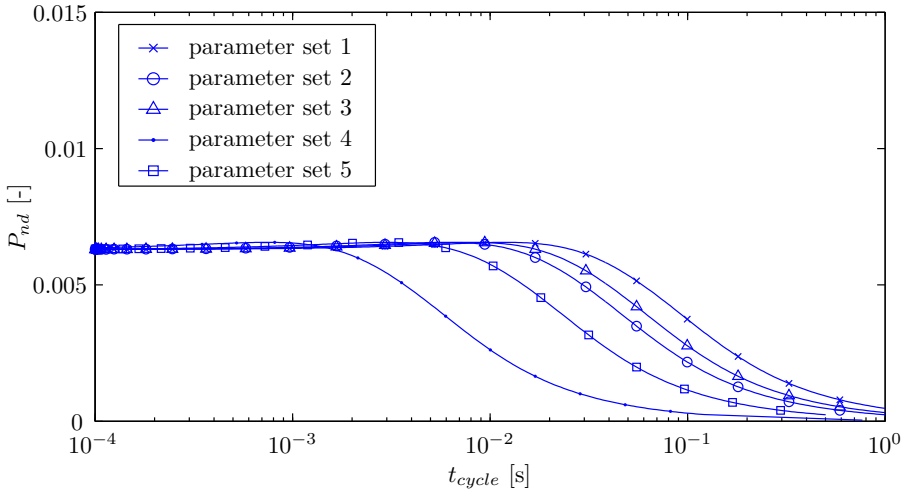

Figure 2.16: Plot of the nondimensional power P_{nd}, defined by Equation (2.34), plotted versus the engine cycle time for different parameter sets. The values used for these sets are given in Table 2.1.

for the EB model, which closely resembles the CA model, the potential is defined as $C_h T_h$. Note that in theory the cold temperature T_c also determines the potential, but in reality the cold temperature will always be equal to the ambient temperature and is considered as a constant here. Dimensional parameters are defined here as engine parameters that have a dimensional unit, for instance the volume of the working fluid V [m] or C_h [W/K]. To see if the statement is true for the EB model, a similar nondimensionalization is applied as was done in the previous section:

$$P_{nd} = \frac{P}{C_h T_h}. \tag{2.34}$$

The dimensional parameters of the EB model are the amount of working fluid n, a characteristic volume of the working fluid V_1, the heat conductance C_h, working fluid heat capacity c_v, heat reservoir T_{hot} and cycle time t_{cycle}. The non dimensional power can be plotted against various engine parameters sets, as is done in Figure 2.16. The parameter sets that are used are given in Table 2.1. Again, the cycle time functions as the plotting variable just like was done in the previous figures. Also similar to the previous section, the ratio's f_{t1}, f_{t2}, f_c, θ and γ are kept constant. It is seen that the maximum non dimensional power is independent of the parameter set used, as is predicted by the statement. The maximum power point does occur at different cycle times, because the right balance between the parameters shifts for every different parameter set.

Parameter	Set 1	Set 2	Set 3	Set 4	Set 5	Unit
T_{hot}	423	473	523	1273	373	K
V_1	0.001	0.002	0.001	0.001	0.002	m^3
n	0.002	0.001	0.002	0.005	0.001	mole
C_h	10	20	30	40	20	W/K
c_v	20.76	41.52	41.52	20.76	20.76	J/mole/K

Table 2.1: Parameters used in Figure 2.16.

So at least for the EB model, the statement is true. This makes it easier to predict what exactly determines the maximum power output of these types of engines. The most important parameter is the potential to generate power $C_h T_h$, which directly determines the absolute maximum of the power. The other parameters only need to be set up such that they are in balance with each other. This balance was found for the CA model in the form of Π, but for the EB model this is not know. To find the maximum power of a certain set of engine parameters, the procedure shown in Figure 2.17 is proposed. First a certain set of engine parameters is chosen, based on constrains that apply in the situation of the FWM. Then the steady state is found using the analytical part of the EB model. The performance is evaluated using numerical integration. These steps are repeated for every possible cycle time until the maximum power is found.

In other words, the procedure of Figure 2.17 searches for an optimal value for Π, even though it is not entirely sure how Π is defined for the EB model. The found performance specifications are not only valid for the found set of parameters, but is also the best performance that the engine will produce for a given potential.

This procedure is applied in Section 2.5, to find the scaling behavior of the EB model. In Chapter 4 a model much like the EB model is used to predict the power output of Concept 3, one of the candidates for the FWM engine discussed in the report. A procedure much like the one shown in Figure 2.17 is used to find the power characteristics of that more complicated model.

For the H_2O_2 engine we learn that the Curzon Ahlborn model is a good indication of what characteristics can be expected for certain engine parameters, but only in a qualitative way. It helps to understand what effects are important for the power and efficiency of a basic hot air engine. It is seen that the rate at which energy can be added to the cylinder determines not only the maximum produced power but also the maximum efficiency that is obtainable. It is also observed that the trade off between produced power and efficiency becomes less significant if a loss term is added to the model because the optimum point for both criteria come closer together if the loss term is increased. Also the importance of timing is illustrated, since its influence on the performance is just as important as the rest of the engine parameters. The energy balance tests the assumptions made with Curzon Ahlborn model, and it was observed that the

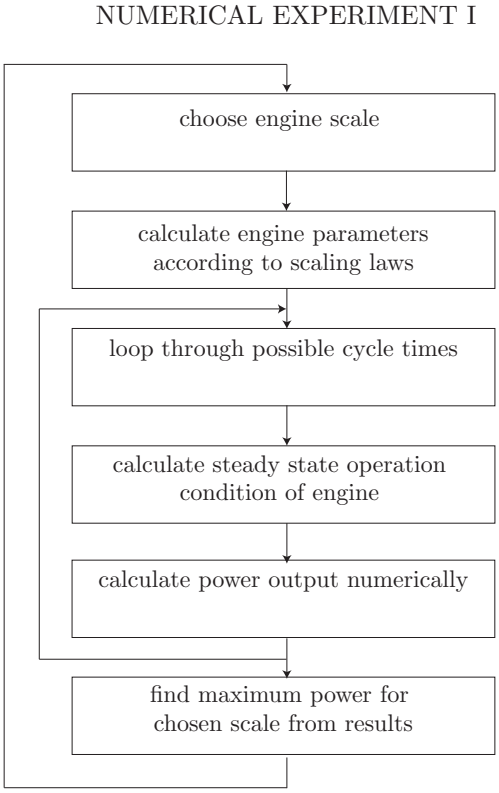

Figure 2.17: Layout of numerical experiment 1

same characteristics can be observed. The importance of the compression ratio was shown via the energy balance.

2.5 Scaling

The scaling behavior of the power output of a certain engine type is one of the interests of this thesis. The Curzon Ahlborn model showed that for an engine that uses heat conduction to transfer energy, the power is proportional to the heat conduction constant C_h. To investigate how the engine model from the previous section behaves during scaling down the the geometric dimensions, the following numerical experiment is proposed. For a certain reservoir temperature difference, an engine configuration is chosen that has a reasonable performance output. This means that it is close to the maximum power - efficiency point as is seen in Figure 2.14. Then for every point of interest, all geometric parameters of the engine are scaled according to their physical scaling law, as was discussed in Section 1.3. To obtain the maximum power output for this set of engine parameters, the cycle time of the engine is varied until the maximum power point is found. This way an indication is obtained of the scaling behavior of the power output of the engine, assuming that the cycle time is unconstrained.

This method is chosen because of the findings of the non dimensional Curzon Ahlborn model. The parameter Π shows that a decrease of one parameter can be compensated with a increase of another. For instance, decreasing the heat transfer rate with 50% can be compensated by increasing the the cycle time with 50%. In the EB model, the parameters that are sensitive for scaling are: heat conduction constants C_h, C_c, the loss factor C_l, the initial working fluid volume V, the amount of working fluid n and the cycle time t_{cycle}. They are scaled with scaling factor S according to:

$$\begin{aligned} C_{h,c,l} &\propto S, \\ V &\propto S^3, \\ n &\propto S^3. \end{aligned} \tag{2.35}$$

The optimal cycle time is found using the described method, shown in Figure 2.17. The timing parameters of the engine are kept constant during the scaling. It was observed that the efficiency at the maximum power point does not change if the timing parameters are kept constant. This gives reason to assume that the optimal configuration of the timing variables is independent of the geometric scale of the engine, as long as the energy inflow and outflow rates of the engine have the same scaling behavior. Two different boundary conditions

are used for investigating the scaling of the energy balance model, one with a hot reservoir temperature of 150°C and one with 900°C. The parameters used during the simulations are given in Table 2.2.

C. Cheng et al. [14] did measurements with a Stirling type engine, which also uses conduction to transfer energy into the working fluid. For the numerical experiment, the parameters given by Reference [14] are used as a starting point. The parameters of the energy balance model are chosen such that the power output of the model is approximately the same as the measurement results of [14]. An exact fit cannot be made because the Stirling also uses a regenerator, which is not modeled in the energy balance model.

In Figure 2.18 the results are shown for both the 900°C and the 150°C case. At $S = 1$, the measurements of Reference [14] to which the EB model is fitted are shown. It is seen that the power output is proportional to the scaling factor, just like it was found with the Curzon Ahlborn model of Section 2.3. As shown in Table 2.2, the working fluid volume at $S = 1$ is 24cm^3. For the H_2O_2 engine the expected volume is below 1cm^3, which corresponds to a $S \approx 0.05$ and a power output in the order of milliwatts.

In the left part of Figure 2.18, it is seen that the optimal cycle time for a given scale is proportional to S^2. This confirms that the energy balance model has the same characteristics regarding their parameters C and n, and the cycle time. The scaling of the optimal cycle time can be predicted with the parameter Π of Section 2.3. Using the definition of Π and the scaling of the parameters given by Equation (2.35), the optimal cycle time dependence of S^2 is also found.

The next step is to add a more complex model for the loss terms of the engine. As it is shown in Section 3.2, the heat loss characteristic is not fully captured by heat conduction. Also radiation and heat convection have influence at these scales. Also, different methods of adding energy to the expansion unit need to be investigated, as was pointed out in Section 2.1. This is done in the next chapter.

2.6 Work Generation by Momentum

As discussed in Section 2.1, the method of generation work used in Concept 2 is fundamentally different from the other concepts. In this section a model of a Tesla turbine will be discussed. Similar to the previous approach of analyzing thermodynamics, first a simple 1 dimensional model will be discussed. It will help understand the basic characteristics of Concept 2. It will also show that similar characteristics can be found as were found with the Curzon Ahlborn model.

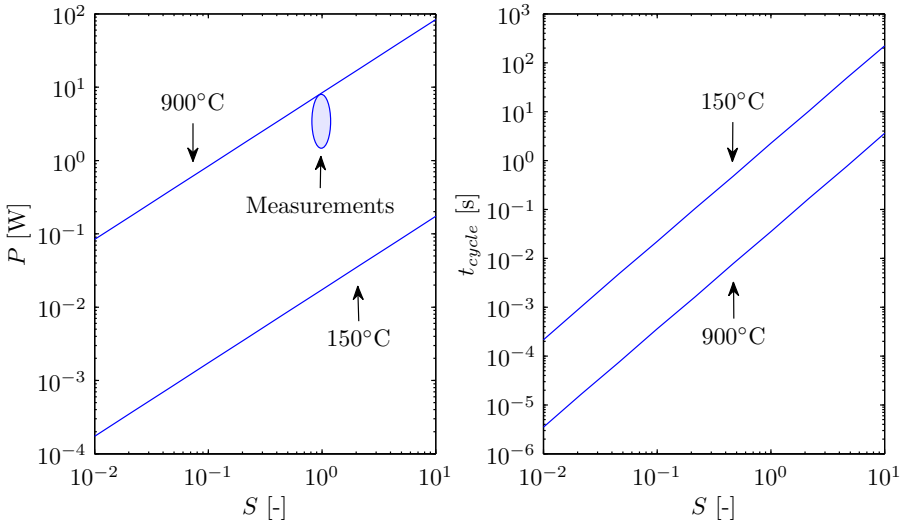

Figure 2.18: Results of numerical experiment 1. Left: the scaling of the output power of the EB model. The measurements of Reference [14] are also shown. Right: the optimal cycle time that is found for different engine scales.

Parameter	Value when $S_g = 1$	
Cylinder radius r	$1 \cdot 10^{-2}$	[m]
Cylinder height h	$0.5 \cdot 10^{-2}$	[m]
Heat conduction area A	$2\pi rw = \pi \cdot 10^{-4}$	[m^2]
Thermal conductivity k	160	[W/(m·K)]
Material thickness t	$1 \cdot 10^{-3}$	[m]
Heat conductance constant C_{hot}	$kA/t = 16\pi$	[W/K]
Minimum working fluid volume V_1	24.6	[mL]
Maximum working fluid volume V_3	$V_1\theta = 5$	[mL]

Constants	Value	
Timing ratio f_{t1}	0.3	
Timing ratio f_{t2}	0.4	
Conductance ratio f_c	5	
Conductance ratio f_l	0.1	
Heat capacity c_v	20.30	[J/(mol·K]
Compression ratio θ	5	
Hot temperature T_{hot}	473	[K]
Cold temperature T_{cold}	293	[K]

Table 2.2: Rate constant k for different types of catalyst material, all normalized for the mass of the material.

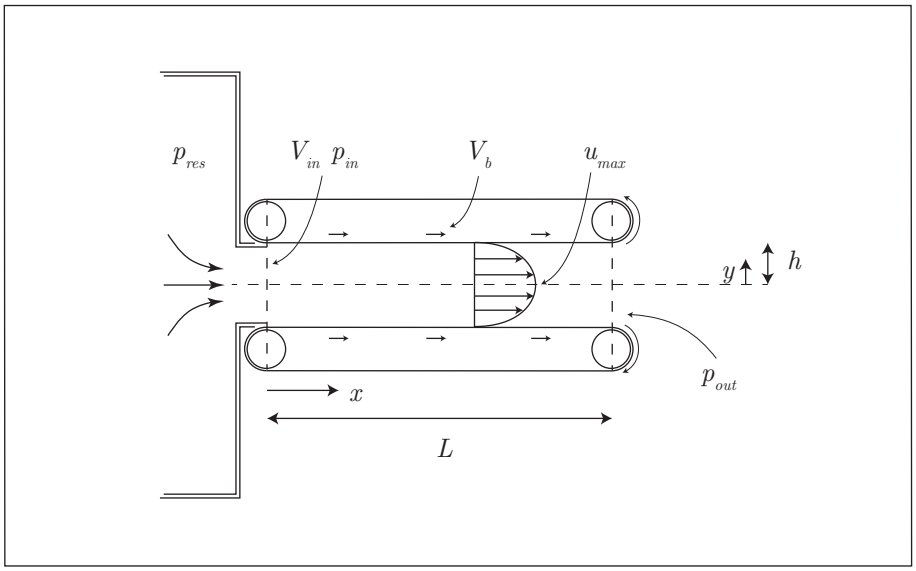

Figure 2.19: Viscous force work generation

One Dimensional Model

In literature several models can be found for modeling the flow between two closely spaced disks. A good starting point is the relatively simple model shown in Figure 2.19, which is discussed by R.T. Deam et al. [43]. Here this model will be discussed and extended to observe the characteristics that are also found in the Curzon Ahlborn model. In the model there is a pressure reservoir and two belts that are moved by the fluid passing along them. The belts are moving such that the sides have a velocity V_b. In the model it is assumed that the fluid flow is incompressible, such that the fluid velocity relative to the belt u is constant over the length L [68]:

$$\frac{\partial u}{\partial x} = 0. \tag{2.36}$$

This means that the gradient of the pressure p is constant over length L and is given by:

$$\frac{dp}{dx} = \frac{p_{out} - p_{in}}{L}, \tag{2.37}$$

where p_{in} is the entrance pressure, p_{out} the pressure at the exit. It is assumed that the flow between the belts is laminar and reaches a fully developed state before it comes into contact with the belts, such that entrance effects can be neglected. In that case, the velocity profile $u(y)$ is given by the Poiseuille parabola

[68], also shown in Figure 2.19. The entrance pressure is given by the energy balance of the flow. Assuming that the fluid is at rest in the reservoir, the absolute velocity of the fluid at the entrance V_{in} is given by:

$$\begin{aligned} p_{in} &= p_{res} - \frac{1}{2}\rho V_{in}^2, \\ V_{in} &= \sqrt{\frac{2}{\rho}\left(p_{res} - p_{in}\right)}. \end{aligned} \tag{2.38}$$

Note that the entrance velocity is an average over height h. The average of relative velocity of the flow between the belts is given by [68]:

$$\begin{aligned} u_{avg} &= \frac{1}{A}\int u dA = \frac{2}{3}u_{max}, \\ V_{in} &= u_{avg} + V_b, \end{aligned} \tag{2.39}$$

here u_{max} is the peak of the velocity, as defined in Figure 2.19. The last relation needed is given by the pressure gradient due to the viscus forces in the fluid [68]:

$$-\frac{dp}{dx} = \frac{2\mu}{h^2}u_{max}. \tag{2.40}$$

The previous equations can be solved for V_{in}:

$$\begin{aligned} V_{in} &= \frac{\sqrt{b - 4ac} - b}{2a}, \\ a &= \frac{1}{2}\rho, \\ b &= \frac{3\mu L}{h^2}, \\ c &= p_{out} - p_{res} - \frac{3\mu L}{h^2}V_b. \end{aligned} \tag{2.41}$$

To calculate the power output of this system, the shear stress of the viscus forces on one belt is needed:

$$\tau = \frac{2\mu}{h}u_{max} = \frac{3\mu}{h}\left(V_{in} - V_b\right). \tag{2.42}$$

The power output P_{out} is given by total forces on both belts times the velocity:

$$P_{out} = 2\tau L w V_b = \frac{6\mu L w}{h} V_b \left(V_{in} - V_b\right), \tag{2.43}$$

where w is the width of one belt. This last formula shows a familiar characteristic of the system. If the belt velocity is zero, the power output will be zero. Similar, if the belt velocity is equal to the average fluid velocity, the power output will also be zero. This characteristic was also found with the Curzon Ahlborn engine, where the parameter of interest was the cycle time of the engine. The similarity between the belt velocity and the cycle time is not true for the efficiency, as will be shown next.

To obtain the efficiency of the belt system, the maximum energy that this system could extract from the pressurized fluid needs to be defined. This energy is given by work done if the gas would be expended adiabatically to ambient pressure. For a unit volume of pressurized fluid, this work would equal:

$$\begin{aligned} &p_{res} V_1^{\gamma} = p_{out} V_2^{\gamma}, \\ &V_2 = V_1 \left(\frac{p_{res}}{p_{out}}\right)^{\frac{1}{\gamma}}, \\ &W_{adi} = p_{res} V_1 \frac{V_2^{1-\gamma} - V_1^{1-\gamma}}{1-\gamma} = \frac{p_{res}}{1-\gamma} \left(\left(\frac{p_{res}}{p_{out}}\right)^{\frac{1-\gamma}{\gamma}} - 1 \right) \end{aligned} \tag{2.44}$$

The power that could have been generated with this work is determined by the total volume flow of the fluid between the belts:

$$\begin{aligned} &\frac{dVol}{dt} = 2hwV_{in}, \\ &P_{adi} = W_{adi} 2hwV_{in}. \end{aligned} \tag{2.45}$$

This allows an efficiency to be defined for this system, given by the energy that is extracted from the reservoir divided by the energy that could have been extracted:

$$\eta = \frac{P_{out}}{P_{adi}}. \tag{2.46}$$

Assume that the belt velocity is zero, such that all the pressurized fluid can escape without doing any work. In this case the efficiency will be zero because no power is extracted from the fluid. This is also true for the other extreme, where the belt velocity equals the average fluid speed. Combining this with the characteristic of the supplied power, a power versus efficiency plot is obtained

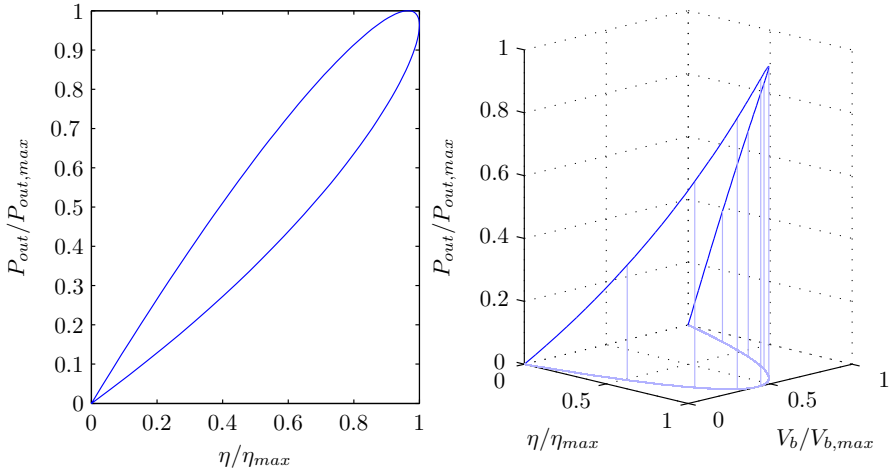

Figure 2.20: Left: typical normalized power versus normalized efficiency of the belt system. Right: same as left but with the normalized belt velocity added.

that has the same loop shape as was found with Curzon Ahlborn model where a loss term was included, see Figure 2.20.

Results of One Dimensional Model

For the plots in Figure 2.20 a pressure difference of 1000 Pa was used, with a length of the belts of 1 meter and a gap height of 2 mm. This results in a maximum power output of 8 mW and an efficiency of 14 %. Unfortunately no non dimensional parameter was found for this system like it was done with the Curzon Ahlborn engine. The three paramters of interest in this model are the reservoir pressure p_{res}, belt lenght L and the gap height h. To see their influence on the perfomance of this system, a procedure is used similar to the one used to investigate the scaling behaviour of the energy balance model in Section 2.5. For all three parameters, a range of interest is chosen. For every point in that range, a plot similar to Figure 2.20 is construced and the maximum power $P_{out,max}$ and η_{max} are plotted. The results of this procedure are shown in Figure 2.21. Note that the given power output on the left side of the figure does not necesarly have to match the with the efficiency given in the right plot. This can be understood from the loop shape of the power-efficiency curve, where the maximum power point is not the same as the maximum efficiency point. See for example Figure 2.20, where the efficiency at the maximum power output is lower than the maximum efficiency.

As can be seen in the top two plots of Figure 2.20, the optimal pressure difference is a trade off between efficiency and power output. For the belt length, both the efficiency and the power output increase for increasing L. For the gap height, an

optimum can be found in the power output. This optimum is also close to the maximum efficiency which is highest for small gap heights. As can be seen in the efficiency plots, the maximum efficiency seems to converge to a value between 40% and 50% for all cases. A similiar limit was also found in Reference [43], with an absolute limit of 38%. The difference comes from a different definition of the efficiency of this system. Measured values of Tesla turbines powered by compressed air show a maximum efficiency up to 44% [43].

Conclusions for Concept 2

Now that the characteristic of these types of systems is known, it can be applied to some measured data found in literature. As mentioned in Section 1.4, a research team at the university of Berkeley did multiple tests with small scale Tesla systems [56]. Multiple rotors and housing configurations where used, to see how the performance is influenced by different parameters. With a pressure difference in the order of 10^4 Pa, power outputs in the order of milliwatts were found. The maximum efficiency that was measured was 40%, but at the maximum power outputs the efficiency is around 10 %. The scale of the tested system match exactly the scale needed for the FWM in its current size (1 cm rotor diameter). Also, the efficiency appears to be appropiated in terms of needed flight time of the FWM. The output power on the other hand is much to low. To increase the power, the pressure difference over the turbine needs to be increased significantly.

It can be assumed that the configurations tested by V.G. Krishnan et al. [56], were not far from the optimal Tesla turbine design. From the one dimensional model and from the observations of Reference [56], it can be concluded that the efficiency of the Tesla turbine drops as the pressure is increased. Since the pressure difference needs to be increased significantly to meet the power requirements of the FWM, it can be concluded that Concept 2 is not suitable for this project.

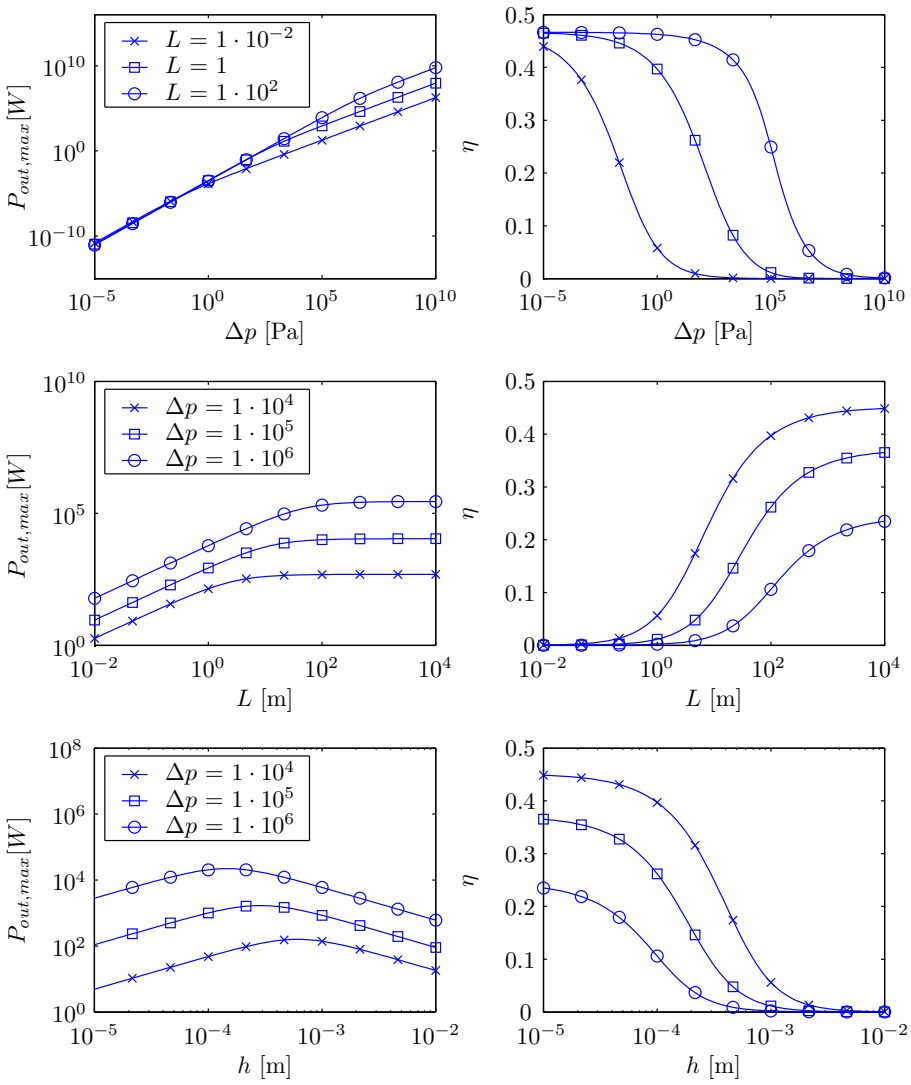

Figure 2.21: Power and efficiency plots as function of the pressure difference (top), the belt length (middle) and height of the duct (bottom).

Chapter 3

Energy Flows

3.1 Introduction

Chapter 2 showed that engine performance is directly related to the characteristics of the energy flows that go through the engine. In this chapter a more detailed analysis is given of the different energy flows found in Concepts 1 and 3. In Section 3.2 the heat flow across the engine boundary is studied using a FEM model. It will given an indication of the magnitude of the influence that heat leakage has on the FWM engine.

The source of energy for both concepts, the catalytic decomposition of H_2O_2, is described in Section 3.3. First a general introduction is given about the physics involving a catalytic decomposition. Then a model is presented that is used to predict peak pressures and fuel reaction times. This model is tested against measured data given by Meskers [60].

In Concept 1, energy leaves the system via the exhaust ports. In Section 3.4 this fluid flow is approximated by looking at the momentum balance of a fluid flowing through a round nozzle. The relation between cylinder pressure and mass flow is used to make an estimated of the rate of energy exchange between the engine and the environment. The nozzle model is a first order approximation of the real situation found at the exhaust port of Concept 1, but it will be useful for performance predictions. The models presented in this chapter are used in Chapter 4 to estimate the performance of Concept 1 and 3.

3.2 Heat Transfer

As was indicated in the previous chapters, heat leakage has a significant effect on the performance characteristics of an engine. Whatever the design of the H_2O_2

engine will look like, it will also suffer form this effect. To see in what order the heat transfer coefficients and time constants of heat leakage are for small engines, a finite element model is set up. Since the shape of the H_2O_2 engine is not yet determined, a simple cylinder shape is assumed, see Figure 3.1. It is assumed the found characteristics with the cylinder shape will be representative for other possible shapes of the engine. The cylinder is filled with a gas that has a certain elevated temperature and heat energy flows through the cylinder walls via conduction. At the outer surface of the cylinder the heat energy is transfered by fluid flow convection and radiation [61]. The rate at which heat is transfered via conduction is given by the Fourier law:

$$\frac{dQ_{cond}}{dt} = \frac{kA}{L}\Delta T, \tag{3.1}$$

with thermal conductivity k, surface area A and characteristic length scale L. For convection the rate is given by:

$$\frac{dQ_{conv}}{dt} = h_{conv}A\Delta T, \tag{3.2}$$

with the convective heat transfer constant h_{conv}, which depends on the type of flow. For radiation the rate is [61]:

$$\begin{aligned} \frac{dQ_{rad}}{dt} &= \epsilon A\sigma\left(T_1^4 - T_2^4\right), \\ &\approx \epsilon A\sigma 4T_{avg}^3\Delta T, \end{aligned} \tag{3.3}$$

where ϵ is the emittance of the surface, σ the Stefan-Boltzmann constant, T_1 the temperature of the surface of interest, T_2 is the surrounding surface temperature and T_{avg} the average temperature. The linearization shows that in approximation, the heat radiation is proportional to the surface temperature of cylinder with a exponent of 4, because the temperature of the surrounds is fixed. The constant σ is small ($5.67{\cdot}10^{-8}$ W/m^{2}K^4), which means that radiation will only play a role if the temperature of the cylinder surface is high.

The thermal conductivity k is a material property and will be considered constant throughout the temperature range of interest. The convective heat transfer constant h, depends on the type of flow around the system. The heat from the cylinder flows into the surrounding air, which elevates in temperature. Since the specific density of hot air is lower than that of cold air, a fluid flow is taking place around the heated cylinder. This phenomena is called natural convection. To indicate if the convection around the cylinder is either turbulent or laminar, one can look at the Grashof number [61]. It is a dimensionless group that gives

an indication how big the buoyancy forces caused by the heating of the air are in relation to the viscous forces caused by the fluid flow:

$$Gr = \frac{\beta \Delta T g x^3}{\nu^2}, \tag{3.4}$$

where β is the volumetric expansion coefficient of air, ΔT is the temperature difference, x is the distance between the start of the flow (for example the bottom of the cylinder) and ν is the viscosity coefficient of the fluid [61]. If a Grashof number below 10^9 is found, it means that the buoyancy forces are small compared to viscous forces and the fluid flow around the cylinder is laminar. By considering the standard properties of air, the fact that the H_2O_2 will have dimensions in the order of centimeters and a temperature difference in the order of melting points of metals, it is seen that the convection around the engine can be considered laminar, which is typical for small scale systems [46].

Another interesting dimensionless group often used in heat transfer analysis is the Biot number. It is defined as the ratio between the internal heat flow resistance and the external resistance. In the case of the cylinder, the internal heat flow resistance is the resistance found in the gas and the cylinder wall, the external resistance is characterized by the convection and radiation. It gives insight in the question if it is beneficial to add extra insulation material to the engine to help reduce heat leakage. If the FEM analysis indicates that the external heat flow resistance at the cylinder surface is much larger than the internal resistance, adding some extra material to the cylinder is probably not going to have much influence.

For normal sized systems a lot of research is done on heat transfer. For convection, one usually finds a relation between the temperature and the heat transfer constant based on empirical observations. A. F. Mills [61] proposes two models for modeling convective heat transfer, one based on a heated vertical wall and the other on a cylinder shaped as seen in Figure 3.1. Especially convection characteristics are sensitive to scaling [61], which makes the empirical based formulas less accurate. Another complication is that we are not only interested in convection, but also conduction, radiation and the transient behavior of the system. That is why a FEM model is used in the software package Comsol Multiphysics®, that conveniently combines all these aspects. In the 2D model seen in Figure 3.1 a cross section of the cylinder is modeled. In the third dimension, the cylinder has a height h which is two times as large as the cylinder radius r.

The cylinder is placed in air that can move freely but is subjected to gravity. Because of the expected low Grashof numbers, the flow around the cylinder is restricted to laminar flow. In order to model the heat radiation, the cylinder is surrounded by walls, which are not shown in Figure 3.1 for illustration purposes. The size of the box surrounding the cylinder is dimensioned ten times as large as the outer diameter of the cylinder.

The objective of this simulation is to obtain a definition for the heat transfer that can be easily implemented in the simulations done in the previous section. To do this an overall heat transfer coefficient U [W/K] is defined, just like it was used in the previous section (C_r from Equation (2.27)):

$$U = \frac{dQ/dt}{\Delta T^n}, \tag{3.5}$$

where Q represents the energy flowing out of the cylinder due to heat loss. This is a linearization of the real heat transfer characteristics, described by Equations (3.1) to (3.3). Since there is no expansion work done in this case, Q is equal to the rate of change in internal energy of the cylinder, so:

$$U = \frac{1}{\Delta T^n}\frac{dE}{dT}\frac{dT}{dt} = \frac{\rho V c}{\Delta T^n}\frac{dT}{dt}, \tag{3.6}$$

where ρ is average specific density of the cylinder, V the volume, c the heat capacity and T the average temperature. The exponent n is determined by which heat transfer mode is dominant. When conduction is the main heat transfer mode, n will be 1. For heat transfer via radiation, which is proportional to the quadruple of the temperature difference, n will be 4. For convection, also a temperature dependence of h_{conv} is expected. For this combined heat transfer problem a n between 1 and 4 can be expected. At small scale heat conduction is dominant so n will be close to 1 in this situation. The FEM model can be used to fit the data to Equation (3.6) to find a appropriate n.

The scaling behavior of this problem can be estimated from the governing equations of the different heat transfer modes. The definitions of the transfer rates show that conduction will scale with a characteristic length of the problem, convection and radiation both scale with a characteristic surface. With the prediction of a low Biot number, it is likely that the overall heat transfer rate U will also scale with a characteristic surface.

To get a good estimate of the heat loss coefficient and see the effect of scaling, the model is scaled such that the outer radius of the cylinder has range between 10^{-3} and 10^{-1} meters. The overall heat transfer coefficient for the different sizes are plotted in Figure 3.2. As the cylinder radius decrease, U decreases in the double logarithmic plot with a slope of approximately 1.5. This is one of the reasons why small engines have trouble with heat loss effects and have a bad performance track record [46], since most engines have a power output that is proportional to its volume flow. If the power output scales with volume flow, its slope in Figure 3.3 will be 3, meaning that heat loss has an increasingly more dominant role on performance as the dimensions get smaller. In the same figure on the right, the time needed to cool down the cylinder from 700 K to 400 K is plotted. It can be seen that for this small cylinder radius, a lot of heat energy is lost in a relatively short time. The effect of this on the engine performance was discussed in Section 2.4.

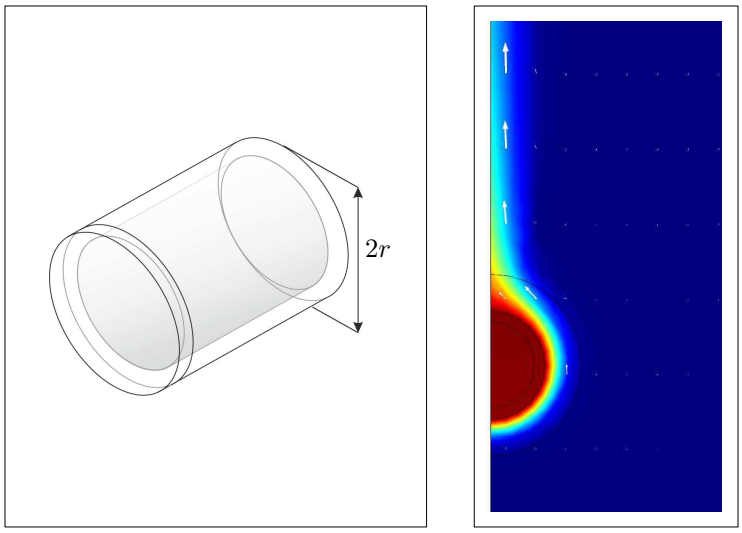

Figure 3.1: Left: Schematic representation of the cylinder that is used for the FEM model. Right: the colors represent a typical temperature distribution around the cylinder, the arrows indicate the speed of the surrounding air.

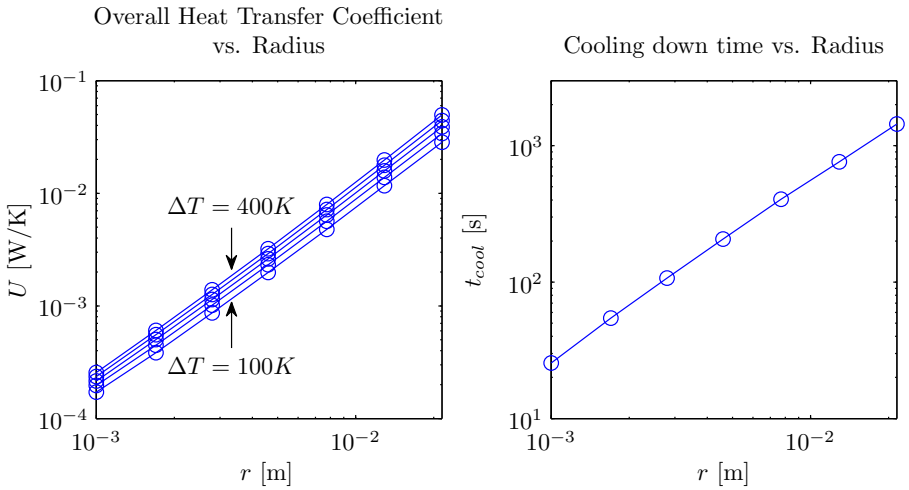

Figure 3.2: Results of the FEM simulation. Left: the overall heat transfer coefficient U for different cylinder temperatures, as function of the cylinder radius r. Right: the time t_{cool} needed to cool the cylinder from 700K to 400 K

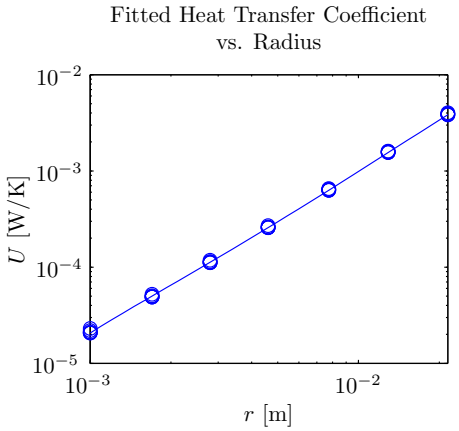

Figure 3.3: Fitted data of the FEM model, useful for the numerical simulations of the engine concepts. Circles: the overall heat transfer coefficient U, with a exponent of the heat transfer n of 1.4. Line: Equation (3.7).

a	b	c	d
-55.24	8.61	0.0189	$-6.759 \cdot 10^{-6}$

Table 3.1: Coefficients of Equation (3.7).

The data from the FEM results can be used in the numerical simulations of the engine concepts. To do this, it would be convenient to have a single formula for the overall heat transfer coefficient U. The exponent n in Equation (3.6) can be fitted with the data, as is done in Figure 3.3. A n of 1.4 matches the data and is in the expected range considering the different heat transfer modes. Then the following polynomial function can be fitted:

$$U_{fit} = ar^3 + br^2 + cr + d. \tag{3.7}$$

The coefficients are listed in Table 3.1. This function is also plotted in Figure 3.3. Note that Equation (3.7) is only valid in the given range of Figure 3.3 and the assumptions made in this section. This includes the assumed shape of the cylinder, with a height to diameter ratio of 1. Since the data found from the FEM model is proportional to the height of the cylinder h_{cyl}, a correction can be done for different cylinder shapes:

$$U_{loss} = U_{fit} \frac{h_{cyl}}{2r}. \tag{3.8}$$

This formulation for U is used in the simulations in the upcoming chapters.

Conclusions of FEM Model

With the Curzon Ahlborn model and energy balance model from the previous chapter the effect of heat leakage was described. The FEM model shows that the power lost caused by heat leakage can be as large as 0.4 Watt for a cylinder diameter of 1 centimeter, a depth of 2 centimeter and a cylinder temperature of 150°C. This is in the same order as the desired power output for H_2O_2 engine. To get a rough indication of the engine efficiency that can be expected based on the Carnot efficiency and heat leakage only, assume that H_2O_2 engine has the previous mentioned specifications as average values. The Carnot efficiency in that case is 30%, so to obtain the required power output of 0.5 Watt, the amount of energy that needs to be put into the engine is:

$$\frac{dE_{in}}{dt} = 0.5\frac{100}{30} + 0.4 = 2.1 \text{ Watt} \tag{3.9}$$

which gives an overall efficiency of 24%. As was seen in the previous Chapter, this efficiency will be lower if the timing of the engine, the compression ratio and other effects are also considered. For the H_2O_2 engine, a trade off must be made to choose the right operation temperature of the engine. High temperature means high Carnot efficiencies, but also large heat leakage losses. Somewhere between a high and a low operating temperature an optimum can be found for the engine efficiency.

The temperature distribution shown in Figure 3.1, which was representative over the whole range of cylinder radii tested, shows that the Biot number for this system is small. This means that the added value for extra insulation will be small. This might form a problem for Concept 3, which depends on a temperature difference inside the engine. As the dimensions of this system are decreased, it will be harder and harder to maintain this temperature difference. The low Biot number also means that the type of the material of the cylinder will not have much influence on the found conclusions.

3.3 Catalytic Reactions

3.3.1 In General

The energy supplied to the H_2O_2 engine comes from, as the name suggests, the chemical decomposition of hydrogen peroxide. This is an exothermic reaction that releases the elements water and oxygen. The heat that is released by the reaction is absorbed by the reaction products. If there is enough energy available, the water will be evaporated such that the only product of the reaction is a hot gas. The amount of water that needs to be evaporated depends on the original concentration of the fuel. Commercially available hydrogen peroxide

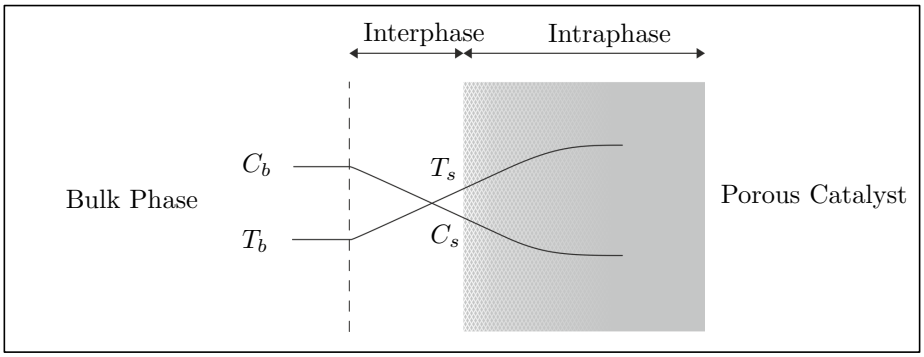

Figure 3.4: Schematic representation of the situation at the surface of the catalyst, with on the left fuel and on the right the catalyst which could be a small particle to form a powder or can be on top of a substrate surface. Based on image from [67]

is usually diluted with water with a certain weight ratio f_{rw}. The higher this ratio, the more H_2O_2 is present en less water needs to be evaporated. Since the mixture is not stable, over time some of the H_2O_2 present in the fuel will decompose without it being trigged by a catalyst. The rate at room temperature is approximately 1% concentration reduction over a period of a year, and doubles for every increase in temperature of 8°C [59]. To reduce this, stabilizers can be added to the mixture, but these also have negative influence on the performance of the catalyst. Since it is expeceted that the maximum flight time of the flapping wing device is in the order of hours, this will not be a problem in this context. Even if the fuel reaches a temperature equal to the boiling point of water, the self-decomposition rate will only be around 1% a day.

To increase understanding of the reaction, a short overview of the theory behind catalytic reactions is given here, mainly inspired by References M. Albert Vannice [67] and A. F. Mills [61]. A basic catalytic reaction occurs when the reactant molecules come in contact with the catalyst. Normally the catalyst is deposited on a porous material, so the active sites are not only on the surface of the catalyst but also deeper in the layer. The total area of the catalyst that the reactant can use is called the BET (Bruanauer, Emmett and Teller) surface, and is usually determined with a gas absorption experiment for different types of catalyst surfaces. The reactant must go through 5 steps in order to complete the reaction [67]:

1. Transport to the catalytic surface
2. Absorption of reactants on the active sites
3. Reaction
4. Desorption of reaction products from active sites
5. Transport back to the bulk phase

This situation is sketched in Figure 3.4. The reactants are transported from the bulk phase (fuel that is on top of the catalyst) through a boundary layer called the interphase, to the internal pores of the catalyst called the intraphase [67]. The interphase is defined as the boundary layer around catalytic surface where no convection of fuel occurs because of viscous forces, which means that transport occurs via diffusion only. Diffusion of the reactants is mainly driven by a spatial concentration gradient [61]. There is a linear relation between the rate of diffusion and the concentration gradient, which is called the Flicks law. It is comparable to other relations found in physics that relate a potential to a rate at which something occurs, for example Fourier's law for heat conduction described in the previous section. There are other possible potentials that can cause diffusion, for example a temperature gradient. In that case it is called thermal diffusion. In the temperature range of interest (below 200°C), the magnitude of these other types of diffusion is usually small compared the concentration gradient based diffusion [61]. This means that the transport rate j_t of H_2O_2 through the interphase is given by:

$$j_t = k_t \left(C_b - C_s\right), \tag{3.10}$$

with the rate constant k_t and concentrations of the bulk C_b and at the surface C_s [67]. The units of j depend on the normalization factor that is used for the rate constant k, which in most cases is the catalyst surface area. When the reactants actually arrive at the active site of the catalyst, the reaction can take place. The reactants are absorbed, react and desorbed. The reaction itself can be explained using the colliding molecules model. The more collisions occur between the reactants and the catalyst, the higher the reaction rate is. These steps can be characterized by the Arrhenius relation in most cases [61], which gives a relation for the reaction rate constant:

$$\begin{aligned} k_r &= Ae^{-E_0/RT}, \\ j_r &= k_r \left(C_s\right)^n, \end{aligned} \tag{3.11}$$

where A is pre-exponential factor, E_0 is the activation energy of the reaction, R is the gas constant, T is the temperature at which the reaction occurs and n is the order of the reaction. This relation shows the usefulness of the fact that the catalyst lowers the activation energy of the reaction. As E_0 is lowered, the rate of the reaction increases. The pre-exponential factor depends on the type of catalyst and reactants that are used and is determined empirically. At this point the reaction products are transported back into the surrounding area via the same mechanisms which brought the reactants to the active sites: mass diffusion and convection. This step is considered to be much faster than the first two steps [30], so it will have no influence on the overall rate of the decomposition. The overall rate R at which the reactants are consumed from the bulk phase is a function of the transportation rate and the reaction rate [61]:

$$\begin{aligned} f_n j_t &= f_n j_r = R, \\ R &= -f_n \frac{k_r k_t}{k_r + k_t} C_b = -f_n k C_b, \end{aligned} \tag{3.12}$$

where f_n is a normalization factor and k the overall reaction rate constant. If j_t and j_r are normalized for the catalytic surface area s_c, then $f_n = s_c$. Another frequently used normalization is the catalyst total weight. The reaction of H_2O_2 has first order kinetics for most types of catalysts [30, 38, 44]. That means that over time, the decay in the concentration in the bulk phase can be found by combining Equations (3.10), (3.11) and (3.12):

$$\begin{aligned} \frac{dC_b}{dt} &= R, \\ C_b &= C_{b,ini} e^{-f_n k t}. \end{aligned} \tag{3.13}$$

At this point two types of processes can be identified [61]: a reaction limited process or a transport limited process. When the process is reaction rate limited, the speed at which the reactants are consumed can be increased by increasing the temperature or decreasing the activation energy according to Equation (3.11). In this situation the transportation rate is so fast that the surface concentration is almost equal to the bulk concentration. For some types of catalyst, the active sites at the catalyst become saturated when C_s is high enough, which results in zero order kinetics [67, 48]. This means that the reaction rate is no longer dependent of the fuel concentration (n=0). The nature of the limiting step of the decomposition is related to the diffusive based Damköhler number, which is defined as the ratio between the reaction rate and transportation rate [67], which for a first order reaction becomes:

$$Da \equiv \frac{\text{reaction rate}}{\text{transportation rate}} = \frac{k_r}{k_t} = \frac{C_b - C_s}{C_s}. \tag{3.14}$$

Notice that (3.13) does not account for volume changes of the bulk because of the catalytic reaction. In the case of H_2O_2 decomposition with high weight ratio's of the fuel, the water from the bulk phase is also evaporated. At some point the rate at which the bulk is evaporated and the rate at which the reactants are consumed is equal and C_b is independent of time. When this situation occurs depends on the temperature and the heat and mass transfer properties associated with the chosen catalyst.

Catalyst material	$k[1/s/g]$	Source
MnO_2	$0.02 \rightarrow 0.25$	[13]
$CoFeO_4$	0.12	[30]
-	0.45	[50]
Cr	$0.5 \rightarrow 1.3$	[42]
$MgCo_2O_4$	0.632	[50]
$MgFe_2O_4$	0.067	[50]
$MnCo_2O_4$	0.33	[50]
$Ag - NiO$	0.03	[53]

Table 3.2: Rate constant k for different types of catalyst material, all normalized for the mass of the material.

3.3.2 Temperature Dependence

Since k_r is strongly dependent on the temperature, Da is also temperature dependent. Experiments with catalyst cobalt-iron oxide ($CoFeO_4$) have shown that a transition of Da occurs at a temperature of approximately 50°C, where the reaction switches from k_r limited to k_t limited [30]. Below this temperature, the consumption rate increased according to the Arrhenius law. For another catalyst, manganese dioxide (MnO_2), A.B. Kanungo et al. [13] report a strong temperature dependence of the consumption rate below 25°C, suggesting the Arrhenius dependence. Between 25 and 35°C a linear dependence was reported, suggesting some sort of transition region. Above 40°C the consumption rate decreased slightly, suggesting diffusion limited kinetics [13].

As the process temperature increases (because of increasing H_2O_2 concentration in the fuel), not only the peroxide will be consumed, but also the water will be evaporated. That means that the bulk concentration C_b is not only dependent of its consumption rate as described by Equation (3.13), but also on the evaporation rate of the water.

If the reaction temperature is above 150°C, the hydrogen peroxide will also evaporate which will result in a efficiency loss of the decomposition system [21]. Thermal decomposition does occur, but the rate is very small compared to catalytic decomposition [23]. When temperatures above 800°C are obtained, thermal decomposition starts to have a considerable rate [18]. Gas decomposition with use of a solid catalyst can also be achieved, but requires a lot more surface area as is the case with liquid fuel, because the concentration is much lower in the gas. At these temperatures other diffusion mechanisms might become significant, further increasing the reaction rate. For the FWM, these temperature ranges will not be considered. Based on the measurements of References [13] and [30], it is assumed that the reaction is diffusion limited and temperature has no influence on the reaction rate.

3.3.3 Surface Area Dependence

A distinction can be made between the geometric surface area of the catalyst and the total available surface area, or BET surface. The geometric surface area is defined as the macroscopic area, for instance a patch of 2 mm by 2 mm. The BET area is an indication of the total available area, which includes surface areas inside the pores of the catalyst material. For a catalyst in the form of small particles (powder), J.R. Goldstein et al. [30] report that the reaction rate is not proportional to the BET surface area, as might be expected. This is because the turbulent nature of the H_2O_2 decomposition. The gas bubbles that are released drive the reactant out of the pores such that a much smaller portion of the BET area is available. Therefore, it has been suggested that the outer (geometric) surface of the catalyst particles is a better normalization parameter than the BET surface [30]. Based on these conclusions, in the remainder of this report it is assumed that if the H_2O_2 concentration in the fuel is high enough, the reaction produces enough heat such that no fuel reaches the pores of the catalyst. That means that k is also proportional to the outer geometric surface of the catalyst.

3.3.4 Catalyst Material

Prior to this work, A.J.H. Meskers [60] investigated which catalyst material might be suitable for the H_2O_2 engine. Based on literature and experiments, MnO_2 was identified as a suitable catalyst. As can be seen from Table 3.2, MnO_2 has not the highest specific rate constant but it is cheap and relatively easy to produce. Different MnO_2 samples were constructed by Reference [60] by using two precursors (nitrate and acetate) with different support layers. During the experiments a small drop of 30% H_2O_2 fuel was dropped on the catalyst and various measurements were obtained. One observation was that the water of the fuel was not fully evaporated and was absorbed by the porous catalyst. Between sequent experiment runs the absorbed water was partially evaporated again because of the heat of the reaction. Since this a turbulent procdure, the surface structure of the catalyst was destroyed. For the engine, durabilty is an important factor which means that MnO_2 in combination with the used production method of Reference [60] is not the best option. Other experiments desribed in literature [13, 50, 38] do not report on such destruction of the catalyst material.

Homogeneous catalyzation is also a option, but C. M. Spadaccini et al. [15] report on a severe limitation of the chemical reaction rates because of mixing problems in small scale systems. High surface to volume ratios in small scale systems cause most fluid flows to be laminar. Mixing of fluids is much faster in turbulent flows, making homogeneous catalyzation unattractive for small scale engine design.

3.3.5 Droplet Decomposition

Up to this point it was assumed that volume of fuel that is decomposed per second is many times smaller than the bulk volume of the fuel. If the H_2O_2 engine is going to use small droplets to control the decomposition rate, this assumption will not be valid. Droplet decomposition might be attractive for the engine design if the energy release rate is fast enough. During the experiments done by Reference [60] a drop of 30% H_2O_2 fuel was decomposed using MnO_2 supported by a porous ceramic layer. The experiment was done in a sealed glass container to observe the rise in pressure and temperature as function of time. With a fixed drop size of 22 μL and cylinder volume of 0.1 L, peak pressures of 12kPa have been measured. The minimum consumption time, defined as the time needed to reach maximum pressure in the cylinder after the reaction has started, was 50 ms. As was indicated by Reference [60], this time depends on the size of the droplet and on the concentration of the fuel. It is also expected that the reaction time depends on the conditions of the surrounding air and catalyst material temperature. Since 50 ms is 50% longer than the total cyclic time that is needed for H_2O_2 engine, it is known that the 22 μL dropsize of 30 % fuel is too large for the engine design. By reducing the drop size, the reaction time will be shorter. To know if droplet decomposition is suitable for the H_2O_2 engine, three questions need to be answered:

1. What is the maximum droplet size such that the consumption rate is in the correct order, considering the fixed cycle time of 30Hz of the engine?
2. What is the total volume of droplets needed for one cycle?
3. What facilities does the engine need to have in order to generate such droplets?

Maximum droplet size

No clear relation between droplet size and consumption time was found in literature, but the droplet decomposition process is in some ways similar to droplet evaporation on a hot plate. With droplet evaporation the consumption rate depends on the contact surface area of the drop, the plate's temperature and the conditions of the surrounding air (dry of saturated air) [52]. With droplet decomposition, the reaction releases heat at the surface so in both situations there is a hot surface and a droplet. That is why it is expected that similar droplet dynamics can be found with droplet decomposition as is found with droplet evaporation.

With droplet evaporation, 2 temperature regions can be identified [52]. Around the boiling temperature T_b of the droplet there is slow film evaporation, where most part of the droplet is in contact with the surface. At the other extreme the temperature of the plate is high enough such that vapor layer forms between the droplet and the surface. This is called the spherical state [36], and the

temperature at which this occurs is called the Leidenfrost temperature. T.Y. Xiong et al. [52] report for water droplets with a diameter D_0 in region of $0.1mm$ up to $2mm$ ($1{\cdot}10^{-4}\mu L$ up to $4\mu L$) a consumption time that is proportional to D_0^n. The exponential factor n depends on the surface temperature T_s and is close to 2 for temperatures in the film evaporation region and goes to 1.4 for temperatures around 150°C. As droplets get smaller (become lighter) and surface temperatures get higher, the droplets start to bounce up and down from the surface because of the turbulent nature of the process. In this region, n is smaller than one [52].

The upper limit of n of 2 when the temperatures are in the low region might be explained by looking at the energy transfer between the plate and the droplet. At low temperatures almost all of the droplet is in contact with the surface, so the heat energy is transfered to the droplet by conduction. Assuming Fourier's law of conduction again, the rate of energy transfer Q is:

$$Q = C\Delta T, \tag{3.15}$$

where C is a function of the surface area divided by a characteristic length of the region through which the conduction occurs. The total energy E_{evap} that is needed to evaporate the droplet is directly proportional to the total volume of the droplet. So if an average of Q is taken, the consumption time of the droplet becomes:

$$\tau = \frac{E_{evap}}{Q_{avg}}. \tag{3.16}$$

Considering the geometric scaling factor $(S_g)^n$ as it was used in Section 1.3, the numerator scales with $n = 3$ and the denominator with $n = 1$, so the consumption time scales with $n = 2$.

At the other extreme in the spherical state, L. H. J. Wachters et al. [36] describe a more complicated model for the energy transfer that considers the convection below the droplet. The evaporation rate in that case scales with $n = 1.35$ for small droplets and $n = 1.5$ for large droplets, so the consumption time with $n = 1.65$ and $n = 1.5$, respectively. Very small droplets that bounce up and down of the surface are not modeled by [36], so the observed $n < 1$ cannot be explained that way.

With droplet decomposition, there is only heat release when the droplet is in contact with the catalyst surface. So the fuel drop will not go into the spherical state. But with temperatures in the lower region, the droplet will experience disturbances from gas release similar to the water droplet on a hot plate. It is uncertain how the reaction step will scale considering the droplet characteristics described above. That is way the worst case scenario is assumed, where $n = 1$. In that case very small fuel droplets are needed in order to obtain a fast enough

consumption time. If this value turns out to be critical for the H_2O_2 engine design, the scaling of droplet decomposition must be tested first.

With the assumed $n = 1$ scaling exponent, the data measured by Reference [60] can be extrapolated to smaller droplet sizes. To calculate the maximum droplet diameter D_{max}, a maximum consumption time τ_{max} needs to be chosen, which is taken here as 10% of the cycle time of the engine. The found maximum diameter is:

$$\begin{aligned} D_{max} &= \frac{\tau_{max}}{\tau_1} D_{0,1} = \frac{1/300}{50 \cdot 10^{-3}} 3.35 \approx 0.22 \ mm \\ V_{max} &= 0.006 \ \mu L \end{aligned} \tag{3.17}$$

To calculate the diameter D_0 as function from the droplet volume and vice versa, a sphere shape is assumed [52]. This value can be used to check different engine designs that use droplet decomposition. J. Duncre [8] discusses a droplet generator based on inertia effects with a droplet diameter of 60 μm, an order smaller than what is calculated here. To be absolutely sure what the needed droplet size is, the effect of droplet size on consumption time should be tested experimentally. But based on rough approximations it can be stated that the droplets can be made small enough such that the consumption time is fast enough for a 30 Hz cycle engine. This is especially true if the fuel concentration is increased from the 30% used for the analysis here.

Needed fuel per cycle

To get an indication of how big the total droplet volume should be in terms of the energy that is needed per engine cycle, the energy that is released as function of the drop size is approximated. The decomposition of H_2O_2 occurs according to:

$$H_2O_2(aq) \rightarrow H_2O(l) + \frac{1}{2} O_2(g) + \bar{E}_{react} \tag{3.18}$$

The released energy can be calculated by taking the sum of the changes in enthalpy of each species, which results in 98.2 kJ per mole H_2O_2 [60]. This value is tabulated in Table 3.3, just like some other properties used in following calculation. The energy is used to: evaporate the water released by reaction and the water already present in the fuel, heat the reactants and heat the catalyst material. It is assumed that at steady state conditions the catalyst is already hot, such that most of the released energy goes into heating the reaction products. To calculated the energy needed to evaporate all the water, first it is needed to know how much water is present per mole H_2O_2 in the fuel. A molar ratio $\bar{n}_{H_2O}$ is defined, which is the ratio between the amount of moles of water and the amount of moles of hydrogen peroxide:

Property	Symbol	Magnitude	Unit
Molar mass H_2O_2	$M_{H_2O_2}$	$34.02{\cdot}10^{-3}$	$kg/mole$
Molar mass H_2O	M_{H_2O}	$18.02{\cdot}10^{-3}$	$kg/mole$
Density H_2O_2	$\rho_{H_2O_2}$	$1.450{\cdot}10^{3}$	kg/m^3
Density H_2O	ρ_{H_2O}	$1.000{\cdot}10^{3}$	kg/m^3
Energy released by reaction	$\bar{E}_{react}$	$98.21{\cdot}10^{3}$	$J/mole$
Enthalpy change evaporation H_2O	ΔH_{evap}	$40.65{\cdot}10^{3}$	$J/mole$
Average heat capacity O_2	C_{O_2}	29.38	$J/mole/K$
Average heat capacity H_2O(l)	$C_{H_2O,l}$	75.33	$J/mole/K$
Average heat capacity H_2O(g)	$C_{H_2O,g}$	37.47	$J/mole/K$
Evaporation temperature H_2O	T_{evap}	373.15	K

Table 3.3: Overview of properties involving H_2O_2 decomposition used in calculation

$$\bar{n}_{H_2O} = \frac{1 - f_{r,w}}{f_{r,w}} \frac{M_{H_2O_2}}{M_{H_2O}}, \tag{3.19}$$

where $f_{r,w}$ is the weight ratio of H_2O_2 per total weight of the fuel and M is the molar mass of the species in the subscript. The amount of energy that is needed to evaporate the water per mole of H_2O_2 that is decomposed is:

$$\bar{E}_{H_2O,evap} = (\bar{n}_{H_2O} + 1)\, \Delta H_{evap}, \tag{3.20}$$

with the evaporation heat of water ΔH_{evap}. For a weight ratio $f_{r,w}$ of 30%, $\bar{E}_{H_2O,evap}$ is equal to 219 kJ/mole. Since this is lower than the energy released during the decomposition, not all water will be evaporated, as was reported by Reference [60]. Now assume that a process temperature T_p of 150°C is achieved, the fuel has an initial temperature $T_{f,ini}$ of 25°C and $f_{r,w}$ is 80%. The energy $\bar{E}_{heating}$ needed to heat the reaction products up to the process temperature is:

$$\begin{aligned} \bar{E}_{heating} = {} & C_{O_2} (T_p - T_{f,ini}) + \\ & (\bar{n}_{H_2O} + 1)\, C_{H_2O,l} (T_{evap} - T_{f,ini}) + \\ & (\bar{n}_{H_2O} + 1)\, C_{H_2O,g} (T_p - T_{evap}), \end{aligned} \tag{3.21}$$

where the first term accounts for the heating of the oxygen gas, the second for the heat of liquid water to the boiling point and the last term for the heat of the water vapor to the process temperature. The energy $\bar{E}_{work}$ left from the reaction to do work is:

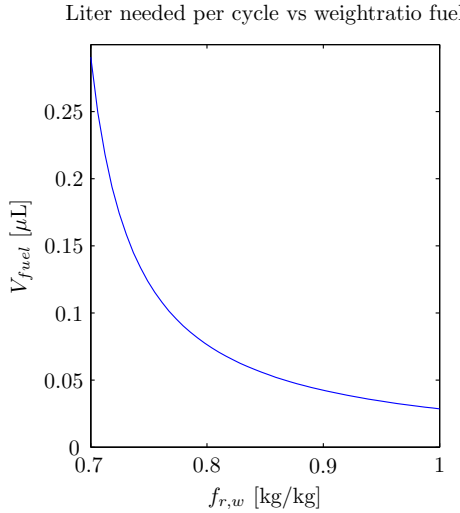

Figure 3.5: Plot of needed amount of fuel per cycle, Equation (3.23), as function of the weight ratio of the fuel. Parameters used: $P_{out} = 0.5$ Watt, $f_{cycle} = 30$Hz, $T_p = 150°$C, $T_{f,ini} = 25°$C

$$\bar{E}_{work} = \bar{E}_{react} - \bar{E}_{H_2O,evap} - \bar{E}_{heating}, \tag{3.22}$$

which is approximately 21 kJ per mole H_2O_2 decomposed, for the given process conditions. Notice that pressures effects have been neglected. A more precise calculation would also account for changes in internal energy of the gas due to pressure increase and changes in the evaporation enthalpy due to pressure change. The needed amount of fuel per cycle to generated a certain amount of power P_{out} is:

$$V_{fuel} = \frac{P_{out}}{\bar{E}_{work}\eta_{Carnot}f_{cycle}} mv_{avg}, \tag{3.23}$$

with Carnot efficiency η_{Carnot}, cycle frequency f_{cycle} and average molar volume of the fuel mv_{avg}. With a Carnot efficiency of 30%, the amount of fuel that needs to be decomposed per cycle to have a net output of 0.5 Watt, is in that case 0.08 μL. This value rapidly increases for a decreasing weight ratio of the fuel, as can be seen in Figure 3.5. The first reason is because less H_2O_2 is present in the fuel, the second reason because more water needs to be evaporated in order to bring the gas up to the process temperature. This figure also shows that the minimum mass fraction that is needed to fully evaporate the water is about 70%.

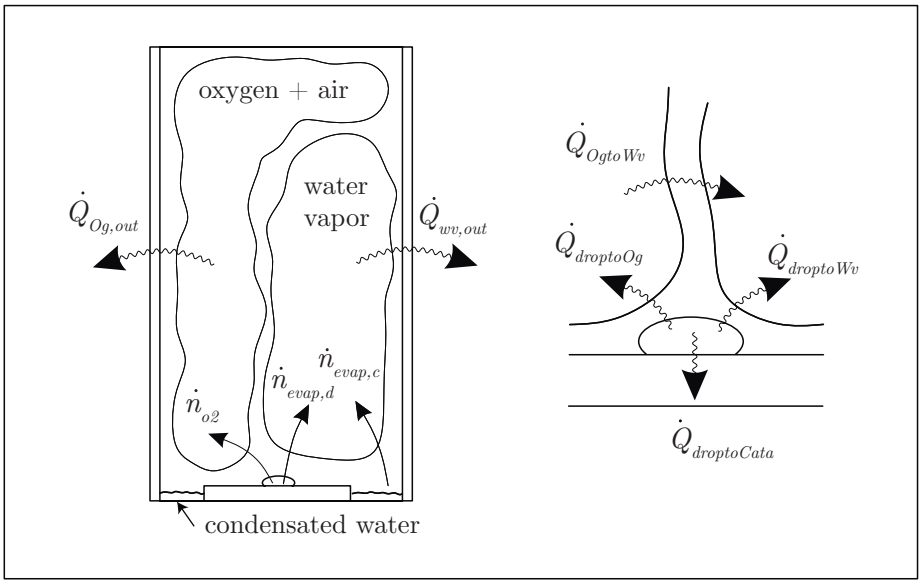

Figure 3.6: Schematic representation of the decomposition model for low fuel concentrations. On the left the chamber is shown in which the decomposition occurs, on the right a close up of the fuel droplet is shown.

3.3.6 Decomposition Model

In this section a model will be presented that can be used for modeling the catalytic reactions in combination with the engine simulations done in the previous chapter. First a drop of low concentration hydrogen peroxide fuel will be simulated. The parameters of this model can than be fitted to the data measured by Reference [60]. The next step is to increase the concentration of the fuel to see what rate of energy release can be expected for the H_2O_2 engine.

Low Fuel Concentrations

To construct a model of the decomposition process, the energy balance of the fuel drop, water vapor and gas inside the chamber are used. The general form of the energy balance looks like [37]:

$$\sum (n_i cp_i) \frac{dT}{dt} = \frac{dp}{dt} V + \sum \left(\frac{dn_i}{dt} h_i \right) + \frac{dQ_{in}}{dt}, \tag{3.24}$$

where n_i is the amount of mole of species i, cp_i the heat capacity and h_i the enthalpy. The different terms account for the heating of the species, the change in pressure, the change in species and the heat transfer, respectively. There

are three different temperature's inside the chamber: the droplet temperature T_{drop}, the water vapor temperature T_{wv} and the temperature of the oxygen and air gas T_{og}. The pressure inside the chamber is assumed to be uniform and is given by the ideal gas law:

$$p = \frac{(n_{o2} + n_{air})\, R_{gas} T_{og}}{V_{og}} = \frac{n_{h2o,g} R_{gas} T_{wv}}{V_{wv}}. \tag{3.25}$$

The decomposition rate $\dot{n}_{h2o2}$ is given by Equation (3.12). The concentration that determines the reaction rate k can be calculated with the known quantities of H_2O_2 and H_2O inside the droplet. The droplet dynamics that influence the rate constant, discussed in the previous section, are not considered in this model for simplicity. Other changes in species are also determined by the decomposition but also by the evaporation of water:

$$\begin{aligned}
\frac{dn_{o2}}{dt} &= -\frac{1}{2}\frac{dn_{h2o2}}{dt}, \\
\frac{dn_{h2o,l,drop}}{dt} &= -\frac{dn_{h2o2}}{dt} - \frac{dn_{evap,d}}{dt}, \\
\frac{dn_{h2o,g}}{dt} &= \frac{dn_{evap,d}}{dt} + \frac{dn_{evap,c}}{dt}, \\
\frac{dn_{h2o,l,cham}}{dt} &= -\frac{dn_{evap,c}}{dt}.
\end{aligned} \tag{3.26}$$

The first step after the drop has come in contact with the catalytic material is the internal heating of the drop because of the released energy. If the fuel concentration is high enough, the droplet temperature will reach the saturation temperature of water. At this point the water starts to evaporate. The saturation temperature T_{sat} changes during the evaporation because of the change in pressure inside the chamber. The relation between T_{sat} and p is given by J. R. Cooper et al. [29], who suggest a fitted quadric function which can be differentiated. It is assumed that during the evaporation of the water in the droplet, the temperature change is given by:

$$\frac{dT_{drop}}{dt} = \frac{dT_{sat}}{dp}\frac{dp}{dt}, \tag{3.27}$$

which means that the droplet temperature will follow the saturation temperature. This means that the evaporation rate of the water inside the dorplet $\dot{n}_{evap,d}$ can be calculated from the energy balance, which will use all the remaining energy for evaporation. As the water vapor is transported to the chamber, heat will flow out from it via the cylinder walls and the surrounding gas. This

means that a part will condensate back into liquid. The rate at which this occurs is shown in Figure 3.6 as $\dot{n}_{evap,c}$ and will be negative.

An important aspect during the decomposition process is the heat transfer rate between the different species. In Figure 3.6, a diagram of the heat transfer between the droplet and its surroundings are shown. The general formula for heat transfer rates is assumed to be:

$$\frac{dQ}{dt} = A\bar{u}\left(T_{sur} - T\right), \tag{3.28}$$

where the product $A\bar{u}$ is called the rate constant. As can be seen in Figure 3.6, there are 6 different heat transfers, each with their own rate constant. The overall rate constant $A\bar{u}_{cyl}$ of the heat transfer to the environment ($Q_{Og,out} + Q_{wv,out}$) was investigated in Section 3.2. It is assumed that the effective area over which $\dot{Q}_{Og,out}$ occurs is in proportion with the effective area of $\dot{Q}_{wv,out}$ according to the mole fraction of the gas in the chamber, such that:

$$\begin{aligned} AU_{og,out} &= A\bar{u}_{cyl}\frac{n_{o2} + n_{air}}{n_{o2} + n_{air} + n_{h2o,g}}, \\ AU_{wv,out} &= A\bar{u}_{cyl}\frac{n_{h2o,g}}{n_{o2} + n_{air} + n_{h2o,g}}, \end{aligned} \tag{3.29}$$

which will be valid if the different species are perfectly mixed. The heat transfer between the different mixed gas is more complicated, because there is not a clear surface over which the heat transfer occurs. No model was found in literature to describe mixed gas heat transfer, but consider the schematic representation of a mixed gas in Figure 3.7. Imagine that every separate molecule transfers heat to all its surrounding molecules. The sum of all heat transfer rates in that case is proportional to the amount molecules of the species with the lowest mole fraction inside the gas. In the situation as it was tested by Reference [60], the water vapor will have the lowest mole fraction, that is why for the heat transfer $\dot{Q}_{OgtoWv}$ the following is assumed:

$$\frac{dQ_{OgtoWv}}{dt} = \bar{u}_{gastogas} n_{h2o,g}\left(T_{og} - T_{wv}\right), \tag{3.30}$$

where $U_{gastogas}$ is a constant that has to be fitted to the experimental data. The heat transfer from the drop to the gas is expected to be small because of the small conductivity of the gas, but the heat transfer to the catalytic material might be large if the temperature difference is large. During the experiments of Reference [60], the catalytic surface on which the drop was decomposed was at ambient temperature at the beginning of the reaction. Because of the large heat capacity of the catalytic material compared to that of the droplet, it is assumed the catalytic material remains at constant temperature T_{env}. The values for the

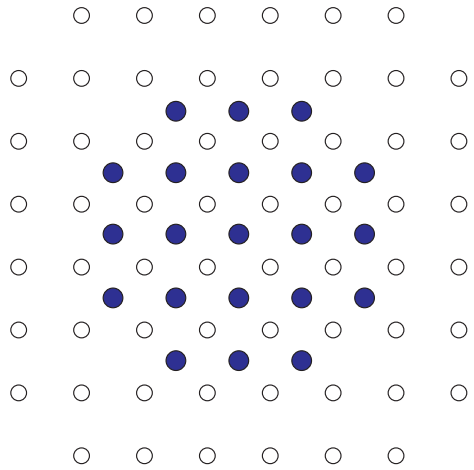

Figure 3.7: w

rate constant concerning the heat transfer out of the drop will be fitted to the experimental data of Reference [60].

What remains is the condensation rate of the water vapor, or its opposite $\dot{n}_{evap,c}$. For low fuel concentrations all the energy released by the decomposition will be used to evaporated the water present in the drop. This means that the temperature of the water vapor will always be equal to the saturation temperature. This means that the energy balance of the water vapor can be used to determine the condensation rate.

Combining Equations (3.25), (3.26) and the three equations resulting from Equation (3.24) results in 6 equations for the six unknown variables: $\dot{T}_{drop}$, $\dot{T}_{og}$, $\dot{T}_{wv}$, $\dot{p}$, $\dot{n}_{evap,d}$ and $\dot{n}_{evap,c}$. These six differential equations are implemented into a numerical solver that can handle conditional statements. The fitted parameters U_{drop}, $U_{droptocata}$ and $U_{gastogas}$ are given in Table 3.4. There are three other parameters that are important: the reaction rate constant k, the initial volume of the fuel drop $V_{drop,ini}$ and the amount of water that was initially present on the substrate. For convenience, this last parameters is incorporated into the model as a correction factor f_{iwc} that is multiplied with the water initially present in the fuel drop itself. These three parameters change for every test that was done by Reference [60]. Because of deactivation and surface irregularities the reaction rate constant was not constant between different runs. Because a low concentration fuel was used, not all water from the fuel was evaporated, so between different runs some water might have been left on the catalytic surface. This influences the total heat capacity of the fuel drop and that is why the correction factor f_{iwc} is used. Finally, the initial volume of the fuel drop was not constant between different test runs either, which can be seen from the different steady state pressures in Figure 3.8. The best fit of these parameters for every experiment run are given in Table 3.5.

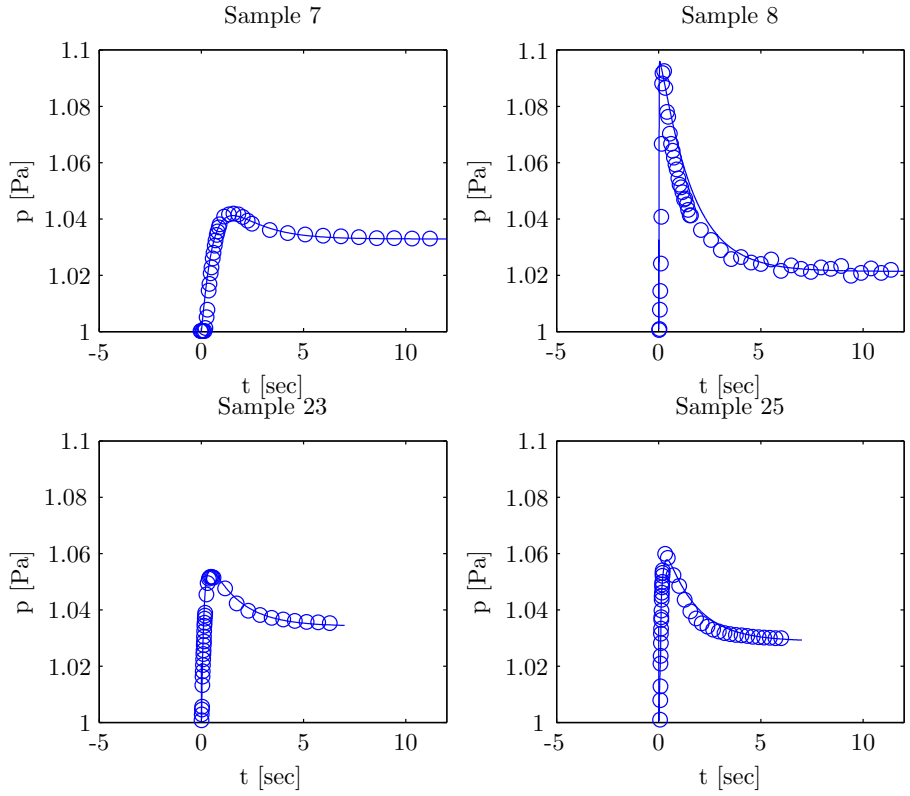

Figure 3.8: Results of the fitted model (line) compared with the measured data of Refenence [60] (circles). The sample numbers correspond to different catalytic materials used in Reference [60].

Heat transfer between	Symbol	Fit	Expected Order	Unit
Drop to gas	$\bar{u}_{droptogas}$	$5{\cdot}10^2$	10^2	$W/[m^2K]$
Drop to catalytic surface	$\bar{u}_{droptocata}$	$5{\cdot}10^4$	10^4	$W/[m^2K]$
Gas to gas	$\bar{u}_{gastogas}$	$1{\cdot}10^4$	?	$W/[molK]$

Table 3.4: Fitted parameters of the decomposition model that are constant for different experiment runs

Sample Number	7	8	23	25
Reaction rate constant k_{react} [1/m^2/s]	0.0025	0.400	0.0270	0.0115
Volume fuel drop V [μL]	25.6	16.5	26.5	22.5
Correction factor initial water f_{iwc} [-]	1	2.6	1.9	1

Table 3.5: Fitted parameters of the decomposition model that change for different experiment runs

As can be seen in Figure 3.8, the decomposition model for low concentration fuel can be fitted to the experimental data of Reference [60]. The largest deviation occurs after the peak pressure has occurred, when the gas inside the cylinder is cooled. This might be because of the definition of the heat transfer rate, Equation (3.28). In this model the heat transfer is taken as a linear function of the temperature difference, which corresponds to assuming all heat transfer occurs via conduction. In reality there is also heat transfer via convection and radiation, which have different rate equations. Also the perfect mixing assumption and the gas to gas heat transfer assumptions have influence on the cooling down characteristic. The accuracy of the fitted heat transfer variables between different species is not that important for the steady state engine simulations, because the gases will have almost equal temperature in those situations.

$$
\begin{aligned}
&\bar{u} = \frac{k}{L}, \\
&k_{gas} \approx 1 \cdot 10^{-2}[W/mK], \\
&k_{liq} \approx 1 \cdot 10^{-1}[W/mK], \\
&k_{sol} \approx 1 \cdot 10^{2}[W/mK], \\
&r_{drop} \approx 1 \cdot 10^{-3}[m],
\end{aligned}
\tag{3.31}
$$

High Fuel Concentrations

When the fuel concentration is increased, more water will be evaporated. At some point, there will be no water left in the drop and the fuel concentration is equal to 1. Increasing the fuel concentration in the decomposition model described above, the lowest fuel weight ratio $f_{r,w}$ at which this occurs is around 65 %. This is similiar to the approximation given in the previous section. Even though all water from the initial drop is evaporated, there is still some water formed at the decomposition. Since the released energy of the decomposition is larger than the energy needed to evaporate this water, it will be directly evaporated such that:

$$\frac{dn_{evap,d}}{dt} = -\frac{dn_{h2o2}}{dt}. \tag{3.32}$$

The energy that remains is used for heating the drop. This means that the fuel drop temperature can increase further up to the evaporation point of H_2O_2, which is 150°C at ambient pressure. At this point, the hydrogen peroxide itself will evaporate. No explicit relation was found for the saturation temperature of hydrogen peroxide, but G. Scatchard et al. [24] give an experimentally fitted function for the saturation pressure. This relation is converted to an explicit relation for temperature via curve fitting, since it is easier to use in the numerical solver:

$$\begin{aligned} &T_{sat,h2o2} = p^3 a + p^2 b + pc + d, \\ &\\ &a = 1.058 \cdot 10^{-15}, \\ &b = -1.089 \cdot 10^{-9}, \\ &c = 4.897 \cdot 10^{-4}, \\ &d = 383.5. \end{aligned} \tag{3.33}$$

This equation and the relation given by Reference [24] are both plotted in Figure 3.9. When the saturation temperature is reached, the rate of the evaporation of the H_2O_2 can be calculated with the energy balance of the drop, Equation (3.24). At this point two choices can be made for the high concentration fuel decomposition model: the evaporated H_2O_2 is added to gas inside the chamber or it is assumed that the engine has the means to also decompose the evaporated fuel. In this section it is assumed that the engine does not have these kind of measures. If it turns out that the droplet decomposition is attractive for the H_2O_2 engine, one can look at the other situation to get an indication of the added value of the extra measures needed to decompose the evaporated hydrogen peroxide.

In Figure 3.10 the results of the high concentration model are shown. In the simulations, a similar cylinder is assumed as was used by Reference [60]. The

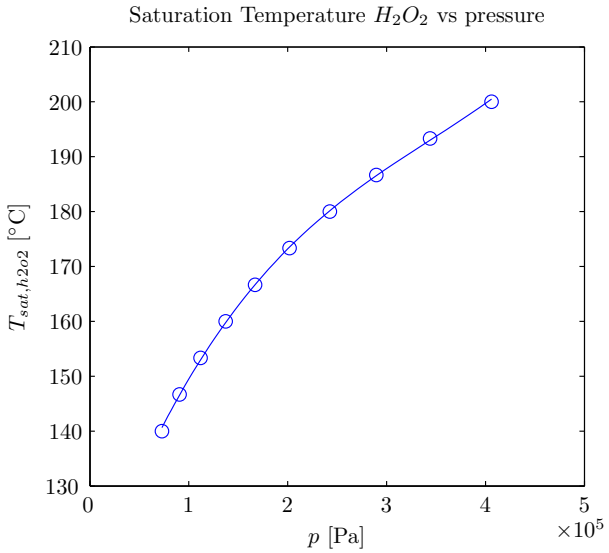

Figure 3.9: Saturation temperature of hydrogen peroxide. The circles represent the data from Reference [24] and the line is Equation (3.33).

peak pressures that are obtained for different reaction rates and fuel concentrations is shown on the left. It is observed that at some point, an increase in the fuel concentration does not increase the peak pressure. This can be understood from the right plot of Figure 3.10, which shows that more and more H_2O_2 is evaporated as the fuel concentration is increased. The amount of evaporated H_2O_2 is expressed as a fraction $f_{h2o2,evap}$ of the initial amount of H_2O_2 present in the fuel drop.

Considerations Engine Design

1. One of the problems that was encountered by Reference [60] was the absorption of fuel by the porous support layer, which caused deactivation of the catalyst. As was pointed out earlier, the porous material does not contributed much to the decomposition rate. To provide durability of the engine design, porous catalysts should be avoided.

2. The maximum droplet size and minimum needed droplet volume are approximated. Various subsystems that can generate such droplets need to be considered.

3. The maximum droplet size is assumed based on a comparison with droplet evaporation on a hot plate, so if during the subsystem design the droplet size turns out to be critical, the scaling characteristics of droplet decomposition need to be tested.

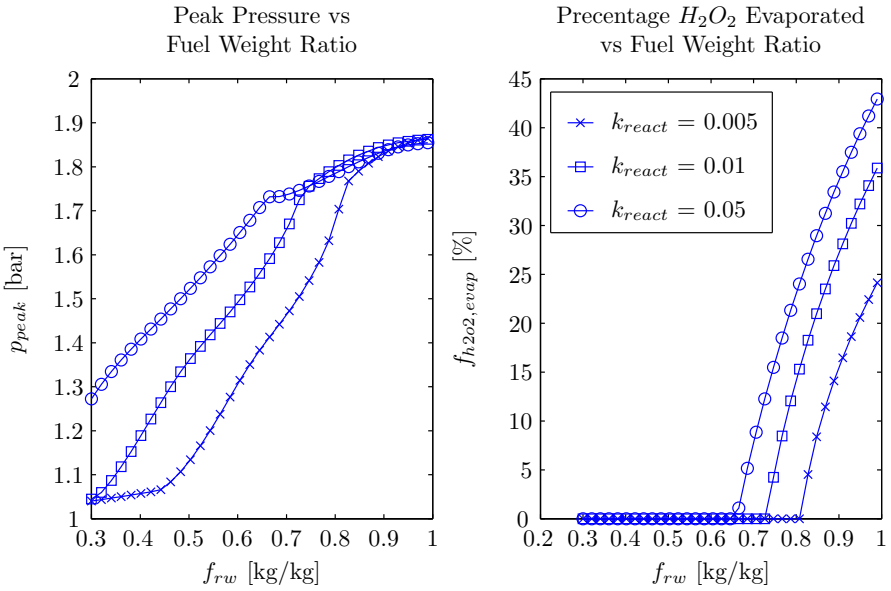

Figure 3.10: Results of the high concentration model. Left: peak pressures in the cylinder as function of the fuel weight ratio for different reaction rates. Right: the amount of hydrogen peroxide that is evaporated, expressed as % of the amount that was initially present in the droplet.

3.4 Exhaust Flow

The exhaust flow found in Concept 1 will determine its performance characteristics and will therefore be important for the conclusions of this report. Due to time restrictions, a fully detailed analysis will have to be done in a follow up study on the engine of the FWM. For now, the basic equations and characteristics are discussed, mainly inspired by F.M. White [68].

The gas that is released by the decomposition is a compressible substance, which means that if the pressure difference over the exhaust is large enough the flow will be supersonic. The important dimensionless number for compressible flows is the Mach number [68], which is defined as:

$$Ma = \frac{V}{a}, \tag{3.34}$$

with gas velocity V. The speed of sound a in a gas is typically above 300 m/s and a function of temperature T:

$$a = \sqrt{\frac{kR_{gas}T}{M_{avg}}}, \tag{3.35}$$

with adiabatic index k, average molar mass of the gas M_{avg} and universal gas constant R_{gas}. This means that pressure waves inside the cylinder take very little time to travel from one side to the other, and a uniform pressure can be assumed. A flow is supersonic if $Ma > 1$. If an isentropic and adiabatic flow is assumed and the ideal gas law can be applied, then [68]:

$$\frac{p_s}{p_0} = \left(\frac{2}{k+1}\right)^{k/(k-1)}, \tag{3.36}$$

with stagnation pressure p_0 and sonic pressure p_s. The stagnation pressure is defined as the pressure when the fluid is completely at rest. When the velocity is increased, the pressure decreases according to the energy balance of the fluid. At some point, the sonic pressure is reached which matches with $Ma = 1$. For air and oxygen gas, $k = 1.4$ and for water vapor $k = 1.3$. Using this with Equation (3.36), it is known that the sonic pressure is approximately 53% of the stagnation pressure. In the situation of Concept 1, the stagnation pressure is inside the cylinder. Fixing the sonic pressure to ambiant conditions, the needed pressure inside the cylinder to obtain sonic flow through the exhaust is approximatelly 1.8 bars. Above this pressere, the flow is called choked.

As a first approach, the flow in the exhaust is approximated by the situation shown in Figure 3.11, which shows a compressible flow through a round nozzle. The flow is considered to be isentropic, which means that friction and other losses are neglected. In this situation, Reference [68] gives the following relation for the mass flow at the exit of the nozzle, if the flow is subsonic:

$$\dot{m}_{sub} = p_a A \sqrt{\frac{M_{avg}}{R_{gas} T_0} \frac{2k}{k-1} \left(\frac{p_a}{p_0}\right)^{2/k} \left(1 - \left(\frac{p_a}{p_0}\right)^{(k-1)/k}\right)}, \tag{3.37}$$

with flow area A and stagnation temperature T_0 If the flow is choked, the flow will be supersonic at the exit and the mass flow is given by:

$$\begin{aligned} \dot{m}_{super} &= \rho_0 A_s \left(\frac{2}{k+1}\right)^{1/(k-1)} \left(\frac{2k}{k+1} \frac{R_{gas} T_0}{M_{avg}}\right)^{1/2}, \\ A_s &= A \; Ma \left(\frac{1 + \frac{1}{2}(k-1) Ma^2}{\frac{1}{2}(k-1)}\right)^{(k+1)/(2-2k)}, \end{aligned} \tag{3.38}$$

with sonic flow area A_s. The distinction between sub and super sonic is shown in the plot of Figure 3.11. If the flow is subsonic, the pressure at the exit will be equal to the ambient pressure. This will be true up to the sonic point. When the flow reaches the super sonic state, the exit pressure will no longer be equal to

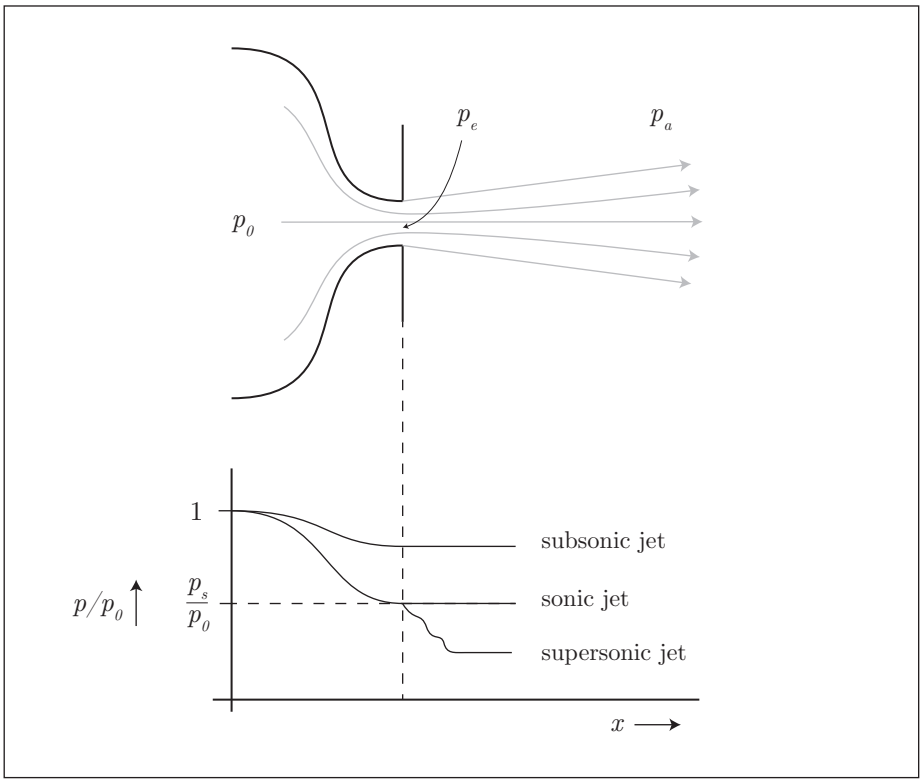

Figure 3.11: Compressible flow through a nozzle, used for modeling the exhaust. (Source: [68]).

the ambient pressure. Decreasing the ambient pressure will no longer influence the conditions inside the nozzle itself.

The model presented here will be used for estimating the performance of Concept 1, but it has to be kept in mind that influences of viscosity and heat transfer are neglected. A fully detailed analysis of the exhaust flow will consider the shear stress found in the flow, caused by the wall and the air outside the engine. Also, since the flow is compressible, shock waves can occur in this problem which can have significant influence on the flow.

To get a feeling of how important the viscus forces are, one can look at the Reynolds number. To do this, the exit pressure is fixed to ambient conditions, as the nozzle model predicts for subsonic flows (Figure 3.11). Then for different stagnation pressures, the conditions of the flow at the nozzle exit can be calculated with the model. The results are shown in Figure 3.12 and 3.13. The stagnation temperature is chosen to be 480 K, which is rather large in context of the H_2O_2 engine. This is done because of the desire to display the sonic point in the plots, which require high pressure differences. When the sonic point is reached at the exit of the nozzle, the fluid temperature has dropped considerably from the stagnation temperature, as is seen in Figure 3.12. At some point, the water vapor in the gas starts to condensate which further increases the complexity the problem. The high stagnation temperature of 480 K prevents this from happening.

With a known exit speed, the other properties can be calculated such that the Reynolds number can be evaluated. This is done in Figure 3.13, where the Reynolds number is plotted for different stagnation pressures and different nozzle radii r. In this plot the viscosity of the gas mixture is used, as it is evaluated in Appendix B. A fuel ratio f_{rw} of 0.9 is assumed. It is seen that at some point when the stagnation pressure is high enough, the Reynolds number converges to a maximum. This is because the velocity is increasing, but the density of the gas is decreasing just as fast. Also, since the properties of the gas do not depend on the radius r of the nozzle, the Reynolds number ($\rho V 2r/\mu$) is proportional to r.

Figure 3.13 shows that in most cases the Reynolds number of the flow is well above the transition region. The transition region starts at Reynolds numbers below 10^4, and indicates the switch from momentum dominated flow to viscosity dominated flow. This benefits the nozzle model, since it is based on the momentum equation of the gas, where friction is neglected. If the stagnation temperature is lowered, the viscosity of the gas is lowered (Appendix B) such that the Reynolds number will only be higher.

In terms of geometric scaling, it is observed that according to Equation (3.37) the mass flow is proportional to the area of the nozzle. The energy flowing out the nozzle depends on the specific enthalpy of the gas according to:

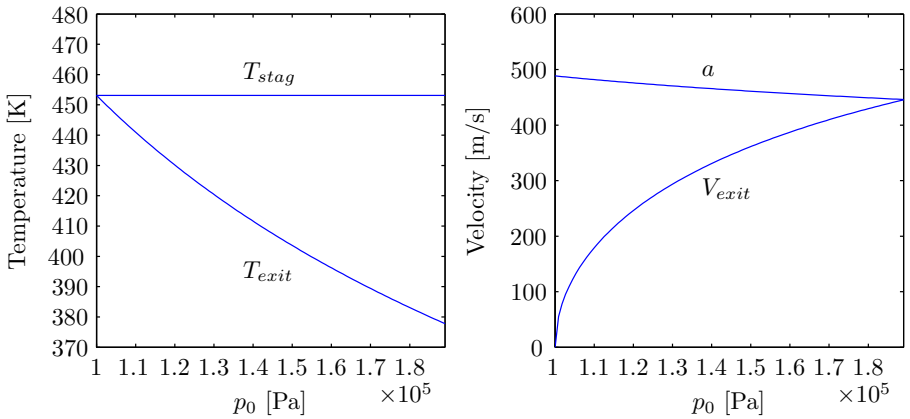

Figure 3.12: Conditions of flow through the exhaust assuming the nozzle model, with $T_{stag} = 480$ K, as function of stagnation pressure p_0. In the left plot, speed of sound a is also given. At $p_0 \approx 1.9 \cdot 10^5$, the sonic point is reached.

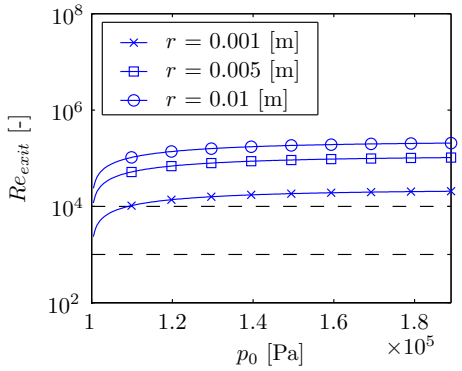

Figure 3.13: Reynolds number at the exit of the nozzle, for different stagnation pressures p_0 and different nozzle radii r. To calculate the viscosity, a fuel ratio f_{rw} of 0.9 is assumed. The Reynolds transition region is shown between the dashed lines.

$$\begin{aligned} \frac{dE_{nozzle}}{dt} &= \sum \frac{dn_i}{dt} h_i, \\ \frac{dn_i}{dt} &= \frac{dm}{dt} \frac{\gamma_i}{M_{avg}}, \end{aligned} \tag{3.39}$$

with mole fraction γ_i and molar mass M_i of species i in the gas. This means that the energy flow out of the engine is proportional the area of the nozzle. Referring back to the geometric scaling factor S_g from Section 1.3:

$$\frac{dE_{nozzle}}{dt} \propto S_g^2, \tag{3.40}$$

The nozzle model is used to model the exhaust flow found in Concept 1. In the next chapter, performance evaluations are made of both remaining concepts.

Chapter 4

Performance Evaluations

4.1 Intro

In Chapter 1, the requirements and possibilities for the FWM engine were discussed. In Chapter 2, the fundamentals of performance of engine models were explained with the Curzon Ahlborn model. Also, it was observed that Concept 2 is definitely not suitable for the FWM, a conclusion that was made by combining the Curzon Ahlborn characteristics with measurements done with real Tesla engines. In the previous chapter, the important aspects that are associated with power generation by using H_2O_2 where explained. In this Chapter, these aspects are applied to numerical models of Concept 1 and 3. With the results of these models, a first estimate is made of the performance that can be expected of these concepts. Also, for each concept a list of considerations is given, concerning both model limitations, practicalities and gut feeling.

The approach to accomplish this is similar to the method used in Section 2.5. First the initial scale of the engine is chosen. This means that the working fluid volume and other characteristic length scales are set. Then a set of engine parameters is formed, based on either an approximate calculation or trial and error. For instance, the heat transfer constants of Concept 3 can be estimated using the definition of Fourier's heat transfer. Suitable timing parameters need to be found with trial and error. In this situation, suitable means that the engine shows nearly optimal performance for the engine.

After a good set of initial parameters is chosen, the performance of the engine at the chosen scale can be evaluated. To see the effect of geometric scaling, the scaling laws can be used for engine parameters depending on physical dimensions. The other parameters that are not influenced by scaling, are changed until the optimal engine performance is found. This results in a estimate of the power output and efficiency of the two remaining concepts on different scales, which

can be used to make a design decision of the engine of the FWM. The results found using this method depend on the initial parameter estimates that are used. That is why for each concept a optimistic and a pessimistic set will be used.

4.2 Concept 3, Heat Engine

4.2.1 Model

The basis of the engine model for Concept 3 was described in Section 2.4. For reference, a schematic overview of the model is shown in Figure 4.1. Just like with the Carnot engine, there are two heat sinks. The hot heat sink with temperature T_{hot} represents the combustor of Concept 3. The cold heat sinks represents the ambient environment of the engine and has a constant temperature. As explained in Section 2.2, the sink temperatures are important for the overall performance of the engine. A higher temperature difference of the sinks generally means higher performance. In Section 3.3, it was seen that if no gas phase decomposition is used, the upper limit of the temperature of the gases released by decomposition is approximately 150°C. Higher temperatures can be obtained, but gas phase decomposition is required. In Section 3.2, it was seen that small scale systems have low Biot numbers, meaning that the external heat resistance of the system is much larger than the internal heat resistance. This means it will require a lot of effort to keep a temperature difference within the system. Combining the temperature limit of the catalytic reaction with the fact that it will be hard to maintain this temperature difference in the first place, it is considered that a temperature of 150°C for the combustor is an optimistic estimate. This is used for the optimistic parameter set. For the pessimistic set, a hot temperature of 100°C will be used. The cold sink temperature is fixed to ambient temperature.

The temperature of the heat sinks also gives an indication of which compression rate should be used, as was shown with the Carnot engine. If the optimal compression ratio for Carnot is used, it means that if the working fluid temperature is equal to the cold sink temperature at maximum volume and equal to the combustor temperature at minimum volume. To calculate the needed compression rate θ, the polytropic relation of adiabatic compression can be used:

$$\begin{aligned} pV^{\gamma} &= constant, \\ \theta = \frac{V_{max}}{V_{min}} &= \left(\frac{T_{hot}}{T_{cold}}\right)^{\frac{1}{\gamma-1}}, \end{aligned} \tag{4.1}$$

with adiabatic index γ of the working fluid. Heat loss shifts the temperature of the working fluid down over the whole cycle. Also, there might be a small

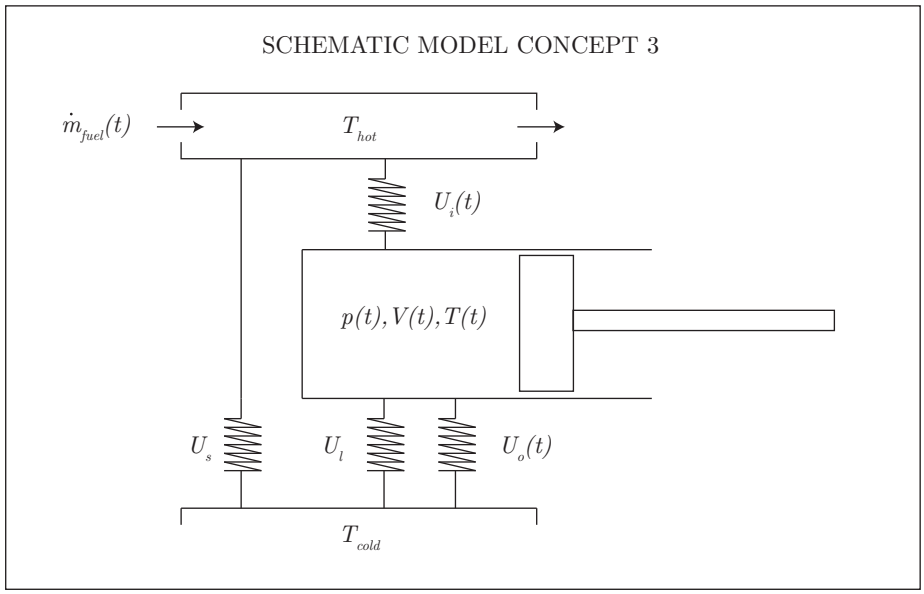

Figure 4.1: Schematic overview of the model used for Concept 3.

performance gain if the temperatures of the working fluid do not exactly match the sink temperatures, since it increases the heat transfer rate. For a first guess the value found with Equation (4.1) will be used. With a hot temperature of 150°C and a cold temperature of 20°C, this results in $\theta = 2.5$. The maximum volume of the working fluid V_{max} is determined by size restrictions of the FWM, as discussed in Section 1.2. It was observed that for the current size of the FWM, a volume of 15 cc is available for the engine. Considering that Concept 3 needs a combustor, cold heat sinks, a spring and a fuel reservoir, it is assumed here that half of the available volume can be used for the working fluid: 7.5 cc.

The working fluid is connected to the sinks via the heat conductors with heat transfer rate factors U_i of the inlet and U_o of the outlet. These are a function of time, since the working fluid switches between these two sinks in order to generate work. As shown in Figure 4.1, there are two other connections to the cold sink, which represents the heat loss of the working fluid U_l and the heat loss of the combustor U_s. One can argue if U_l should also be a function of time, since the contact area of the working fluid with the surroundings is a function of its volume. But since the total contact area of the engine itself with the environment is constant and to keep things simple, it is assumed that it is constant.

To bring the model closer to the operating principle of Concept 3, a different timing scheme is used compared to the one used in Section 2.4. The timing scheme used here is shown in Figure 4.2. The volume V of the working fluid

is a normal sinus function and as described earlier, the heat transfer factors U_i and U_o are a function of time, according to:

$$U_i = \begin{cases} U_{hot,max} \frac{V_1 - V}{V1 - V_{min}} & \text{if } t_1 < t < t_2 \\ 0 & \text{else} \end{cases}$$
$$U_o = \begin{cases} U_{cold,max} \frac{V - V_0}{V_{max} - V_o} & \text{if } t_3 < t < t_4 \\ 0 & \text{else} \end{cases} \tag{4.2}$$

where V_i represents the volume of the working fluid at time t_i. The maximum values $U_{hot,max}$ and $U_{cold,max}$ are determined by assuming a certain shape, as shown in Figure 4.3. Using Fourier's heat transfer law again for the heat transfer between the sinks and the working fluid, for the combustor and cold heat sink:

$$U_{hot,max} = \frac{k_{mat} 2\pi r_c h_c}{t_c},$$
$$U_{cold,max} = \frac{k_{mat} 2\pi r_s h_s}{t_s}, \tag{4.3}$$

with thermal conductivity k of the material and the other variables as they are defined in Figure 4.3. A higher thermal conductivity means less resistance to heat flow, which means better performance. The thermal conductivity of aluminum is $k = 27$[W/m/K], which is a representative value for most metals. This value will be a valid k_{mat} if the temperate inside the combustor and inside the working fluid are completely uniform, such that there is only a temperature gradient over the metal. In reality, there will also be a temperature gradient inside the working fluids which will also results in a resistance to heat flow. The thermal conductivity of gas is much lower compared to aluminum: $k_{gas} \approx 0.03$. This means that the gas resistance is much higher than the metal resistance and will dominated the heat transfer rate. A k_{mat} of 0.03 is more appropriate in this situation. In reality, the heat transfer between the sinks will also have a convective term. In a full detailed study, a model should be used similar to the one used in Section 3.2. Here an estimate of the length t_c and t_s will be used, which indicate the length scale of the heat affected region of the working fluid as defined in Figure 4.3. For the optimistic parameter set a length $t_c = t_s = 0.1 r_e$ will be used, for the pessimistic set $t_c = t_s = r_e$. For convenience, the dimension r_c is also fixed to the main engine radius r_e. What remains is the height of both heat sinks, w_s and h_c. By constraining the other parameters as described above, the ratio between these two dimensions has a similar role as f_c of Section 2.4:

$$f_c = \frac{w_s}{h_c}. \tag{4.4}$$

The height of the combustor h_c will be fixed to one fifth of the main engine dimension w_e. An appropriate ratio f_c will be found by trying different values

in the numerical model. For the loss term U_l and U_s, the data found with the FEM model in Section 3.2 can be used. For the shape correction factor of Equation (3.8), a width over diameter ratio of 4 is assumed for Concept 3:

$$\begin{aligned} w_e &= 8r_e, \\ U_l &= U_{fit}\frac{w_e}{2r_e} = 4U_{fit}, \end{aligned} \tag{4.5}$$

where w_e is the height of the cylinder used in the FEM model of Section 3.2, in this case representing the largest dimension of the engine. For the heat loss of the combustor, the correction factor becomes:

$$U_s = \frac{h_c}{2r_c}U_{fit} = \frac{0.2w_e}{2r_e}U_{fit} = \frac{4}{5}U_{fit}. \tag{4.6}$$

This is based on the drawing of Concept 3 shown in Section 1.6 and Figure 4.3. As explained, the sketches for the concepts are based on intuition. Further investigation should indicated if the shapes assumed for the concepts are in any realistic bounds. The form factor used in Equation (4.5) can also be used to couple the maximum working fluid volume V_{max} to radius of the engine r_s:

$$\begin{aligned} V_{max} &= w_e A = 8\pi r_e^3, \\ r_e &= \left(\frac{V_{max}}{8\pi}\right)^{1/3}. \end{aligned} \tag{4.7}$$

The remaining parameters are the contact times of the sinks and the working fluid, t_{inlet} and $t_{exhaust}$ defined as shown in Figure 4.2. The duration of the energy exchange periods of the cycle are a trade off between power and efficiency. Longer periods generally means more energy exchange, which results in more power but less efficiency. Just like was done in Section 2.3, two timing parameters are defined as:

$$\begin{aligned} f_i &= \frac{t_{inlet}}{0.5t_{cycle}}, \\ f_e &= \frac{t_{exhaust}}{0.5t_{cycle}}. \end{aligned} \tag{4.8}$$

These two parameters need to be tuned by hand in order to get a cycle with reasonable performance. For a f_i and f_e of 1, the power will be highest but the efficiency lowest. The maximum efficiency is obtained when these parameters approach zero, as shown in Section 2.4.

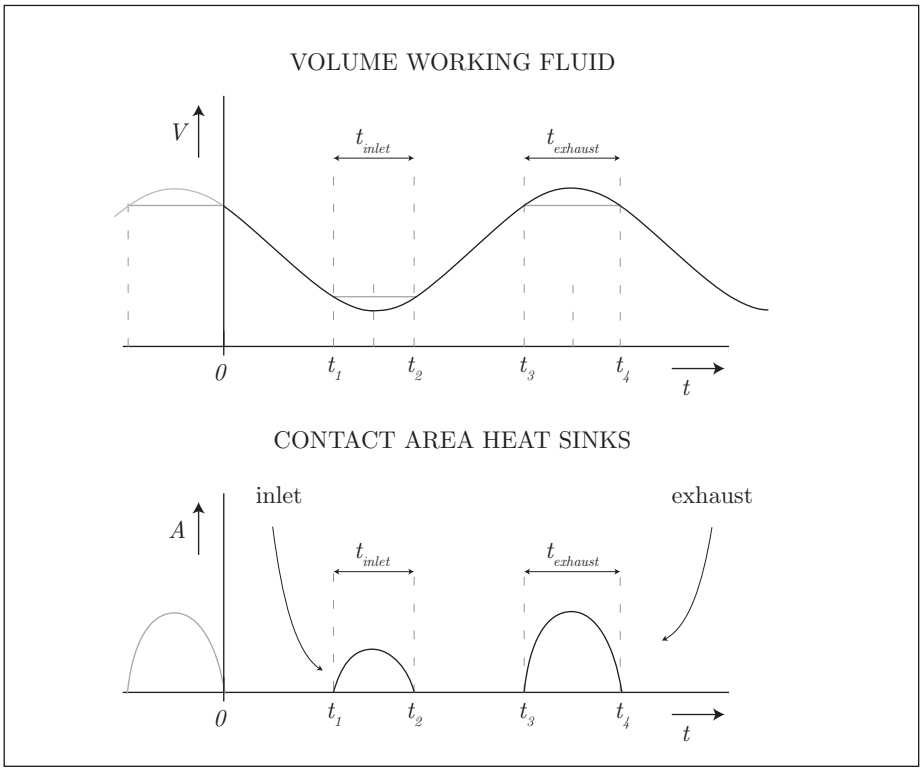

Figure 4.2: Timing used for the model of concept 3. Top: volume of working fluid. Bottom: contact area between working fluid and heat sinks of the engine.

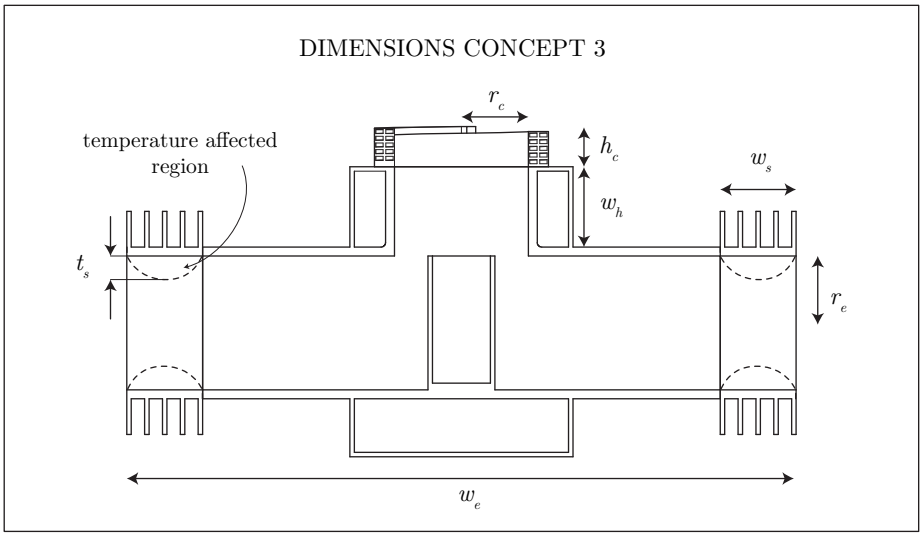

Figure 4.3: Definition of dimensions used for form factors of Concept 3

The missing component of the model for Concept 3 is the combustor efficiency. In steady state and honoring the mass balance, just a much mass has to leave the combustor as is coming in. Since the gas leaving the combustor will have energy in it, the engine efficiency is further reduced. To account for this loss, one can look at how much mass needs to enter the combustor for every unit of energy that goes into the working fluid. An equal amount of mass needs to leave the combustor with a certain reduced energy content. In the ideal situation, all the energy released from the decomposition is still inside the gas when it enters the heat exchange area. Per unit of mass of fuel, this energy e_{in} [J/kg] is equal to:

$$e_{in} = \left[\frac{f_{rw} h_{h2o2}}{M_{h2o2}} + \frac{(1 - f_{rw})\, h_{h2o}}{M_{h2o}} \right]_{T_{in}}, \tag{4.9}$$

with molar mass M_i and molar enthalpy h_i of species i at the inlet temperature T_{in}. The ratio f_{rw} indicates how much H_2O_2 is in the fuel per kilogram. Assuming that no hydrogen peroxide is evaporated, the molar ratios of the species in the gas at the exit of the combustor are given by the stoichiometry of the decomposition:

$$\begin{aligned} & a\ H_2O_2 + b\ H_2O \rightarrow c\ H_2O + d\ O_2, \\ & a = \frac{f_{rw}}{M_{h2o2}}, \\ & b = \frac{1 - f_{rw}}{M_{h2o}}, \\ & c = a + b, \\ & d = 0.5a. \end{aligned} \tag{4.10}$$

Note that both sides of Equation (4.10) represent one kilogram of matter. The energy that leaves the exit e_{exit} per unit mass is given by:

$$e_{out} = [h_{h2o} c + h_{o2} d]_{T_{exit}} \tag{4.11}$$

The other energy outlet of the combustor is via heat loss, $\dot{Q}_s$, which will be modeled according to Fourier's heat transfer law with use of the linearized heat transfer constant U_s. The effective heat transfer to the working fluid $\dot{Q}_{in}$ is also modeled with Fourier's law, just like was done in Section 2.4:

$$\begin{aligned} \frac{dQ_s}{dt} &= U_s \left(T_{hot} - T_{cold}\right), \\ \frac{dQ_{in}}{dt} &= U_i \left(T_{hot} - T\right). \end{aligned} \tag{4.12}$$

At this point, one could introduce a finite heat capacity of the combustor into the model, such that a time dependence of T_{hot} is obtained. Here the decomposition rate becomes important, because it needs to be set such that the average temperature of the combustor remains at a acceptable level. Then the fluid flow resistance becomes important, since it determines how much hot gas is present inside the combustor and how fast the gas goes trough it. For the model, it means that direct control is lost over the combustor temperature T_{hot}, the most important parameter of the engine.

To avoid dealing with the complexity of the decomposition and to keep the interpretation of the phenomena seen in the results of the model simple, a constant uniform temperature of the combustor is assumed. It implies that just enough fuel is decomposed in order to keep the temperature in the combustor constant:

$$\begin{aligned} T_{hot} &= constant, \\ T_{exit} &= T_{hot}. \end{aligned} \tag{4.13}$$

Using the energy balance of the combustor and the constant temperature assumption, the following governing equation for the combustor results:

$$\frac{dm_{fuel}}{dt}\left(e_{in} - e_{out}\right) = \frac{dQ_s}{dt} + \frac{dQ_{in}}{dt}, \tag{4.14}$$

with fuel mass flow $\dot{m}_{fuel}$. The combustor efficiency η_c is defined as the amount of energy flowing into the working fluid Q_{in} divided by the amount of energy E_{max} that could have been extracted from the hydrogen peroxide. Note that E_{max} is equal to the reaction enthalpy times the amount of H_2O_2 that is used:

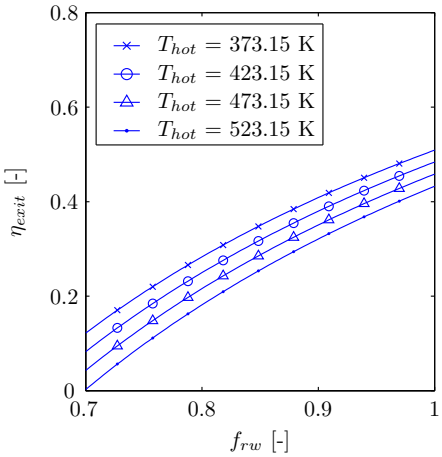

Figure 4.4: Efficiency of the combustor concerning only the exit losses via the gas flow, plotted against the fuel mass ratio for different combustor temperatures.

$$
\begin{aligned}
E_{max} &= m_{fuel} a \left[h_{h2o2} - h_{o2} + h_{h2o} \right]_{T_{env}} , \\
\eta_{thermal} &= \frac{Q_{in}}{Q_{in} + Q_s}, \\
\eta_{exit} &= \frac{e_{in} - e_{out}}{a \left[h_{h2o2} - h_{o2} - h_{h2o} \right]_{T_{env}}}, \\
\eta_c &= \frac{Q_{in}}{E_{max}} = \eta_{thermal} \eta_{exit},
\end{aligned}
\tag{4.15}
$$

where m_{fuel} is the total amount of fuel that is used in a period t, Q_{in} the heat energy absorbed by the working fluid of the cylinder and Q_s the heat energy lost to the environment via the combustor. The last equation reveals the characteristic of the model of the combustor. The efficiency $\eta_{thermal}$ depends on the heat flows across the combustor boundary. If the heat loss Q_s is large, the efficiency of the combustor will be small. The second efficiency η_{exit} shows how much of the energy entering via the inlet is lost in the form of hot gases leaving the exit, even if no heat is extracted from the combustor at all. It depends on the fuel ratio f_{rw} and the combustor temperature, both dependencies are plotted in Figure 4.4.

It is seen that maximum obtainable efficiency of the combustor is obtained when the fuel ratio is highest, without considering the heat loss $\dot{Q}_s$. This can be explained looking at the required mass flow $\dot{m}_{fuel}$. When the fuel ratio is low, the gas at the exit contains relatively much water vapor, which has a lot of evaporation energy in it. Therefore, the energy that is available to do work is much smaller for a small fuel ratio's. Hence, to keep a constant temperature, the mass flow needs to be large and a lot of heat is lost via the exit. The total efficiency of the engine η is defined by both the combustor efficiency and the efficiency η_w of the work generation process of the cylinder:

$$\eta = \eta_c \eta_w \tag{4.16}$$

The constant temperature assumption has influence on both the power production capabilities of the engine and on the engine efficiency. In reality, the average combustor temperature will always be lowered if the cylinder working fluid extracts some energy from it. For the produced power, it means it will be lower since a lower average temperature means less power. For the combustor, a lower average temperature means less heat loss Q_s and less energy in the exit gases so η_c is lower with the constant temperature assumption. For the efficiency η_w, it is less clear what the influence of the assumption is. A lower inlet temperature means that less heat flows into the working fluid and so less heat is lost. But the Carnot efficiency will be lower because of the lower inlet temperature. Looking at the other projects at similar scale in Section 1.4, it is likely all the power that can be generated with Concept 3 is needed for the FWM. So in reality the engine will be set up such that there is a high average combustor temperature and the exit temperatures are hot.

The search method of the numerical experiment done in Section 2.5, which will also be used here, might take advantage of this assumption. If the heat capacity of the combustor is small and the cycle time of the engine is short, the fuel needs to be decomposed very rapidly in order to keep a constant temperature of the combustor. If this is not possible, considering the nature of the catalytic decomposition described in Section 3.3, the model might show unrealistic high performance. Fortunately, the total heat capacity of the combustor and the working fluid both are proportional to their volume, so the validity of this assumption is not influenced by scaling.

4.2.2 Experiments

With the combustor added to the engine model of Section 2.4 and the other modifications described above, the engine performance can be evaluated numerically. The engine model described in Section 2.4 was set up such that the steady state can be calculated analytically. In this situation, the equations are too complex. That is why the following procedure is used to find the steady state of the engine, shown schematically in Figure 4.5. First an initial working

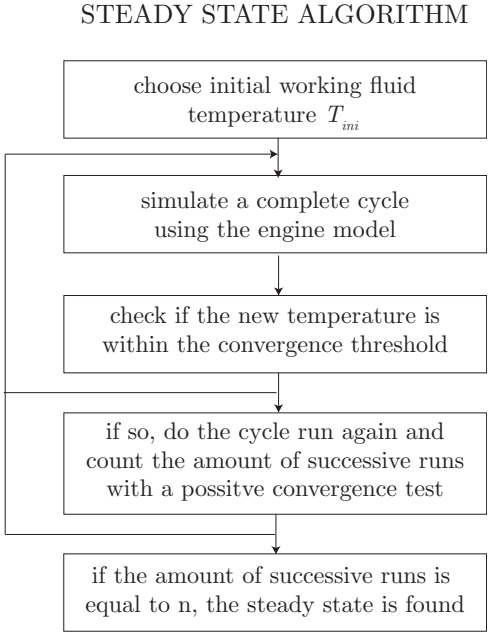

Figure 4.5: Algorithm to find the steady state of the model described in this section. The convergence test is given by Equation (4.17)

fluid temperature is assumed. Then using the differential equation of the model, a complete cycle is simulated. At the end of this cycle, a new working fluid temperature is obtained. If this new temperature is within the convergence threshold, the engine is considered at its steady state. This algorithm can be tested using the analytical model of Section 2.4. While doing that, the following convergence test has proven to work:

$$\frac{T_{new} - T_{old}}{T_{old}} < 10^{-5}, \tag{4.17}$$

with T_{old} as the working fluid temperature at the beginning of the cycle and T_{new} as the working fluid temperature after one complete cycle has passed. As a second test, the algorithm searches for three successive cycle runs with a positive convergence test (n=3 in Figure 4.5). For large cycle times, it is likely that the temperature at the end of the heat dump step of the cylinder is equal to the ambient temperature. To reduce the number of iterations, this temperature is used as initial temperature T_{ini} for the algorithm.

Now that the steady state of the engine is found, a suitable set of parameters can be tested to find an engine layout with suitable engine performance. For the parameters of the engine that depend on geometrical dimensions or on physical

Parameter	Optimistic Set	Pessimistic Set	Unit
T_{hot}	423	373	K
T_{cold}	293	293	K
V_{max}	$7.5{\cdot}10^{-6}$	$7.5{\cdot}10^{-6}$	m^3
k_{mat}	0.03	0.03	W/m/K
r_e	$6.7{\cdot}10^{-3}$	$6.7{\cdot}10^{-3}$	m
w_e	$5.4{\cdot}10^{-2}$	$5.4{\cdot}10^{-2}$	m
t_e,t_s	$6.7{\cdot}10^{-4}$	$6.7{\cdot}10^{-3}$	m
h_c	$1.1{\cdot}10^{-2}$	$1.1{\cdot}10^{-2}$	m

Table 4.1: Parameters used for the numerical simulations of this section.

properties, an estimated was given of what might be expected in a optimistic and pessimistic situation. Note that in Section 2.4 it was found that for these types of engines the performance mainly depends on a certain potential to generate work, which for the EB model was given as $C_h T_h$. Since the model of Concept 3 described in this section and the EB model have the same fundamentals, it is assumed that this is also true for the model of Concept 3. That means that the potential to generate power is the same, $U_{hot,max}T_{hot}$, although different symbols are used. The other parameters determine how well this potential is utilized by the engine, but it was shown that for this type of engines the utilization is only determined by the ratio's between the parameters. For example, if a characteristic volume of the working fluid is decreased by 50%, there is a new cycle time such that the utilization of the power potential is the same. In this case, the power potential does depend on the volume via Equation (4.3) and (4.7), so the absolute maximum power would be influenced by the decrease in volume. For details, see Section 2.3 and 2.4. Note that after the previously desribed constrains on the engine parameters, the only remaining ratio parameters that are free to choose are the compression ratio θ, inlet timing f_i, exit timing f_e and heat conductance ratio f_c

Our main concern is the power potential $U_{hot,max}T_{hot}$. For the combustor temperature, a optimistic and a pessimistic value was given based on the nature of the catalytic reaction. For the heat conductance of the combustor, an estimate was made base on the definition of the heat conductance constant in the Fourier law. This approach might be too simplistic since it neglects effects like convection. To be absolutely certain that the made estimates are in the correct order a more detailed study is needed. This was done for the case of the heat transfer to the environment, described in Section 3.2. So with relative certainty, it can be said that U_l is correct for this engine. Note that with the made assumptions, $U_{hot,max}$ is 15 times larger than U_l for the optimistic parameter set. This is 1.5 times for the pessimistic set. It is assumed that this is achievable for the FWM engine.

Parameter	Optimistic Set	Pessimistic Set
θ	2.4	1.8
f_i	0.5	0.9
f_e	0.6	0.9
f_c	5	5

Table 4.2: Parameters used for the numerical simulations of this section.

The compression ratio θ, inlet timing f_i, exit timing f_e and heat conductance ratio f_c determine how well the available power potential is used. An appropriate set of these parameters has to be found by hand tuning the model. For the compression ratio, a first estimate is given by the Carnot engine. The timing ratios have a range between 0 and 1. In Section 2.4 it was shown that when they approach zero, the engine efficiency approaches to a maximum. When close to one, then during almost half of the cycle the inlet is open and the other half the outlet is open. This will result in bad efficiency, so a balance between power and efficiency has to be chosen. Note that in Section 1.2 is was seen that if 5% of the energy contents of hydrogen peroxide can be used, the FWM has enough power available to hover approximalty 6 minutes. In real situations the FWM probaly needs more power than just for hovering, but the 5% efficiency will be used as guide line. The remaining parameter is the ratio between the heat conducatances f_c. In Section 2.3 it was seen that the power output improves for larger f_c until it converges to a limit, see Figure 2.7. So idealy f_c is very large, but in reality it is constrained by size and weight limits of the engine. Here a ratio of 5 is assumed.

For the hand tuning of the parameters θ, f_i and f_e, a search method similar to the one described by Figure 2.17 is used. A certain parameter set is chosen, the steady state is found using the algorithm of Figure 4.5 and the performance is evaluated. This is repeated for every possible cycle time. The maximum power that is found is labeled as the performance of the engine using the chosen parameter set. The results of these steps are shown in Table 4.2.

4.2.3 Results

For the optimistic set, the maximum power output is 0.1 W with an efficiency of 11%. For the pessimistic set, the maximum power output is 6 mW with an efficiency of 4%. To translate these results back to the requirements of the FWM descibed in Section 1.2, one needs to look at the power density of the engine. For this, a certain function for the mass of the engine is needed. Here the shape of Concept 3 is assumed as it was drawn in Figure 1.16. The volume V_{mat} of the material that makes up the engine can be obtained from the 3d model, which results in the following volume function:

$$V_{mat} = 0.02 w_e^3. \tag{4.18}$$

Assuming that the entire engine is constructed from aluminum results in an engine weight of 8 gram. This is a very rough estimate of the engine mass, since the 3d model of Figure 1.16 is not designed based and requirements and constrains but by intuition. An actual realization of this engine might weigh less because the design used here is over dimensioned. Including 4 grams of fuel and the 0.6 gram of the FWM, a total system mass of approximately 12.6 gram is obtained. Using the optimistic parameter set, it would have a power density of 7.9 W/kg. As was indicated in Section 1.2, the needed power density of the current FWM design is around 125 W/kg, while nature needs a power density of 30 W/kg. It is clear that the power output is too low or the volume of the engine is too large. To see what happens with the power output if the engine volume is reduce, geometric scaling is applied to the model.

4.2.4 Scaling

Just like was done with EB model in Section 2.5, geometric scaling can be applied to the model in this section. This analysis will indicate what happens with the performance of Concept 3 if the volume is reduced. To do this all dimensions used in the model described above are scale with scaling factor S. As reference scale, the dimensions described above are used such that they correspond to $S = 1$. For example, if a scaling factor of 0.5 is applied it means the new engine will have a maximum working fluid volume of:

$$V_{max} = 7.5 \cdot 10^{-6} S^3 = 9.38 \cdot 10^{-7}. \tag{4.19}$$

Based on the results of Section 2.5, one could expect that the power density scales with a exponent of -2. Reducing the system size to one tenth of the dimensions used above, the expected power density would be a factor 100 higher. In Section 2.5 all the ratio's of the model were kept constant during the scaling analysis. Here this is a problem, since the loss terms U_l and U_s scale differently then $U_{hot,max}$ and $U_{cold,max}$. First the loss ratio's are defined, similar as was done in Section 2.4:

$$\begin{aligned} f_l &= \frac{U_l}{U_{hot,max}}, \\ f_s &= \frac{U_s}{U_{hot,max}}. \end{aligned} \tag{4.20}$$

In Section 2.4 the loss term was modeled via Fourier's law, similar as the inlet heat flow and outlet flow. Here the two loss terms are modeled based on the

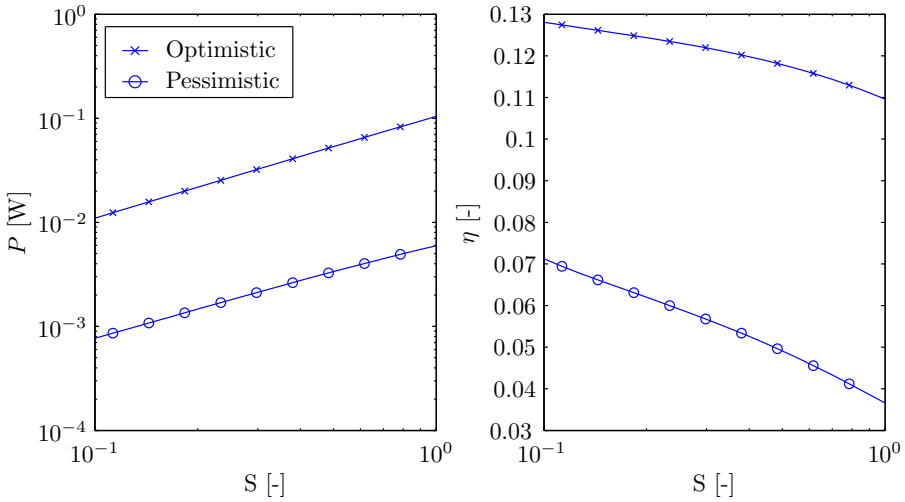

Figure 4.6: The performance of Concept 3 as function of its scale. At the initial scale $S = 1$ the dimensions described above are used. Left: power output for both optimistic and pessimistic parameter set. Left: efficiency of engine.

FEM analysis results of Section 3.2. There a scaling exponent of approximately 1.5 was found, which is different from the unit exponent when the Fourier law is assumed. For the scaling analysis this means that the ratio's f_l and f_s cannot be kept constant. Since the loss terms have a higher scaling exponent compared to the heat inlet and outlet flows, it is expected that the model efficiency increases as the scale is reduced. This could be compensated by shifting the other ratio's to a setting with more power output, but since the precise influence of these ratio's is not known this is not attempted here.

To see if Concept 3 has potential when its size is decrease, its performance is evaluated for a scaling factor between 0.1 and 1. The results are shown in Figure 4.6. Is is seen that the power scales with a exponent of approximately 1. As was expected, the efficiency increases when the scale is reduced. This is more the cases for the pessimistic parameter set, because the loss term is more dominant there. These results can be translated back to the power density of the complete FWM system. Assuming that the mass of the FWM system scales with its volume, the power density is shown for both the optimistic and pessimistic set in Figure 4.7. This plot also shows the required power density, based on what the current FWM mechanism needs and what is found in nature.

4.2.5 Conclusions

The results show that Concept 3 is not suited for the FWM in its current size. The power density is too low. When the geometric dimensions of the engine

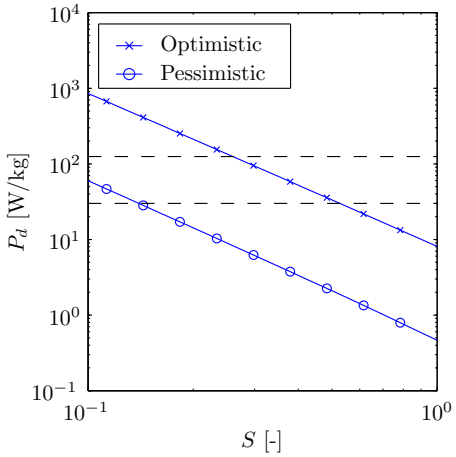

Figure 4.7: Power density of the FWM system when Concept 3 is used. The upper dashed line is the power density requirement of the current FWM design, the lower line is the power density found in nature (Hawkmoth).

are decreased, the power density increases because the power output is linear with the scaling factor S. Figure 4.7 shows that it is expected that the power density approaches the right order when the scaling factor is lower then 0.2. This corresponds to $w_e = 5.4 \cdot 10^{-2} S = 1.1 \cdot 10^{-2}$ [m]. So either the scale of the FWM must be reduced, or a multiple of small scale Concept 3 type engines must be used for the FWM.

The results are the outcome of a model that uses a variety of assumptions. A certain shape of the engine is used in the model to relate working fluid volume, heat sink dimensions and engine weight to each other. Other shapes and engine layouts might results in different relations between these model parameters, but it is not expected that this has much influence on the performance results.

The inlet and outlet heat conductances are approximated using Fourier's law and were verified using the linearized heat loss conductance. Since these parameters are important for the engine performance, these should be verified with a more detailed analysis before this concept is taken to a next step.

The pressure and temperature of the working fluid are assumed to be uniform. The uniform pressure assumption will be valid in these small scale systems, considering the speed of sound and the small dimensions. The time constant for the unsteady temperature response of the working fluid is given by [61]:

$$t_c = \frac{L^2 c_v n}{kV} \tag{4.21}$$

with characteristic length L [m], working fluid heat capacity c_v [J/K/mole], amount of working fluid n [mole], working fluid volume V and thermal conduc-

tivity k [W/m/K]. Using the values of the model described above results in a t_c around 30 seconds, which shows that the uniform temperature assumption might not be valid. This means that the effective heat capacity of the working fluid is lower than what might be expected using the uniform assumption. For instance, when the working fluid comes into contact with the combustor its temperature will increase faster and less energy will flow into it. This is also one of the aspects that should be examined more closely.

The combustor temperature is assumed to be uniform and the heat loss of the combustor to the other parts of the engine is neglected. In reality it becomes more difficult to maintain a temperature gradient when the engine scale is reduced, since the Biot number will become even smaller. This means that the external resistance to heat transfer is much larger than the internal resistance. A relatively large heat conducting barrier must be applied at small scales, which can only increase the system weight.

The constrains of the catalytic reaction are not considered. Note that the shown results mainly depend on the inlet temperature and heat conductances of the engine. To deal with uncertainties and model simplifications, both a optimistic and pessimistic parameter set were used. One has to keep in mind that shown results are only valid for engine with operating conditions that closely resemble the model.

4.3 Concept 1, Two Stroke Engine

4.3.1 Model

The basis of the model for the first concept is the decomposition model presented in Section 3.3. By adding a variable volume function for the chamber in which the droplet is decomposed, work is generated. The energy leaves the engine via fluid flow, which was discussed in Section 3.4. The combination of these different models results in a system with 3 gases, of which 2 can be at or above the saturation temperature, a droplet that can be below, at, between and again at the saturation temperatures of H_2O and H_2O_2 and a exhaust port that can either be open or closed. Each combination of these states results in a different set of differential equations and constraints. For reference, a sketch of Concept 1 is shown in Figure 4.8. Note that the engine is completely symmetrical. In the model only one side will be considered. To get the performance of the complete engine, the power and weight are multiplied by 2.

Most of the equations needed for this model are given in Sections 3.3 and 3.4. New is that the volume is variable, so a new differential for the pressure is obtained. Again, the ideal gas law is assumed:

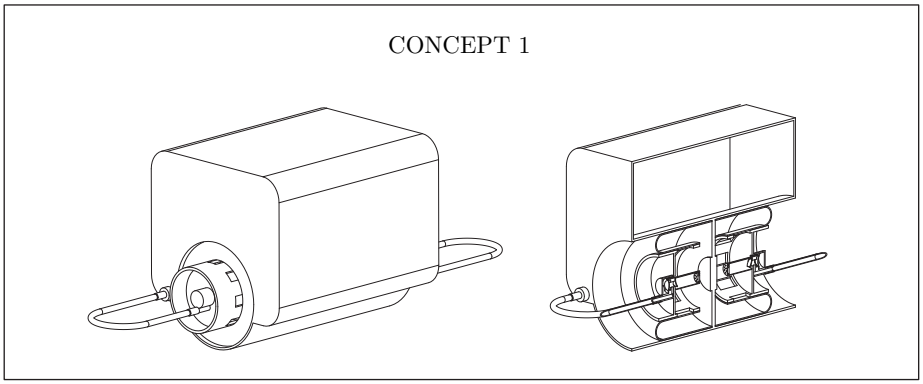

Figure 4.8: Drawing of Concept 1 as it was presented in Section 1.6

$$
\begin{aligned}
p &= \frac{R_{gas}}{V} \sum_i \left[n_i T_i \right], \\
\frac{dp}{dt} &= \frac{R_{gas}}{V} \left(\sum_i \left[\frac{dn_i}{dt} T_i \right] + \sum_i \left[n_i \frac{dT_i}{dt} \right] + \sum_i \left[n_i T_i \right] \frac{1}{V} \frac{dV}{dt} \right)
\end{aligned}
\tag{4.22}
$$

with universal gas constant R_{gas}, amount of species n_i and temperature T_i of species i. The chamber volume V is constrained to a sinus function:

$$
\begin{aligned}
\theta &= \frac{A_1 + A_2}{A_1 - A_2}, \\
V &= A_1 + A_2 sin(\omega t),
\end{aligned}
\tag{4.23}
$$

with compression ratio θ. The start of the decomposition of the fuel is constrained to the time t_1 when the volume of the cylinder is at its minimum. Just like with normal combustion engines, there might be a small performance gain when the start of decomposition is slightly before the minimum volume point. This is not considered here. The volume V and the point in time t_1 are shown schematically in Figure 4.9.

The pressure inside the cylinder is assumed to be uniform, considering the small dimensions of the engine, the aimed cycle time for the FWM and the speed of sound. The different gases (oxygen gas, water vapor and hydrogen peroxide vapor) each have there own temperature. In Section 3.3 this was a problem because the heat transfer rate between two gases in one cylinder is unknown. In this situation, where the cylinder will be at steady state, it is expected that the gases will be at almost equal temperature and the fitted parameters of Section 3.3 will have less influence.

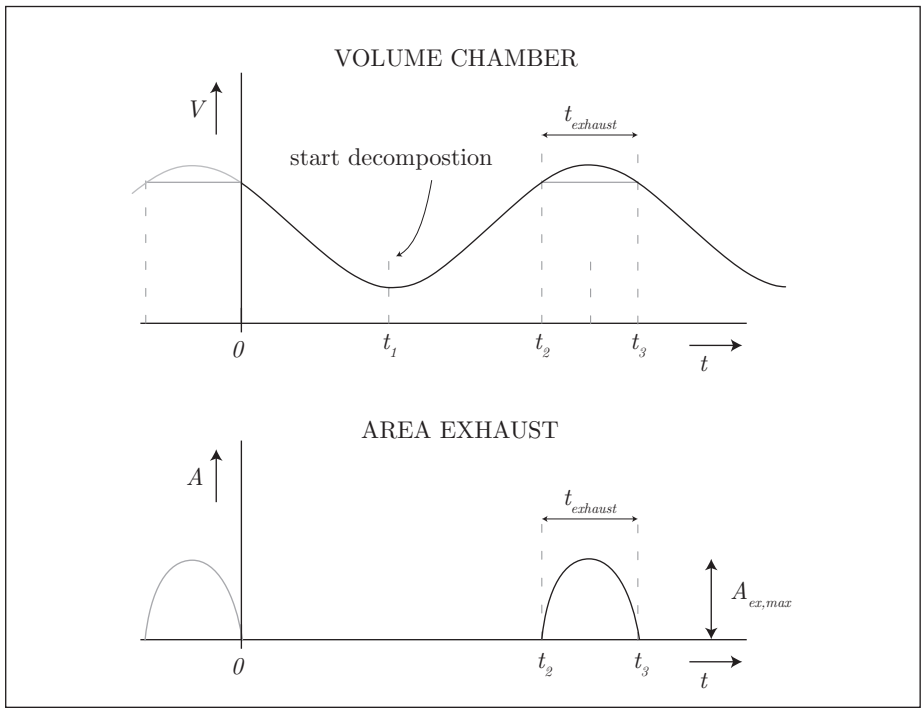

Figure 4.9: Timing used for the model of Concept 1. Top: volume of working fluid. Bottom: area of exhaust opening.

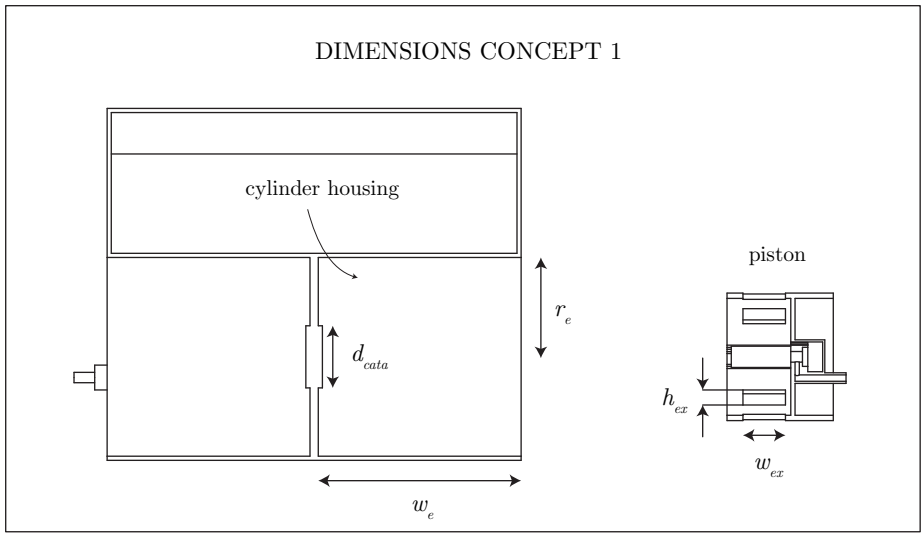

Figure 4.10: Definition of dimensions used for form factors of Concept 1. Left: cross section of the engine housing. Right: cross section of the piston. For a perspective view see Figures 1.14 and 4.8.

The exhaust is given a variable function for its flow area, depending on the position of the piston. The used function is shown schematically in Figure 4.9. The maximum area of the exhaust $A_{ex,max}$ is one of the parameters for which an appropriate magnitude needs to be determined. To do this, a certain shape of the engine is assumed just like was done for Concept 3. The assumed shape is based on the sketches of Concept 1 shown in Figure 4.8. The definition of the different dimensions is shown in Figure 4.10. Just like was done in the previous section, all dimensions will be related to the maximum working fluid volume of the engine:

$$V_{max} = w_e \pi r_e^2. \tag{4.24}$$

with cylinder radius r_e and cylinder width w_e. For this model, a shape is assumed such that:

$$\begin{aligned} w_e &= 2r_e, \\ w_{ex} &= 0.25r_e, \end{aligned} \tag{4.25}$$

with exhaust port width w_{ex}. Note that there are 8 exhaust ports in the pistons of Concept 1. The resistance the fluid flow plays a similar role as the resistance to heat conductance at the cold sinks of Concept 3. In Section 2.3 it was observed that the engine performance benefits if the exit resistance to energy flow is as small as possible. The flow of energy through the exhaust was given in Section 3.4 by:

$$\frac{dE_{out}}{dt} = \frac{dm}{dt} \sum \frac{\gamma_i h_i}{M_{avg}}, \tag{4.26}$$

with mass flow $\dot{m}$, average molar mass M_{avg}, molar ratio γ_i and enthalpy h_i of species i. The mass flow is given by Equation (3.37) and is proportional to the exhaust area A_{ex}. Note that in Section 3.4 the assumed shape of the exhaust was a round nozzle. The shape of the exhaust will have an influence on the performance of Concept 1, but is beyond the scope of this thesis. That is why even though Concept 1 has 8 square exhaust ports, it is assumed that they behave as 8 round nozzles with an area given by:

$$A_{ex} = w_{ex} h_{ex}. \tag{4.27}$$

Similar to the approach of the previous section, an optimistic and pessimistic value is used for the exhaust area. The width of the exhaust was constrained to the other dimensions of the engine, so the height h_{ex} is changed per parameter set. For the optimistic set $h_{ex} = 0.1r_e$ and for pessimistic set $h_{ex} = 0.05r_e$.

With the form factor used in Equation (4.25), the linearized equation for the heat loss factor of Section 3.2 can be used again. With a diameter of height ratio of 1, the resulting loss factor becomes:

$$\begin{aligned} U_{loss} &= U_{fit}(r_e), \\ \frac{dQ_{loss}}{dt} &= U_{loss}\left(T_{env} - T_{wf}\right), \end{aligned} \tag{4.28}$$

with working fluid temperature T_{wf} and environment temperature T_{env}. Concept 1 uses a pump to transport the fuel from the tank to catalytic surface. This pump will have influence on the performance of the engine and perhaps even is a bottle neck, but that is not the main interest of this section. Perhaps other methods are better suited to deliver the fuel to the catalytic surface. Therefore, the pump is considered ideal in this model. In that case, the resistance to energy inflow originates from the catalytic reaction:

$$\frac{dE_{in}}{dt} = k_{react} A_{contact} C_{fuel} \Delta h, \tag{4.29}$$

with reaction rate constant k_{react}, contact surface area $A_{contact}$ between the catalytic material and the fuel, fuel concentration C_{fuel} and decomposition enthalpy Δh. The reaction rate depends greatly on the type of catalyst and in what condition it is, as was observed in Section 3.3 and by A.J.H. Meskers [60]. For the optimistic set, a value of 0.04 [$1/m^2/s$] is used, for the pessimistic set 0.01 [$1/m^2/s$]. From Section 3.3 it is known that when a drop of fluid hits a flat surface, it approximately has the shape of a hemisphere. It was also observed that during evaporation, the contact area between the drop and the surface remains constant. Therefore, $A_{contact}$ is given by:

$$\begin{aligned} A_{drop} &= \pi^{1/3}\left(1.5 V_{drop,ini}\right)^{2/3}, \\ A_{contact} &= n_{drops} A_{drop}, \\ V_{fuel} &= n_{drops} V_{drop,ini}, \end{aligned} \tag{4.30}$$

with the initial fuel drop volume $V_{drop,ini}$ and amount of drops n_{drop}. The maximum contact area possible depends on the amount of droplets that can be generated and the available catalytic surface area. Note that $A_{contact}$ only influences the rate at which the fuel is decomposed. Referring back to the model of Concept 3 of the previous section, it has a similar influence on the performance of the engine as the contact area between the working fluid and the heat sinks. It is known that if $A_{contact}$ is larger, the maximum power output of the engine is larger.

Based on literature describing droplet evaporation on hot plates, it was suggested in Section 3.3 that the the effective contact area between the catalytic surface and drop might have a more complicated relation as Equation (4.30) suggests. This is not considered in this model for now. The only consequence this more complicated relation could have for the engine is that more catalytic surface area is needed to provide the same rate of decomposition. To deal with these uncertainties, a optimistic and pessimistic value for $A_{contact}$ is assumed. For a optimistic setting $A_{contact} = 0.125\pi r_e^2$, for a pessimistic setting $A_{contact} = 0.0625\pi r_e^2$.

An important parameter is the amount of fuel that is used per cycle. In this model it is controlled by the total volume of the fuel drops V_{fuel}. Note that this volume determines how long the decomposition process can go on, which was called the consumption time in Section 3.3. It will play a similar role as the product $f_i t_{cycle}$ had in the previous section. It determines how much energy is put into the engine during every cycle. The compression ratio θ and the exhaust timing $t_{exhaust}$ determine how much of that energy is converted into mechanical work by the piston. A larger compression ratio means that more energy can be extracted, which in turn means that the drop volume can be increased. For the optimistic set, a compression ratio of 3 is assumed, for the pessimistic set $\theta = 2$. This might seem low compared to more traditional engines which can reach ratio's up to 14. It is not likely these values will be reached at small scale. The conventional piston cylinder assemblies experience a lot of leakage, as was observed in Section 1.4. Other approaches that uses flexible materials, like Concept 1, depend on the maximum stress of that material. High compression ratios means that large pressures and temperatures are reach by the working fluid. Most materials that are flexible cannot cope with such heat or pressure.

The volume of the drops and the exhaust timing will be tuned such that the performance is close to what is needed for the FWM specs, which means an efficiency above 5% and 1 W power output. This will have to be done by hand, as is explained next.

4.3.2 Experiments

To find the steady state of the engine, a similar procedure is used to that shown in Section 4.3. A certain initial condition is assumed, which is used as starting point for multiple cycle simulations. After every run the engine comes closer to its steady state operation. Since there is no single parameter to judge if the engine has reached this state, the power output is used as convergence test:

$$\frac{P_{new} - P_{old}}{P_{old}} < 10^{-3}, \tag{4.31}$$

with the power output of the current cycle P_{new} and of the previous cycle P_{old}.

An attempt was made to mold the model of this section into a similar format as was done for the EB model. Even though there are some similarities between the EB model of Section 2.4, no relation was found between the power output and the dimensional parameters of the model of this section. From the equations it is known that both the energy inflow and outflow depend on a characteristic area and therefore are proportional to S_g^2. But since there are more complicated effects in this model, it is suggested that this relation is more complicated than it was for the EB model. For instance, the volume of the fuel drops has an influence on the amount of energy inflow but also on the amount of working fluid n.

Therefore, the procedure to find the optimal power of the engine as it was used in the previous section will not work for this model. There is no guarantee that the maximum engine power is found by only changing t_{cycle} and keeping the ratio's between the dimensional parameters constant. So instead of hand tuning the ratio's between the parameters of the model, the parameters need to be adjusted until a good setting is found. This is done for both the optimistic and pessimistic set, for which the parameters are listed in Table 4.3. The cycle time is fixed to 30 Hz, the opted cycle time for the FWM in its current size.

For the fuel ratio $f_r w$ a value of 0.9 is chosen. While it was observed in Section 3.3 that some part of the fuel is evaporated using high concentration fuel, it does result in the highest temperatures in the engine. This means that less water and hydrogen peroxide are condensed during the expansion of the cylinder. Even for pure hydrogen peroxide as fuel, still some condensation was observed of the gases. This means that there is a liquid build up in the engine during operation. This prevents the model from finding a steady state. To prevent this, after every cycle of the engine a certain percentage of the present liquids is removed from the engine, according to:

$$V_{liq,new} = r_d V_{liq,old}, \tag{4.32}$$

where r_d is called the drain ratio, $V_{liq,new}$ and $V_{liq,old}$ are the new and old volumes of the liquid inside the engine. For the experiment runs a drain ratio of 0.1 is used.

4.3.3 Results

The resulting performance for the optimistic parameter set has a power output of 7.2 W with an efficiency of 6.8 %. In Figure 4.11, the pressure versus volume curve is plotted for this setting. At the maximum volume point, it is observed that the fuel consumption time is short compared to the cycle time of the engine. At the maximum volume point, the exhaust is opened and has a low enough resistance such that the pressure goes down to ambiant conditions. The average exhaust temperature is around 130°C, causing most of the energy loss.

Parameter	Optimistic Set	Pessimistic Set	Unit
V_{max}	$7.5{\cdot}10^{-6}$	$7.5{\cdot}10^{-6}$	m^3
w_e	$2.12{\cdot}10^{-2}$	$2.12{\cdot}10^{-2}$	m
r_e	$1.06{\cdot}10^{-2}$	$1.06{\cdot}10^{-2}$	m
k_{react}	0.04	0.01	$1/s/m^2$
$A_{contact}$	$4.4{\cdot}10^{-5}$	$4.4{\cdot}10^{-6}$	m^2
w_{ex}	$2.7{\cdot}10^{-3}$	$2.7{\cdot}10^{-3}$	m
h_{ex}	$1.06{\cdot}10^{-3}$	$0.53{\cdot}10^{-3}$	m
θ	3	2	-
f_e	0.15	0.15	-
V_{fuel}	$0.5{\cdot}10^{-9}$	$0.5{\cdot}10^{-9}$	m^3
t_{cycle}	1/30	1/30	s
f_{rw}	0.9	0.9	-

Table 4.3: Parameters used for the numerical simulations of this section.

Another significant efficiency reduction is the heat loss of the working fluid to the environment. The peak pressure after the working fluid is compressed is and indication of the heat loss effect. For the optimistic set a compression ratio of 3 is used, which means that if the compression was close to adiabatic the peak pressure would be $4.6{\cdot}10^5$ Pa. The pV curve in Figure 4.11 shows a peak pressure after compression of $4.1{\cdot}10^5$ Pa, meaning a considerable amount of energy is lost.

The pessimistic set results in a power output of 4 W with an efficiency of 3.6 %. Its pV curve is also shown in Figure 4.11. Relative to the optimistic set, the reaction rate and the effective catalytic surface are reduced. This results in a longer consumption time and a lower pressure increase. Because a lower compression ratio is used, the overall pressure difference during the cycle is also lower. At the maximum volume point, the conditions have reached ambient again. This means that the exhaust is not limiting the performance of the engine, even though its available flow area is reduced.

To obtain the power density of these parameter sets, a certain relation between material volume and the characteristic length scale of the engine needs to be determined. Similar to what was done in the previous section, the proportions of the 3d drawing shown in Figure 4.8 are used for this purpose. The resulting correlation is:

$$V_{mat} = 0.06 w_e^3, \tag{4.33}$$

with the total volume V_{mat} of the material that makes up the engine. Assuming an average density of 2700 kg/m^3 (aluminium) and including 4 grams of fuel, the power density of the engine system using the optimistic parameter set is 440 W/kg. For the pessimistic set a power density of 245 W/kg is found.

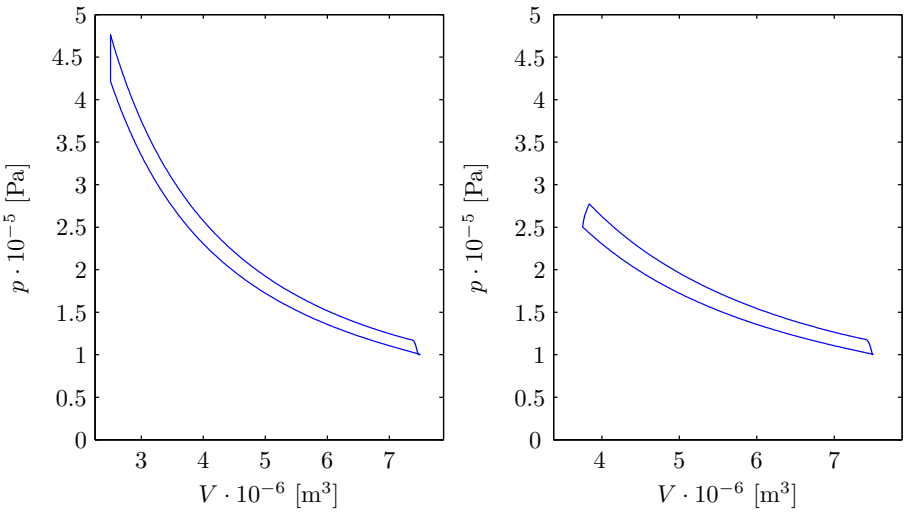

Figure 4.11

4.3.4 Conclusions

The performance found for Concept 1 indicates that it is a suitable candidate for the FWM engine. One has to keep in mind that the model described in this section neglects fuel pumping, viscous forces of fluid flow and droplet dynamics. Each of these effects will have their own contribution to the overall efficiency loss of the engine. But since the found performance is well above the required power density requirement of 125 W/kg, there is still a margin for those extra losses.

In this section it was assumed that the fuel pump can produce any drops that are desired for the engine. The importance of fuel drop size and contact area with catalytic surface was discussed in Section 3.3. The simulations in this section show that for the chosen contact area the consumption time of the fuel is certainly short enough. To further investigate the possibilities and limitations of Concept 1, one should investigate if the chosen contact area in combination with fuel volume per cycle is realistic on this small scale.

Also in Section 3.3, it was observed that droplets have their own dynamics during the evaporation on a hot plat. Since the evaporation on a hot plate and the decomposition on a flat surface are somewhat similar, it is expected that the droplet dynamics also play a role here. This might further reduce the effective contact area, which will result in a slower consumption time.

The model of Concept 1 shows that there is a considerable amount of vapor condensed during every cycle, resulting in a build up of fluids inside the engine. This could not be prevented by increasing the fuel concentration. A next

iteration of Concept 1 should consider this aspect. Perhaps by adding a gas decomposition stage, the temperatures that are reached inside engine are high enough to prevent condensation. This will increase the exit losses of the engine, but since in this model the evaporated fuel is simply discarded via the exit it is not expected this will be a problem. Gas phase decomposition does require much more surface area as liquid fuel decomposition, since the concentration is much lower.

Chapter 5

Conclusions and Future Work

During this thesis different possibilities for the engine project of the FWM designed by Casper Boltzman [2] are discussed. First a selection was made in Chapter 1 based on similar projects and input of the PME department at the Delft University of Technology. This has resulted in three concepts of which the main characteristics are discussed in Chapter 2. Based on measurements and the found characteristics for Concept 2, it is clear the performance of Concept 2 type engines is too low for the requirements of the FWM. More detailed elements of the two remaining concepts are discussed in Chapter 3. This provides the basis for the more complicated engine models of Concept 1 and 3.

According to the model of Concept 3, it can be concluded that Concept 3 type engines do not have enough power density to be suited for the FWM engine in its current size. This it true for the both the optimistic and pessimistic parameter sets. Considering that effects like viscous friction and heat loss from the combustor to the working fluid are not yet implemented in the model, the performance of the real engine is expected to be too low for the FWM. The model does show that the power density has favorable scaling properties. By reducing the system size by approximately one order, the power density comes in the right region. This statement is only true if the effects of viscous friction and heat leak of the combustor to the rest of the engine can be neglected. The magnitude of these effects should be investigated before this concept is taken to the next level. Also the heat transfer between the working fluid and and the heat sinks is subject for further investigation. In this report they are approximated by using an uniform temperature assumption and Fourier's law of heat conduction. The magnitude of the flows were justified by comparing them with the results of the FEM model of heat transfer. Since these parameters are critical for the

engine performance, they should be studied in full detail to check the validity of the assumptions done in this report.

The model of Concept 1 shows that the expected performance of these types of engines is in the right region for the FWM engine. Again a pessimistic and optimistic parameter set are used and both showed performance above the requirements. Also in this model, certain assumptions are done for simplification. These include the gas to gas heat transfer assumption described in Section 3.3. This assumption was considered not to have much influence on the results since the temperatures of the gases are close to each other when the engine is at steady state. The dynamics of the droplet and its effects on the effective contact area between catalyst and the fuel are neglected. Instead a optimistic and pessimistic value for the contact area and the reaction rate are used. Using both sets it was shown that the consumption time of the fuel for the given drop size is in the right order considering the opted cycle time of the FWM. The most important point of attention is the exhaust fluid flow model described in Section 3.4. This model uses the momentum equation of the fluid and neglects friction effects. Although the found Reynolds numbers indicated that the flow is in the turbulent region, friction and a more complicated exhaust port geometry might slow down the flow which decreases the ratio between momentum and friction effects. The performance will be reduced if the exhaust flow experiences more resistance as was modeled in Chapter 4. But since there is still some margin on the found performance, it is concluded that a more realistic exhaust model will not make Concept 1 unsuitable as FWM engine.

Another important aspect to consider before Concept 1 is taken to the next step is the implementation. Concept 1 uses flexible material to prevent leakage between the piston and cylinder wall. Without it, fluid leakage will dominate the engine performance as was found during experiments of other projects. The material used for the implementation is not considered in this thesis. It should have a high stiffness in the direction of the piston movement, but should be flexible in the tangential direction. It should also have a high temperature resistance. Perhaps a composite of a flexible, temperature resistant material surrounded by fibers in the direction of the piston movement provides a solution.

Appendices

Appendix A

Detailed Calculations

A.1 Calculations Chapter 2

A.1.1 Calculation of maximum hover time

Below the calculations are presented for obtaining an approximation of the maximum flight time while the device is hovering at (average) constant height.

The equations of motion of the device:

$$\begin{aligned} I_{tot}\frac{d^2\phi}{dt^2} + F_{wd}L + k\phi &= M_{act} \\ m_{tot}\frac{d^2x}{dt^2} + F_{xd} + m_{tot}g &= F_{lift} \end{aligned} \tag{A.1}$$

Assumption, the mass of the system is constant during period P of the wing rotation, and the consumed fuel is dumped instantly at the end of each period:

$$m_{tot,n} = m_{ini} - \sum_{n=1}^{n} \Delta m_{uf,n} \tag{A.2}$$

Here $\Delta m_{uf,n}$ represents the decomposed fuel during the nth period. Definitions of the external forces acting on the system:

$$\begin{aligned} F_{xd} &= C_x\dot{x} \\ F_{wd} &= C_dL^2\dot{\phi}^2 sgn\left(\dot{\phi}\right) \\ F_{lift} &= C_lL^2\dot{\phi}^2 \end{aligned} \tag{A.3}$$

Assumption, the wing makes a sinusoidal motion:

$$\phi = A_n cos\left(\omega t\right) \tag{A.4}$$

Resulting equation of motion of the wing:

$$A\left(k - I_{tot}\omega^2\right) sin\left(\omega t\right) + C_d L^3 A^2 \omega^2 \left(cos\left(\omega t\right)\right)^2 sgn\left(cos\left(\omega t\right)\right) = M_{act} \tag{A.5}$$

Assumption, the device is operating at the resonance frequency:

$$\begin{aligned} \omega &= \sqrt{\frac{k}{I_{tot}}} \\ M_{act} &= C_d L^3 A^2 \omega^2 \left(cos\omega t\right)^2 sgn\left(cos\omega t\right) \end{aligned} \tag{A.6}$$

Resulting motion in the x direction, assuming that the device mass is constant over 1 period:

$$m_{tot}\frac{d^2x}{dt^2} + C_x\frac{dx}{dt} + m_{tot}g = C_l L^2 A^2 \omega^2 \left(cos\omega t\right)^2 \tag{A.7}$$

Steady state conditions:

$$\begin{aligned} x(0) &= H_0 \\ \dot{x}(0) &= \frac{1}{2}A^2 C_l L^2 \omega^2 \left(\frac{1}{C_x} + \frac{C_x}{C_x^2 + 4m_{tot}^2\omega^2}\right) - \frac{m_{tot}g}{C_x} \end{aligned} \tag{A.8}$$

Solve for x:

$$\begin{aligned} x &= B_1 cos\left(2\omega t\right) + B_2 sin\left(2\omega t\right) + B_3 t + B_4 \\ B_1 &= \frac{A^2 C_l L^2 m_{tot}\omega^2}{2\left(C_x^2 + 4m_{tot}\omega^2\right)} \\ B_2 &= \frac{C_x}{2m_{tot}\omega}B_1 \\ B_3 &= -\frac{2m_{tot}g - A^2 C_l L^2 \omega^2}{2C_x} \\ B_4 &= \frac{C_l A^2 C_x L^2 m_{tot}\omega^2 + 2H_0 C_x^3 + 8H_0 C_x m_{tot}^2\omega^2}{2C_x(C_x^2 + 4m_{tot}^2\omega^2)} \end{aligned} \tag{A.9}$$

The begin and end height of the device can be made equal, such that the device will not lose any height over one 1 period. This is done by choosing A such that:

$$\begin{aligned} B_3 t &= 0 \\ A &= \sqrt{\frac{2m_{tot}g}{C_l L^2 \omega^2}} \end{aligned} \tag{A.10}$$

Assumption, the fuel consumption is proportional to the energy that needs to be added to the system in order to remain at constant average height:

$$\begin{aligned} P_{hover,n} &= M_{act,n}\dot{\phi}_n \\ E_{hover,n} &= \int_{t1}^{t1+\frac{2\pi}{\omega}} M_{act}\dot{\phi}dt = \frac{8C_d}{3\omega}\left(\frac{2g}{C_l}\right)^{3/2} m_{tot,n}^{3/2} \\ \Delta m_{uf,n} &= \frac{E_{hover,n}}{\eta\Phi} \end{aligned} \tag{A.11}$$

With fuel energy density Φ and constant engine efficiency η. To calculate the maximum flight time for a given fuel mass, it is assumed that the variation of the mass over time can be approximated with its average value:

$$\dot{m} = \frac{\Delta m_{uf,n}}{t_p} = \frac{\omega E_{hover}}{2\pi\eta\Phi} \tag{A.12}$$

Combining this assumption with (A.2) results in:

$$\begin{aligned} m_{tot} &= m_{ini} - \int_0^t \frac{8C_d}{6\pi\eta\Phi}\left(\frac{2g}{C_l}\right)^{3/2} m_{tot}^{3/2} dt \\ m_{tot} &= \frac{4}{\left(B_5 t - B_6\right)^2} \\ B_5 &= \frac{8C_d}{6\pi\eta\Phi}\left(\frac{2g}{C_l}\right)^{3/2} \\ B_6 &= \frac{-2}{\sqrt{m_{ini}}} \end{aligned} \tag{A.13}$$

The maximum flight time t_{end} is defined by the time when all the fuel is decomposed:

$$\begin{aligned} m_{end} &= \frac{4}{\left(B_5 t_{end} - B_6\right)^2} \\ t_{end} &= 2\frac{\sqrt{m_{ini}} - \sqrt{m_{end}}}{B_5\sqrt{m_{ini}m_{end}}} \end{aligned} \tag{A.14}$$

Definition of ratio between the initial mass and the mass when all fuel is used:

$$\begin{aligned} \gamma &= \frac{m_{ini}}{m_{end}} \\ m_{end} &= m_{device} \\ t_{end} &= \frac{3\sqrt{2}\pi}{g^{3/2}} \frac{C_l^{3/2}\Phi}{C_d} \left(1 - \frac{1}{\sqrt{\gamma}}\right) \frac{\eta}{\sqrt{m_{device}}} \end{aligned} \tag{A.15}$$

Design objective for the engine:

Maximize: $\frac{\eta}{\sqrt{m_{device}}}$

Constraint: $P_{rated} = E_{hover}/t_{cycle}$

A.1.2 Carnot Heat Engine

Calculations for the efficiency of the Carnot engine. The engine goes trough 4 process steps:

Step	State from→to	Process
1	$1 \rightarrow 2$	Isotropic expansion with hot reservoir attached to the gas
2	$2 \rightarrow 3$	Adiabatic expansion
3	$3 \rightarrow 4$	Isotropic compression with cold reservoir attached to the gas
4	$4 \rightarrow 1$	Adiabatic compression

Assumption: the working fluid of the engine is a gas and it behaves according to the ideal gas law:

$$pV = nR_{gas}T \tag{A.16}$$

Work and heat transfer for a general isotropic process from state A to state B:

$$\begin{aligned} (pV)_A &= (pV)_B \\ W_{A\rightarrow B} &= \int_A^B pdV = nR_{gas}Tln\left(\frac{V_B}{V_A}\right) \\ Q_{A\rightarrow B} &= W_{A\rightarrow B} \end{aligned} \tag{A.17}$$

Work and heat transfer for a general adiabatic process from state A to state B, where the gas behaves according to the polytropic relation:

$$\begin{aligned} &(pV^{\gamma})_A = (pV^{\gamma})_B \\ &W_{A\to B} = \int_A^B pdV = \frac{nR_{gas}\left(T_B - T_A\right)}{\gamma - 1} \\ &Q_{A\to B} = 0 \end{aligned} \tag{A.18}$$

If the engine is reversible, the following volume constrains apply:

$$\begin{aligned} &\frac{V_2}{V_1} = \frac{V_3}{V_4} \equiv R_1 \\ &\frac{V_4}{V_1} = \left(\frac{T_h}{T_c}\right)^{\frac{1}{\gamma-1}} \equiv R_2 \end{aligned} \tag{A.19}$$

The work output of one engine cycle is the sum of all individual steps:

$$\begin{aligned} W_{net} &= W_{1\to 2} + W_{2\to 3} + W_{3\to 4} + W_{4\to 1} \\ &= nR_{gas}T_h ln\left(\frac{V_2}{V_1}\right) + \frac{nR_{gas}\left(T_c - T_h\right)}{\gamma - 1} - \\ &\quad nR_{gas}T_c ln\left(\frac{V_3}{V_4}\right) + \frac{nR_{gas}\left(T_h - T_c\right)}{\gamma - 1} \\ &= nR_{gas}\left(T_h - T_c\right) ln\left(\frac{V_3}{V_4}\right) \end{aligned} \tag{A.20}$$

The efficiency is given by the total work output divided by the total energy output:

$$\eta_{rev} = \frac{W_{net}}{Q_{1\to 2}} = 1 - \frac{T_c}{T_h} \tag{A.21}$$

A.1.3 Curzon Alhborn Heat Engine

Calculation of the dimensionless power and efficiency of the Curzon Alhborn air engine.

Symbols:

Symbol	Summary
$V_{1/2}$	characteristic volumes of the engine
R_{gas}	universal gas constant
n	number of moles working fluid
$T_{h/c}$	temperature of hot/cold resevoir
$Q_{h/c}$	heat transferred from hot/cold reservoir during one cycle
$t_{h/c}$	time duration of heat transfer at hot/cold reservoir during one cycle
$T_{w,h/w,c}$	temperature of working fluid during hot/cold part of the cycle
η_{rev}	energy efficiency of the engine when it is operating reversible
η_{irr}	real energy efficiency of the engine
Π_{rev}	dimensionless engine parameter
P_{nd}	dimensionless power generated per one cycle
η_n	normalized energy efficiency of the cycle as fraction of the reversible efficiency

Heat transfer during the heat exchange steps of the cycle:

$$\begin{aligned} Q_{hot} &= t_h C_h \left(T_{hot} - T_{w,h}\right) \\ Q_{cold} &= t_c C_c \left(T_{cold} - T_{w,c}\right) \\ C_{h,c} &= \frac{kA}{L} \end{aligned} \tag{A.22}$$

With k as the thermal conductivity of the material, A the area of the heat conducting patch between the reservoir and the working fluid and L the thickness of the material. Assuming a reversible conversion process in the internal part of the engine, the entropy balance is given by:

$$\begin{aligned} \frac{Q_{hot}}{T_{w,h}} - \frac{Q_{cold}}{T_{w,c}} &= 0 \\ \frac{Q_{hot}}{Q_{cold}} &= \frac{T_{w,h}}{T_{w,c}} \end{aligned} \tag{A.23}$$

Energy balance of the engine:

$$W_{irr} = Q_{hot} - Q_{cold} \tag{A.24}$$

Assumption: the total cycle time of the engine is given by the sum of the two heat transfer steps:

$$\begin{aligned} t_{cycle} &= t_h + t_c \\ t_c &= t_h f_t \end{aligned} \tag{A.25}$$

With f_t as a dimensionless parameter of the engine. The same is done for the heat transfer constant:

$$C_c = C_h f_c \tag{A.26}$$

Relation between the generated work during one cycle and the process parameters of the engine [17]:

$$W = nR_{gas} ln\left(\frac{V_2}{V_1}\right)(T_{w,h} - T_{w,c}) \tag{A.27}$$

The efficiency and power of the engine cycle are defined by:

$$\begin{aligned} \eta_{irr} &= 1 - \frac{T_{w,c}}{T_{w,h}} \\ P &= \frac{W}{t_{cycle}} \end{aligned} \tag{A.28}$$

Definition of the dimensionless engine parameters:

$$\begin{aligned} \eta_{rev} &= 1 - \frac{T_c}{T_h} \\ \alpha &= \frac{C_h t_{cycle}}{nR_{gas} ln\left(\frac{V_2}{V_1}\right)} \\ \Pi &= \frac{\alpha + (f_t + 1)}{\alpha - \frac{f_t + 1}{f_t f_c}} \end{aligned} \tag{A.29}$$

Definition of the dimensionless performance parameters:

$$\begin{aligned} \eta_n &= \frac{\eta_{irr}}{\eta_{rev}} \\ P_{nd} &= \frac{P}{C_h T_h} \\ P_{ndn} &= \frac{P_{nd}}{P_{nd,max}} \end{aligned} \tag{A.30}$$

With $\tau = nR_{gas} ln\,(V2/V1)$. Combining the heat transfer law (A.22), the entropy balance (A.23),the energy balance(A.24), the time balance (A.25) the generated work (A.27) and the definitions for the non dimensional parameters (A.30) gives a set of equations that can be solved for the unknown process parameters Q_{hot}, Q_{cold}, t_h, $T_{w,h}$, W and $T_{w,c}$. With these results the efficiency

and the average power are given by:

$$\begin{aligned} \eta_n &= \Pi - \frac{\Pi - 1}{\eta_{rev}} \\ P_{nd} &= \frac{f_t f_c \left(\Pi - 1\right) \left(\Pi \eta_{rev} - \Pi + 1\right)}{\Pi \left(f_t f_c + 1\right) \left(f_t + 1\right)} \end{aligned} \tag{A.31}$$

The maximum non dimensional generated power, $P_{nd,max}$, for a given reversible efficiency is determined by the condition:

$$\begin{aligned} \frac{dP_{nd}}{d\Pi} &= \frac{f_t f_c \left(\Pi_{max}^2 \eta_{rev} - \Pi_{max}^2 + 1\right)}{\Pi_{max}^2 \left(f_t f_c + 1\right) \left(f_t + 1\right)} = 0 \\ \Pi_{max} &= \frac{1}{\sqrt{1 - \eta_{rev}}} \\ P_{nd,max} &= \frac{f_t f_c}{\left(f_t f_r + 1\right) \left(f_t + 1\right)} \left(1 - \sqrt{1 - \eta_{rev}}\right)^2 \\ P_{ndn} &= \frac{\left(\Pi - 1\right) \left(\Pi \left(\eta_{rev} - 1\right) + 1\right)}{\Pi \left(1 - \sqrt{1 - \eta_{rev}}\right)^2} \end{aligned} \tag{A.32}$$

The Curzon Ahlborn efficiency, which is the efficiency at the maximum power point is found by substituting Π_{max} into the efficiency formula:

$$\eta_{CA} = 1 - \sqrt{\frac{T_c}{T_h}} \tag{A.33}$$

With differentiation the optimal relation between the ratio parameters f_t and f_c can be found:

$$\begin{aligned} \frac{dP_{nd,max}}{df_t} &= 0 \\ f_t &= \frac{1}{\sqrt{f_c}} \end{aligned} \tag{A.34}$$

The range where Π is valid can be determined with the efficiency formula:

$$\begin{aligned} \eta_n &= \Pi_{begin} - \frac{\Pi_{begin} - 1}{\eta_{rev}} = 0 \\ \Pi_{begin} &= \frac{1}{1 - \eta_{rev}} \\ \eta_n &= \Pi_{end} - \frac{\Pi_{end} - 1}{\eta_{rev}} = 1 \\ \Pi_{end} &= 1 \end{aligned} \tag{A.35}$$

Dissipative term

Energy flow that bypasses the Curzon Alhborn engine:

$$Q_{loss} = t_{cycle} C_l \left(T_{hot} - T_{cold}\right) \tag{A.36}$$

New defintion of the efficiency of the engine, with consideration of the irreversibility and the loss term

$$\eta_{i+l} = \frac{Q_{hot} - Q_{cold}}{Q_{hot} + Q_{loss}} \tag{A.37}$$

Non dimensional form:

$$\eta_{irr+loss} = \frac{1 + (nRev - 1)\,\frac{\alpha + f_t + 1}{\alpha - \frac{f_t + 1}{f_t f_c}}}{1 + f_l\left(f_t + 1 + \alpha\right)\eta_{rev}} \tag{A.38}$$

Maximal efficiency is obtained with the condition:

$$\frac{\partial \eta_{i+l}}{\partial \alpha} = 0$$

$$\alpha_{max} = \frac{f_t + f_t^2 f_c + f_t f_c - f_t f_c \eta_{rev} - f_t^2 f_c \eta_{rev} + 1}{f_t f_c \eta_{rev}} \tag{A.39}$$

$$+ \frac{\left((f_t f_c + 1)(f_t + 1)(1 - \eta_{rev})(1 + f_t + f_t f_c(\frac{1}{f_l} + 1 + f_t))\right)^{1/2}}{f_t f_c \eta_{rev}}$$

A.1.4 Energy Balance Model

Estimating operating conditions

Assumption, the piston of the Curzon Alhborn engine moves such that the volume of the gas is given by:

$$\begin{aligned} V &= \left(A_1 sin\left(\omega t + \phi\right) + A_2\right)^x \\ &= V_n^x \end{aligned} \tag{A.40}$$

Choose the constants A_1 and A_2 such that the maximum and minimum of the volume function are equal to V_3 and V_1 of the Carnot engine model described

above:

$$\begin{aligned} V\left(t=\frac{0.5\pi-\phi}{\omega}\right) &= V_3 \\ V\left(t=\frac{1.5\pi-\phi}{\omega}\right) &= V_1 \\ A_1 &= 0.5\left(V_3^{1/X}-V_1^{1/X}\right) \\ A_2 &= A_1+V_1^{1/X} \end{aligned} \tag{A.41}$$

Energy balance of the working fluid:

$$\begin{aligned} dU &= dQ-dW \\ dW &= pdV \\ dQ &= C_R\left(T_R-T\right)dt \\ dU &= nc_v dT \end{aligned} \tag{A.42}$$

Resulting differential equation for the working fluid temperature:

$$\begin{aligned} \frac{dT}{dt} &= A_3-\left(A_4+A_5\frac{1}{V}\frac{dV}{dt}\right)T \\ A_3 &= \frac{T_R C_R}{c_v n} \\ A_4 &= \frac{C_R}{nc_v} \\ A_5 &= \frac{R_{gas}}{c_v} \end{aligned} \tag{A.43}$$

With the volume function inserted:

$$\frac{dT}{dt} = A_3-\left(A_4+A_5 x\frac{1}{V_n}\frac{dV_n}{dt}\right)T \tag{A.44}$$

For which an explicit solution can be found if x is chosen as the inverse of A_5:

$$\begin{aligned} p &= A_4 + \frac{1}{V_n}\frac{dV_n}{dt} \\ g &= A_3 \\ \mu &= e^{\int p dt} = e^{A_4 t + A6} V_n \\ A_6 &= \frac{2}{\omega} atan\left(tan\left(\frac{\phi}{2}\right)\right) \\ T &= \frac{\int \mu g dt + A_7}{\mu} \\ T &= \frac{1}{V_n}\left(A_2\omega^2 A_8 - A_4 A_8 \frac{dV_n}{dt} + \frac{A_7}{e^{A_4 t}}\right) + A_4^2 A_8 \\ A_8 &= \frac{A_3}{A_4\left(\omega^2 + A_4^2\right)} \end{aligned} \tag{A.45}$$

The constant A_7 depends on the initial conditions of the working fluid:

$$A_7 = e^{A_4 t_{ini}}\left(\left(T_{ini} - A_4^2 A_8\right) V_{n,ini} - A_2\omega^2 A_8 + A_4 A_8 \frac{dV_{n,ini}}{dt}\right) \tag{A.46}$$

Introduction of a relative time (voegt dit iets toe?):

$$\begin{aligned} \tau &= t + \frac{\phi}{\omega} \\ V_n(\tau) &= A1 sin(\omega\tau) + A2 \\ T(\tau) &= \frac{1}{V_n}\left(A_2\omega^2 A_8 - A_4 A_8 \frac{dV_n}{d\tau} + \frac{A_7}{e^{A_4(\tau)}}\right) + A_4^2 A_8 \end{aligned} \tag{A.47}$$

The differential for the entropy of the working fluid:

$$\begin{aligned} dS &= \frac{dQ}{T} \\ &= nc_v \frac{1}{T} dT + nR_{gas} \frac{1}{V} dV \\ &= nc_v \left(\frac{1}{T} dT + \frac{1}{V_n} dV_n \right) \\ S_b - S_a &= nc_v ln \left(\frac{T_b V_{n,b}}{T_a V_{n,a}} \right) \end{aligned} \tag{A.48}$$

Since the expansion (2→3) and compression (4→1) steps are still adiabatic, the following relation between the temperatures of these states applies:

$$\begin{aligned} S_3 - S_2 = S_1 - S_4 &= 0 \\ T_3 V_{n,3} &= T_2 V_{n,2} \\ T_1 V_{n,1} &= T_4 V_{n,4} \end{aligned} \tag{A.49}$$

Combination of the entropy balance and the temperature equation results in the begin and end temperature of each step of the cycle.

Definition of timing parameters:

The heat addition step always starts the minimum volume moment, the heat extraction at maximum volume. The duration of each of these steps is made relative to the cycle time with the parameters f_1 and f_2:

$$\begin{aligned} \omega t_1 + \phi &= 1.5\pi \\ \omega t_3 + \phi &= 2.5\pi \\ t_1 &= t_{cycle} \left(\frac{3}{4} - \frac{\phi}{2\pi} \right) \\ t_2 &= t_1 + f_1 \frac{1}{2} t_{cycle} \\ t_3 &= t_1 + \frac{1}{2} t_{cycle} \\ t_4 &= t_3 + f_2 \frac{1}{2} t_{cycle} \end{aligned} \tag{A.50}$$

Estimating performance:

The heat exchange between the working fluid and the reservoir becomes:

$$dQ = C_r \left(T_r - T\right) dt$$

$$Q_{a\to b} = C_r T_r \left(t_b - t_a\right) - C_r \int_a^b T dt$$

$$\begin{aligned}\int_a^b T dt = &\frac{4\pi A_2 A_8}{t_{cycle}\left(A_2^2 + A_1^2\right)^{1/2}} atan\left(\frac{A_1 + A_2 tan\left(0.5\phi + \frac{t_b \pi}{tcycle}\right)}{\left(A_2^2 + A_1^2\right)^{1/2}}\right) \\ &- A_4 A_8 ln\left(A_2 + A_1 sin\left(\phi + \frac{2\pi t_b}{t_{cycle}}\right)\right) \\ &+ A_4^2 A_8 t_b + const \\ &+ \int_a^b \frac{A_7}{e^{A_4 t} V_n} dt\end{aligned} \tag{A.51}$$

The last part of this integral cannot be written in explicit form. For large values of t_{cycle} the integral converges to a simpler one. This can be used to calculate the maximum efficiency of this engine. The performance parameters are still defined in the same way as with the Carnot engine:

$$\begin{aligned}W_{net} &= Q_{1\to 2} - Q_{3\to 4} \\ P_{rated} &= \frac{W_{net}}{t_{cycle}} \\ \eta_{irr} &= \frac{W_{net}}{Q_{1\to 2}}\end{aligned} \tag{A.52}$$

Maximum efficiency without heat loss:

The maximum efficiency will occur at large values of t_{cycle}. In tat case the implicit part of the heat exchange formula can be approximated with:

$$\begin{aligned}\int_a^b \frac{A_7}{e^{A_4 t} V_n} dt &\approx \int_a^b \frac{A_7}{e^{A_4 t}\left(A_1 sin(\omega t_a + \phi) + A_2\right)} dt \\ &= \frac{e^{A_4 t_a}\left(\left(T_a - A_4^2 A_8\right) V_{n,a} - A_2 \omega^2 A_8\right)}{A_1 sin(\omega t_a + \phi) + A_2} \int_a^b \frac{1}{e^{A_4 t}} dt \\ &= \frac{\left(1 - e^{A_4(t_a - tb)}\right)\left(\left(T_a - A_4^2 A_8\right) V_{n,a} - A_2 \omega^2 A_8\right)}{A_4\left(A_1 sin(\omega t_a + \phi) + A_2\right)}\end{aligned} \tag{A.53}$$

For large cycle times the temperatures T_1 and T_3 converge to the following values:

$$\begin{aligned}\lim_{t_{cycle}\to\infty} T_1 &= T_{1,lim} = T_{cold}\frac{V_{n4}}{V_{n1}} \\ \lim_{t_{cycle}\to\infty} T_3 &= T_{3,lim} = T_{hot}\frac{V_{n2}}{V_{n3}}\end{aligned} \tag{A.54}$$

Combining this with the definition of the timing (A.50), the heat flows (A.51), the approximation valid for large cycle times (A.53), results in the limiting values of the heat inflow and outflow:

$$\begin{aligned}\lim_{t_{cycle}\to\infty} Q_{1\to2} &= Q_{in,lim} = nc_v\left(T_{1,lim} - T_{hot}\left(1 + ln\left(\frac{V_{n2}}{V_{n1}}\right)\right)\right) \\ \lim_{t_{cycle}\to\infty} Q_{3\to4} &= Q_{out,lim} = nc_v\left(T_{3,lim} - T_{cold}\left(1 + ln\left(\frac{V_{n4}}{V_{n3}}\right)\right)\right)\end{aligned} \tag{A.55}$$

The maximum obtainable efficiency becomes:

$$\begin{aligned}\eta_{irr} &= 1 + \frac{Q_{out,lim}}{Q_{in,lim}} \\ &= 1 - \frac{\left(1 - \eta_{rev}\right)\left(1 + ln\left(\frac{Vn4}{Vn3}\right)\right) - \frac{Vn2}{Vn3}}{\left(1 - \eta_{rev}\right)\frac{Vn4}{Vn1} - \left(1 + ln\left(\frac{Vn2}{Vn1}\right)\right)}\end{aligned} \tag{A.56}$$

Looking at the definition of V_n (A.40) and the definition of the timing values (A.50), it is seen that this efficiency only depends on the parameters η_{rev}, A_1, A_2 f_1 and f_2. By taking yet another limit of the efficiency, this time with both f_1 and f_2 approaching zero, it is seen that (A.56) converges to:

$$\eta_{irr} = \frac{2A_1}{A_1 + A_2} \tag{A.57}$$

Which can be larger than the reversible efficiency. This shows that if A_1 and A_2 are chosen such that (A.57) is larger than the η_{rev}, some additional constraints apply for the chosen duration of the heat adding step and the duration of the heat removal step (f_1 and f_2).

Which shows the difference between an endoreversible model and a model based on physics laws.

A.2 Calculations Chapter 3

A.2.1 The Decomposition Model

Low Fuel Concentrations

Energy balance of the droplet:

$$\begin{aligned}(cp_{h2o2}n_{h2o2} + cp_{h2o,l}n_{h2o,l,drop})\frac{dT_{drop}}{dt} &= V_{drop}\frac{dp}{dt} + \frac{dQ_{drop}}{dt} \\ &- \frac{dn_{h2o2}}{dt}\left(h_{h2o2} - h_{h2o,l,tdrop} - 0.5h_{o2,tdrop}\right) \\ &- \frac{dn_{evap,d}}{dt}\left(h_{h2o,g,tdrop} - h_{h2o,l,tdrop}\right).\end{aligned} \tag{A.58}$$

Energy balance of the water vapor in the chamber:

$$\begin{aligned}n_{h2o,g}cp_{h2o,g,Twv}\frac{dT_{wv}}{dt} &= V_{wv}\frac{dp}{dt} + \frac{dQ_{wv}}{dt} \\ &- \frac{dn_{evap,d}}{dt}\left(h_{h2o,g,Twv} - h_{h2o,g,Tdrop}\right) \\ &- \frac{dn_{evap,c}}{dt}\left(h_{h2o,g,Twv} - h_{h2o,l,Twv}\right).\end{aligned} \tag{A.59}$$

Energy balance of the oxygen and air in the chamber:

$$\begin{aligned}(cp_{o2,Tog}n_{o2} + cp_{air}n_{air})\frac{dT_{og}}{dt} &= V_{og}\frac{dp}{dt} + \frac{dQ_{og}}{dt} \\ &\quad - 0.5\frac{dn_{h2o2}}{dt}\left(h_{o2,Tdrop} - h_{o2,Tog}\right).\end{aligned} \tag{A.60}$$

Equation for the pressure inside the room

$$p = \frac{\left(n_{o2} + n_{air}\right)R_{gas}T_{og}}{V_{og}} = \frac{n_{h2o,g}R_{gas}T_{wv}}{V_{wv}}. \tag{A.61}$$

The total chamber volume V_c is the sum of the volumes of the different gases, neglecting the volume of the fluids:

$$V_c = V_{wv} + V_{og} \tag{A.62}$$

Combining the last two equations gives:

$$\begin{aligned}V_{og} &= \frac{\left(n_{o2} + n_{air}\right)T_{og}V_c}{n_{h2o,g}T_{wv} + \left(n_{o2} + n_{air}\right)T_{og}}, \\ V_{wv} &= \frac{n_{h2o,g}T_{wv}V_c}{n_{h2o,g}T_{wv} + \left(n_{o2} + n_{air}\right)T_{og}}.\end{aligned} \tag{A.63}$$

The resulting equation for the pressure and pressure derivative:

$$p = \frac{R_{gas}}{V_c}\left(n_{h2o,g}T_{wv} + \left(n_{o2} + n_{air}\right)T_{og}\right),$$

$$\frac{dp}{dt} =$$

$$\frac{R_{gas}}{V_c - V_{drop}}\left(\frac{dn_{h2o,g}}{dt}T_{wv} + \frac{dT_{wv}}{dt}n_{h2o,g} + \frac{dn_{o2}}{dt}T_{og} + \left(n_{o2} + n_{air}\right)\frac{dT_{og}}{dt}\right) \tag{A.64}$$

The remaining equations are gained from the evaporation rates. If the drop temperature is below the saturation temperature of water, then the evaporation rate of the water in the drop is zero:

$$\frac{dn_{evap,d}}{dt} = 0. \tag{A.65}$$

Otherwise, the drop has reached the saturation temperature, such that the change in temperature of the drop is given by the change in saturation temperature:

$$\frac{dT_{drop}}{dt} = \frac{dT_{sat,h2o}}{dt}. \tag{A.66}$$

In the low fuel concentration case, the water vapor inside the chamber will always be in the saturated state, such that:

$$\frac{dT_{wv}}{dt} = \frac{dT_{sat,h2o}}{dt}. \tag{A.67}$$

Combining all of the equations above gives a set of 6 equations that can be solved for the six unknowns of this problem: $\dot{T}_{drop}$, $\dot{T}_{og}$, $\dot{T}_{wv}$, $\dot{p}$, $\dot{n}_{evap,d}$ and $\dot{n}_{evap,c}$. The results of this model are given in Section 3.3.

High Fuel Concentrations

For high fuel concentrations, the drop temperature reaches the saturation point of H_2O_2, which means it will evaporate. The energy balance of the hydrogen peroxide vapor needs to be added to the previous model:

$$\begin{aligned} n_{h2o2,g} cp_{h2o2,g,Thpv} \frac{dT_{hpv}}{dt} &= V_{hpv} \frac{dp}{dt} + \frac{dQ_{hpv}}{dt} \\ &- \frac{dn_{evap,hpv}}{dt} \left(h_{h2o2,g,Thpv} - h_{h2o2,g,Tdrop}\right) \\ &- \frac{dn_{evap,hpv,c}}{dt} \left(h_{h2o2,g,Thpv} - h_{h2o2,l,Thpv}\right). \end{aligned} \tag{A.68}$$

If all the water of the drop is evaporated, the evaporation rate is equal to the rate of decomposition:

$$\frac{dn_{evap,d}}{dt} = -\frac{dn_{h2o2,d}}{dt}. \tag{A.69}$$

If the saturation point of hydrogen peroxide is reached, the evaporation rate of H_2O_2, $\dot{n}_{evap,hpv}$, can be calculated from the energy balance of the drop.

The condensation rate of the hydrogen peroxide vapor in the chamber can be calculated from the energy balance of the gas itself.

Appendix B

Viscosity of Gas Mixture

In this appendix the effect of the fuel weight ratio $f_{r,w}$ and the temperature on the viscosity of the gas that is released by the decomposition is studied. It is assumed that the gas mixture will consist of water vapor and oxygen gas only. The properties of these individual species will be looked at first.

Water vapor properties have been tabulated by the IAPWS (International Association for the Properties of Water and Steam). For steam viscosity, it is advised to use a certain interpolation function [41], which has been implemented into the Matlab routine XSteam. XSteam is available from the Mathworks file exchange website. In Figure B.1 on the left, a plot of the viscosity as function of the temperature has been plotted. A sharp drop can be seen, caused by the phase change at the saturation temperature. In the gas phase, the viscosity increases when temperature increases.

For the viscosity of oxygen the data presented by [25] is used, who use a certain model that is fitted to data from experiments. In Figure B.1 on the right, the temperature characteristics of μ are plotted. Similar to water vapor, the viscosity increases for increasing temperature.

To calculate the properties of the gas that is released by the decomposition process, the data presented in Figure B.1 must be combined. To do this, a model presented by [3] is used:

$$\mu_{mix} = \sum_{i=1}^{2} \frac{x_i \sqrt{\mu_i}}{\frac{x_i}{\sqrt{\mu_i}} + \sum_{j=1, j\neq i}^{2} \frac{\varphi_{ij}}{\sqrt{\mu_j}} x_j}, \tag{B.1}$$

where x_i is the mole fraction of species i ,μ_i the viscosity and φ a parameter that depends on the polarity, temperature and molar mass of both species. The mole fraction of the species in the hot gas are calculated by assuming that all the water initially present in the fuel is evaporated. This does not happen for

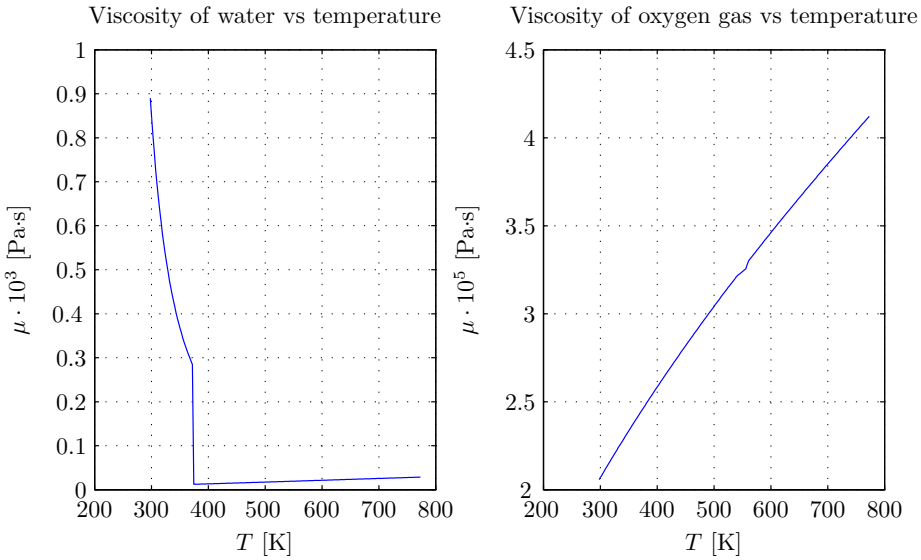

Figure B.1: Left: viscosity of water based on data from [41]. Right: viscosity of oxygen based on data from [25]

a weight ratio of the fuel lower than approximately 0.7 (see Figure 3.5), which is why values lower than 0.7 are not considered. In Figure B.2 the viscosity of the gas mixture is plotted against the weight ratio of the fuel. It is seen that the viscosity slight increases for a increasing $f_{r,w}$, because the mole fraction of oxygen becomes higher for higher $f_{r,w}$. This figure will be used as reference for the rest of the report.

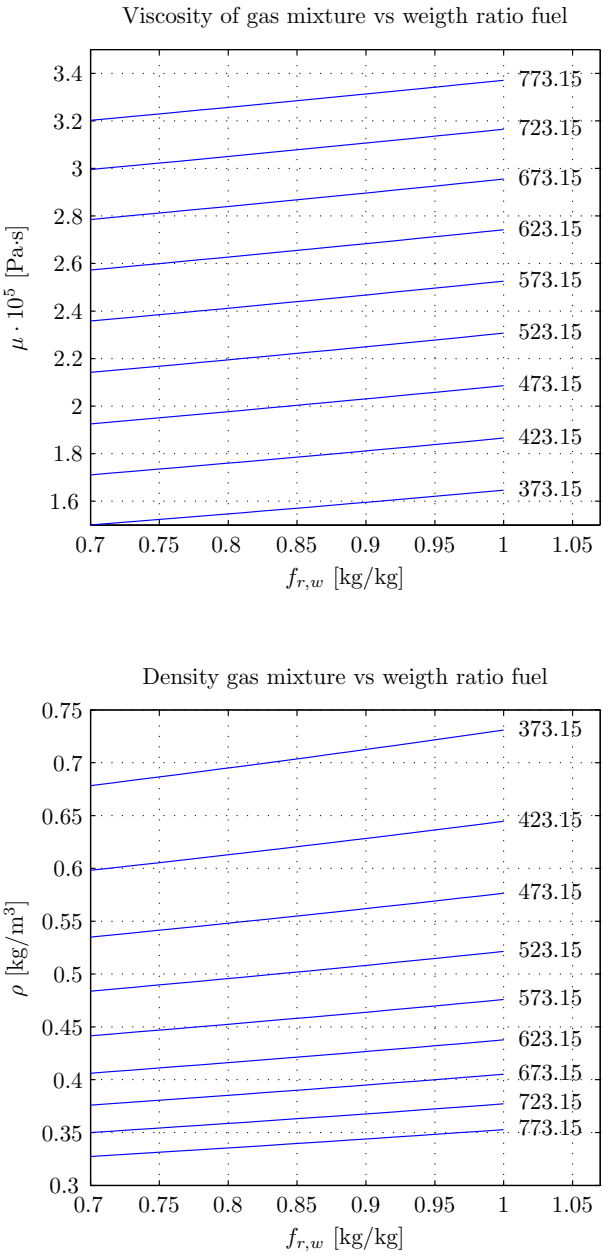

Figure B.2: Viscosity of the gas mixture formed by the decomposition process, for different gas temperatures[K].

373.15

Bibliography

[1] M.F. Ashby. *Materials Selection in Mechanical Design*. Elsevier, 3 edition, 2005.

[2] C.T. Bolsman. *Flapping wing actuation using resonant compliant mechanisms, an insect inspired design*. PhD thesis, TU Delft, Oktober 2010.

[3] R.S. Brokaw. Viscosity of gas mixtures. Technical report, NASA, Cleveland, Ohio, april 1968.

[4] S. Menon C. Cadou. Scaling of losses in small ic aero engines with engine size. *AIAA 2004 690*, 2004.

[5] H. Cohen. *Gas Turbine Theory*. Longman House, 4 edition, 2011.

[6] J.C. Cool. *Werktuigkundige Systemen*. Delft University Press, 2 edition, 2003.

[7] M. de Volder et al. A pdms lipseal for hydraulic and pneumatic microactuators. *Micromechanics and Microengineering*, 17:1232 – 1237, 2007.

[8] J. Duncre. Topspot-a new method for the fabrication of microarrays. *Micro Electro Mechanical Systems*, pages 317 – 322, 2000.

[9] M. Gad el Hak. *The MEMS Handbook*. CRC Press, 1 edition, September 2002.

[10] A.H. Epstein. Millimeter scale mems gas turbine engines. *ASME*, 4:669–696, 2003.

[11] A. Carlos Fernandez Pello et al. Mems rotary engine power system. *IEEJ Trans. SM*, 123(9):326–330, 2003.

[12] A. Fischer et al. Can a quantitative simulation of an otto engine be accurately rendered by a simple novikov model with heat leak? *Non-Equilibrium Thermodynamics*, 29(1):928, 2004.

[13] A.B. Kanungo et al. The kinetics ands mechanism for the catalytic decomposition of h_2o_2 over different crystalline modifications of mno_2. *Electrochimica Acta*, 26(8):1157 – 1167, 1980.

[14] C. Cheng et al. Analytical model for predicting the effect of operating speed on shaft power output of stirling engines. *Energy*, 36(10):5899 – 5908, sep 2011.

[15] C. M. Spadaccini et al. Catalytic combustion systems for micro-scale gas turbine engines. *ASME*, 129(1):49 – 61, January 2005.

[16] C.H. Lee et al. Design and fabrication of a micro wankel engine using mems technology. *Micro Electronic Engineering*, 73 - 74(0):529 – 534, 2004.

[17] D. Kondepudi et al. *Modern themodynamics, from heat engines to dissipative structures.* Wiley, 1 edition, 1998.

[18] D. Sengupta et al. Controlling non-catalytic decomposition of high concentration hydrogen peroxide. Technical report, CFD Research Corparation, 2004.

[19] D. Xie et al. Multi-materials drop-on-demand inkjet technology based on pneumatic diaphragm actuator. *Science China Technological Sciences*, 53(6):1605 – 1611, 2009.

[20] D.E. Park et al. Design and fabrication of micromachined internal combustion engine as a power source for microsystems. *Micromechanics Microengineering*, pages 272 – 275, 2002.

[21] D.L. Hitt et al. Mems-based satellite micropropulsion via catalyzed hydrogen peroxide decomposition. *Smart Materials and Structures*, 10(6):1163, augustus 2001.

[22] F. Eid et al. Design, fabrication and demonstration of a mems steam generator for ejector pump applications. *Micromechanics Microengineering*, 20:104007, 2010.

[23] F.O. Rice et al. The thermal decomposition of hydrogen peroxide. *Physical Chemistry*, 31(9):1352 – 1356, January 1927.

[24] G. Scatchard et al. Vapor-liquid equilibrium. viii. hydrogen peroxide-water mixtures. *Armerican Chemical Society*, 74(15):3715 – 3720, 1952.

[25] H.J.M. Hanley et al. Viscosity and thermal conductivity coefficients of gaseous and liquid oxygen. Technical report, NASA, august 1974.

[26] I. Muller et al. *Rubber and rubber Balloons: Paradigms of Thermodynamics.* Springer, 1 edition, 2004.

[27] J. Bejhed et al. Catalyst microsystem design and manufacture for a monopropellant microrocket engine. *PowerMEMS*, pages 68 – 71, November 2004.

[28] J. Peirs et al. A microturbine for electric power generation. *Sensors and Actuators*, 113(1):86 – 93, 2004.

[29] J. R. Cooper et al. Revised release on the iapws industrial formulation 1997 for the thermodynamic properties of water and steam. Technical report, IAPWS, Lucerne, Switzerland, 2007.

[30] J.R. Goldstein et al. The kinetics of hydrogen peroxide decomposition catalyzed by cobalt-iron oxides. *Journal of Catalysis*, 32:452 – 465, april 1973.

[31] K. H. Hoffman et al. Endoreversible thermodynamics. *Non-Equilib. Thermodyn*, 22(4):311–355, 1997.

[32] K. Isomura et al. Experimental verification of the feasibility of a 100 w class micro-scale gas turbine. *Micromechanics and Microengineering*, 16(9):S254, September 2006.

[33] K. Khu et al. Effects of finite heat input on the power performance of micro heat engines. *Energy*, 36(5):2686 – 2692, May 2011.

[34] L. Chen et al. Influence of internal heat leak on the power versus efficiency characteristics of heat engines. *Energy Conversion and Management*, 38(14):1501 – 1507, 1995.

[35] L. Chen et al. Effect of heat transfer law on the performance of a generalized irreversible carnot engine. *Energy Conversion and Management*, 39(7):643–64, 1998.

[36] L. H. J. Wachters et al. The heat transfer from a hot horizontal plate to sessile water drops in the spherodial state. *Chemical Engineering Science*, 21(10):923 – 936, 1965.

[37] M. J. Moran et al. *Fundamentals of engineering thermodynamics*. Wiley, 4 edition, 2002.

[38] M.A. Hasnat et al. Efficient hydrogen peroxide decomposition on bimetallic ptpd surfaces. *Catalysis Communications*, 12(4):286 – 291, 2010.

[39] N. Nakajima et al. Study on microengines: Miniaturizing stirling engines for actuators. *Sensors and Actuators*, pages 145 –148, feb 1989.

[40] R. Darlington et al. *Stirling and Hot Air Engines*. Crowood Press, 2005.

[41] R. Fernandez-Prini et al. Revised release on the iaps formulation 1985 for the viscosity of ordinary water subtance. Technical report, IAPWS, 2003.

[42] R.B. Fahim et al. Heterogeneous and/or homogeneous chromia-catalysed decomposition of hydrogen peroxide. *Surface Technology*, 12(4):317 – 326, 1981.

[43] R.T. Deam et al. On scaling down turbines to millimeter size. *Engineering for Gas Turbines and Power*, 130:052301 1–9, September 2008.

[44] S. Do et al. Hydrogen peroxide decomposition on manganese oxide (pyrolusite): Kinetics, intermediates, and mechanism. *Chemosphere*, 75:8 – 12, 2009.

[45] S. Mao et al. Lift and power requirements of hovering insect flight. *Acta Mechanica Sinica*, 19(5):458 – 469, 2003.

[46] S. Menon et al. Miniaturization limits of smal ic engines. *PowerMEMS*, December 2009.

[47] S. Whalen et al. Design, fabrication and testing of the p3 micro heat engine. *Sensors and Actuators*, 104(3):290 – 298, 2003.

[48] S.F. Oliveira et al. Kinetic study of the decomposition of hydrogen peroxide catalysed by co(ii) acetylacetonate supported on a silica-proppylpiperazine matrix. *Colloids and Surfaces A: Physicochemical and Engineering Aspects*, 136(1 - 2):151 – 154, April 1998.

[49] T. Huesgen et al. Detailed study of a micro heat engine for thermal energy harvesting. *Micromechanics and microengineering*, 20(10):104004, 2010.

[50] T. Mimani et al. Catalytic decomposition of hydrogen peroxide on fine particle ferrites and cobaltites. *Chemical Science*, 99(4):209 – 215, 1987.

[51] T. Toriyama et al. Design of a resonant micro reciprocating engine for power generation. *Transducers*, 2:1303 – 1306, june 2003.

[52] T.Y. Xiong et al. Evaporation of a liquid droplet on a hot plate. *Heat Mass Transfer*, 34(7):1881 – 1894, 1990.

[53] V. Mucka et al. Decomposition of hydrogen peroxide on silver nickel oxide two-component catalysts and the effects of ionizing radiation. *Radiation Physics*, 26(2):121 – 126, 2011.

[54] V. N. Orlov et al. Power output from an irreversible heat engine with a nonuniform working fluid. *Physical Review A*, 42(12):7230 – 7235, Dec 1990.

[55] V. N. Orlov et al. Power and efficiency limits for internal combustion engines via methods of finite-time thermodynamics. *Applied Physics*, 74(7):4317 – 4322, 1993.

[56] V.G. Krishnan et al. A micro tesla turbine for power generation from low pressure heads and evaporation driven flows. *Transducers*, 11:1851 – 1854, June 2011.

[57] Y. Ge et al. Reciprocating heat-engine cycles. *Applied Energy*, 81:397 – 408, 2004.

[58] J.M. Gordon. General performance characteristics of real heat engines. *Applied Physics*, 72(3):829 – 838, august 1992.

[59] A.V. Jensen. *Chemical Rocket/Propellant Hazards Volume III. Liquid Propellant Handling, Storage and Transportation*, volume 3. Chemical Propulsion Information Agency, 1970.

[60] A.J.H. Meskers. High energy density micro-actuation based on gas generation by means of catalyst of liqiud chemical energy. Master's thesis, TU Delft, 2010.

[61] A. F. Mills. *Basic heat and mass transfer*. Prentice Hall, 2 edition, 1999.

[62] N.T. Nguyen. Mems-micropumps: A review. *Fluids Engineering*, 124(2):384 – 393, June 2002.

[63] A. Carlos Fernandez Pello. Micro power generation using combustion: Issues and approches. *Proceeding of the Combustion Institute*, 29(1):883899, 2007.

[64] R.B. Peterson. Size limits for regenerative heat engines. *Microscale Thermophysical Engineering*, 2(2):121 – 131, may 1998.

[65] P.E. Claire Soares. *Microturbines: applications for distributed energy system*. Elsevier, 1 edition, 2007.

[66] C. M. Spadaccini. *Comprehensive Microsystems*, volume 3. Elsevier, 2008.

[67] M. Albert Vannice. *Kinetics of Catalytic Reactions*. Springer, 2005.

[68] F.M. White. *Fluid Mechanics*. McGraw Hill, 5 edition, 2003.